# Interactive comment on “Analysis of 24 years of mesopause region OH rotational temperature observations at Davis, Antarctica. Part 2: Evidence of a quasi-quadrennial oscillation (QQO) in the polar mesosphere” by W. John R. French et al.

**Anonymous Referee #1**

Received and published: 18 February 2020

Reviewer Report on the manuscript acp-2019-1097

Analysis of 24 years of mesopause region rotational temperature observations at Davis, Antarctica. Part 2: Evidence of quasi-quadrennial oscillation (QQO) in the polar mesosphere

By W.J.R.French, A.R.Klekociuk, and F.J.Mulligan

General Remarks

1) The paper studies multi-annual variability in the lower and middle atmosphere up to the mesopause which is an interesting objective. 2) Emphasis is on quasi-quadrennial oscillations (QQO) observed in mesopause hydroxyl temperatures in a 24 year time series. 3) The variability signal is also seen in many other parameters as temperature, winds , geopotential, trace gas mixing ratios, SST, sea ice. These are obtained from various sources as satellites (MLS, SABER), ground based radar, ERA 5, etc.. 4) The analysis concerns vertical as well as meridional and zonal structures of the middle at- mopsphere. This is very interesting and worth publishing! 5) However: More than half of the paper (pictures) deals with these parameters, only, and not with the Davis temperatures! The title of the paper is, therefore, inappropriate and misleading. It should be changed to something more general, and the manuscript should be rearranged accordingly. I know that this is not an easy task, as the interannual variability of the middle atmosphere is a very extended topic, and the data shown in the paper form only part of it. Nevertheles I recommend rewriting the paper in this direction, rather than turning it down. (To make it clear: I do not recommend that the authors write a review of middle atmosphere interannual variability, but that they state that their work forms an essential part of such a larger overview.) 6) The paper is well written, but many of the figures need improvement. 7) The paper is recommended for publication after major changes have been made.

We thank the reviewer for the comments. As a general response to item 5), thank you for the suggestion regarding the title. This work forms part 2 of a two part series reporting on the long-term measurements of OH rotational temperatures at Davis. In part 1 (acp-2019-1001; “Analysis of 24 years of mesopause region OH rotational temperature observations at Davis, Antarctica. Part 1: Long-term trends.”) we focus on the solar cycle response and long term trend components. In this part, we focus on the residual variability observed in those data (the QQO). We decided to separate these sections as they deal with distinctly separate aspects of the long-term measurements..

The principle and foremost observation in both these reports are the trends and variability in the OH rotational temperature data set from Davis. We use many different (publicly available) data-sets in this part to put the Davis observations in global context and use correlation and composite analyses to understand the source and mechanism of the

apparent QQO in Davis OH residual temperatures. We provide evidence of the feature by comparisons with Aura/MLS and SABER temperatures and search for clues to its origin in wind, pressure and sea surface temperature data. We therefore do not think the title is inappropriate or misleading.

Major Comments

1) Fig.1: a) The period of 4.2 years is not very convincing! In the years before 2006 the agreement of Davis-T, Saber-T, and the 4.2 yr oscillation curve is marginal! Please give an error bar for the 4.2 yr period value (see for instance Kalicinsky et al., ACP 16, 15033, 2016; Kalicinsky et al., JASTP 178, 7, 2018). b) How did you detrend solar cycle and long-term trend? Simultaneously or in an iteration?

a) The period of 4.2 years is obtained with a simple sinusoid fit to the residuals. The period and error estimate is 4.18 ± 0.10 years. Coefficients and errors for all model fit coefficients are provided below. The curve is provided as a guide. It is clearly not a simple sinusoid of 4.2 years which is why the term *quasi*-quadrennial oscillation is used (in much the same way that the *quasi*-biennial oscillation (QBO) is not strictly a 2-year periodicity) .

Formula: y ~ Offset + Amp * sin(2 * pi * (Phase - x)/Period)

Parameters:

| | Estimate | Std. Error | t value | Pr(>\|t\|) |
|---|---|---|---|---|
| Offset(K) | 0.02455 | 0.25801 | 0.095 | 0.925137 |
| Amp(K) | 1.49255 | 0.35868 | 4.161 | 0.000483 *** |
| Phase(year) | 1994.20367 | 0.35537 | 5611.601 | < 2e-16 *** |
| Period(years) | 4.18158 | 0.10287 | 40.647 | < 2e-16 *** |

Signif. codes: 0 ‘***’ 0.001 ‘**’ 0.01 ‘*’ 0.05 ‘.’ 0.1 ‘ ’ 1

Residual standard error: 1.26 on 20 degrees of freedom

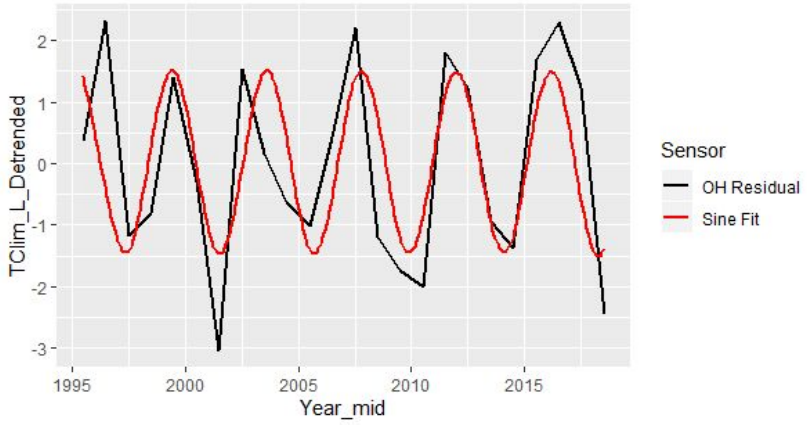


The comparison with SABER is limited as we cannot compare the same winter data interval due to SABERs yaw cycle. As described in the text ‘only days 106-140 and 196-259 are comparable between SABER and Davis-OH over the winter interval and days 141 - 195 (21 May to 14 July) are excluded. We note that the comparison is not as good an agreement as Aura/MLS but still indicates the presence of a QQO feature.

Another version of the wavelet analysis is shown below with 95% confidence contour in white and the ridge as black points, (cone of influence shaded). The ridge varies between 3.29 and 4.46 years.

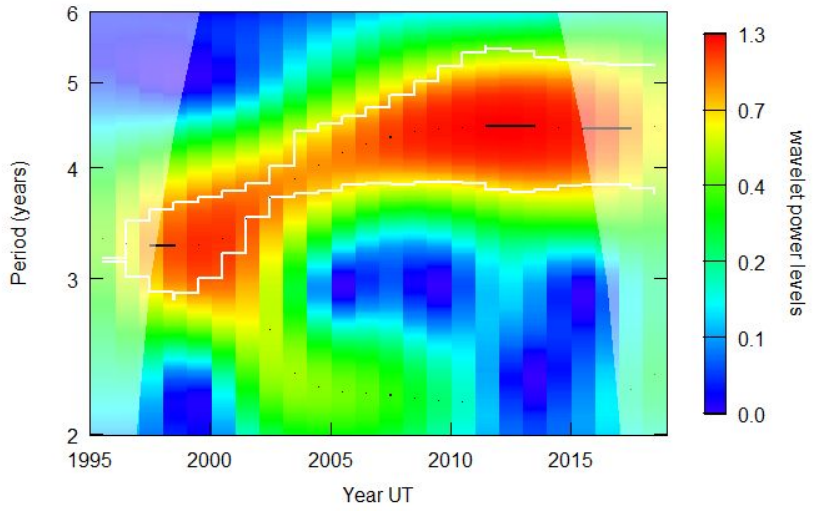


b) The solar-cycle and long-term trends are detrended simultaneously with a multiple linear regression model. This is described in detail in part 1 of this work (acp-2019-1001)

2) Fig. 1 and related text: Figure 10 might be moved to this part of the paper to illustrate that the interannual variability is fairly different in summer, winter, North and South.

Thank you for the suggestion. Figure 1 is specifically the Davis QQO observation. It is the source of our identification of the QQO variation, describes the characteristics of the feature, and provides corroborating evidence of the variation from satellite observations specific to the location of Davis.

Figure 10, on the other hand, is polar cap averages (65-85° North and South) of the MLS 0.00464 hPa pressure level and the summer and winter months (AMJJAS and ONDJFM) in each hemisphere.

Our focus is primarily on the SH and we prefer to keep discussion of the hemispheric and seasonal comparison separate in section 4.5

3) Fig.2: a) This is mostly a global analysis, and only a small part is from OH temperatures. Hence, my General Remark #5 applies. This is also the case in Fig.3 and many other places of the paper, especially for most of Section 4. My suggestions in the following assume a paper version in which title and text have been modified already. b) The “hashed areas” are indicated by crosses. These are difficult to discern! This also applies to the following figures, especially if the background colour is blue! The paper would become much more readable if this was improved! c) Fig.2b shows the vertical structure of the interannual variability, which is very interesting. However, the altitude resolution is poor: it only shows that the mesosphere differs from the stratosphere. As described in Section 2.2 there are more altitude levels available. Therefore please complement the left hand column of Fig. 2 by the altitude levels missing. This should show whether the vertical phase distribution is continuous or steplike (as the ones of Offermann et al., 2015).

a) As stated above, the key result, the new observational data, and the focus of the investigation reported here is to explain the QQO feature observed in the Davis OH

temperatures. We would argue that explanation of the QQO variability in the OH temperatures are the whole reason for the study. We have examined the temporal and spatial extent of the QQO signal with available global data sets to place the observation in context and to attempt to identify its source. We believe this is a reasonable title.

b) We have made appreciable efforts to re-work the figures to improve the hashed/stippled areas which indicate significance. Perhaps this option of applying a border to grid cells that pass the significance criterion improves visibility and clarity? We are happy to defer to editorial and publication recommendations on this.

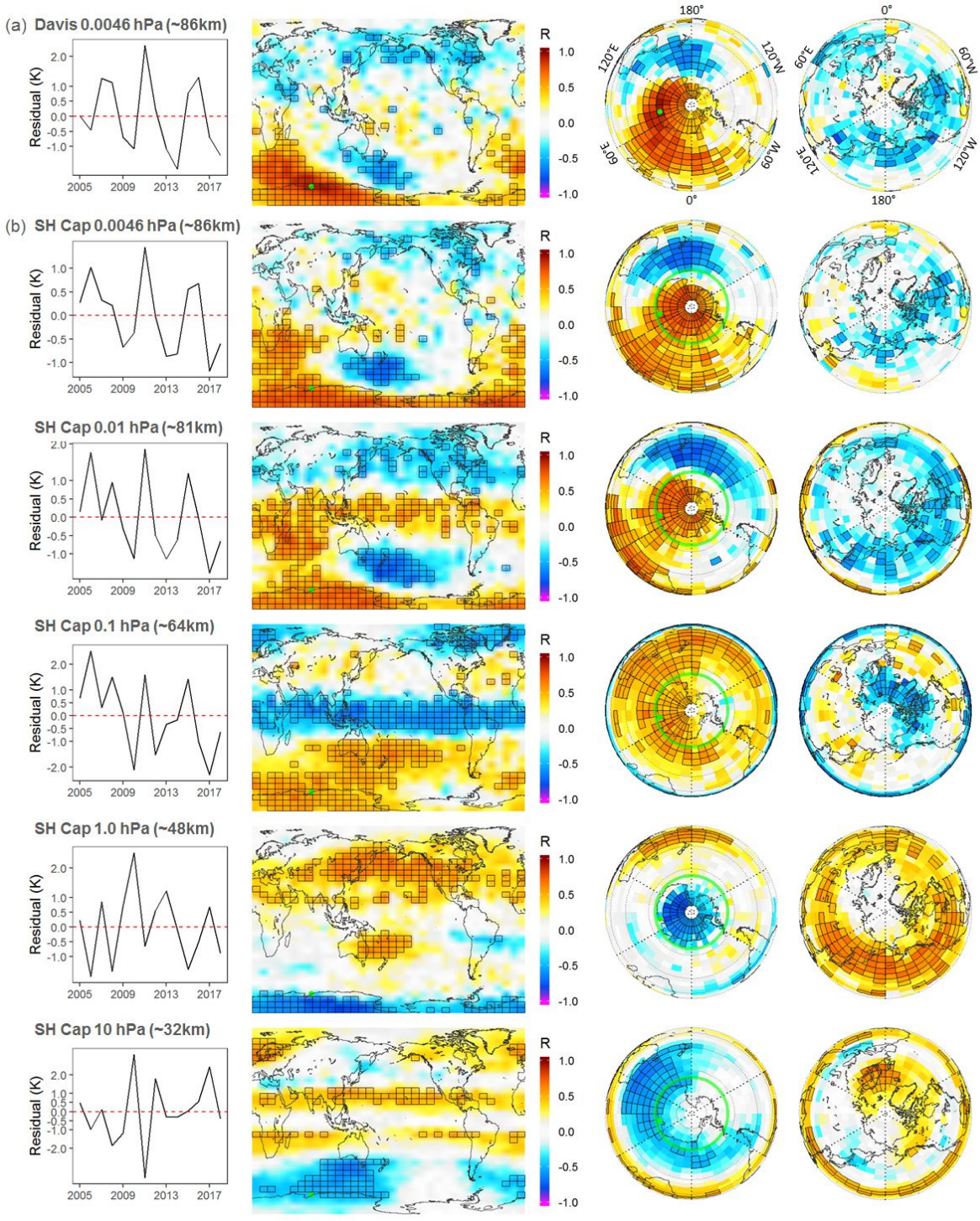

c) Indeed, 55 pressure levels are available in the Aura\MLS data set but we have selected levels which are representative of the stratosphere, stratopause region, mesosphere and mesopause region (see fig right).

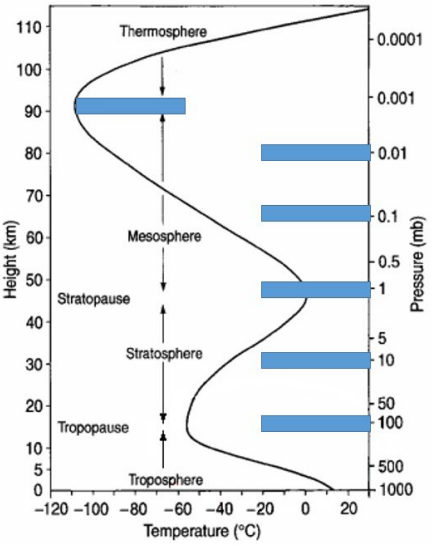


Plotted below are the additional time series of Aura/MLS [AMJJAS] polar cap (65-85°S) averages at each of the MLS native pressure levels compared to the Davis OH time series. The y-axis temperature scale is common to all series, but they are offset by the pressure (log scale) indicated by the labels.

These plots show the QQO feature is common through the range 0.0046 - 0.1 hPa, (represented by the 0.0046, 0.01 and 0.1 hPa panels in our figure) then there is a transition between 0.1 and ~1hPa (1hPa is shown) followed by a reasonably consistent pattern to the time series below 1hPa (10hPa is shown). The selected levels of fig 2 thus reasonably encompass the range of variability shown over the polar cap and are representative of the 3 different regimes. This figure is added to the supplementary material as figure 2S.

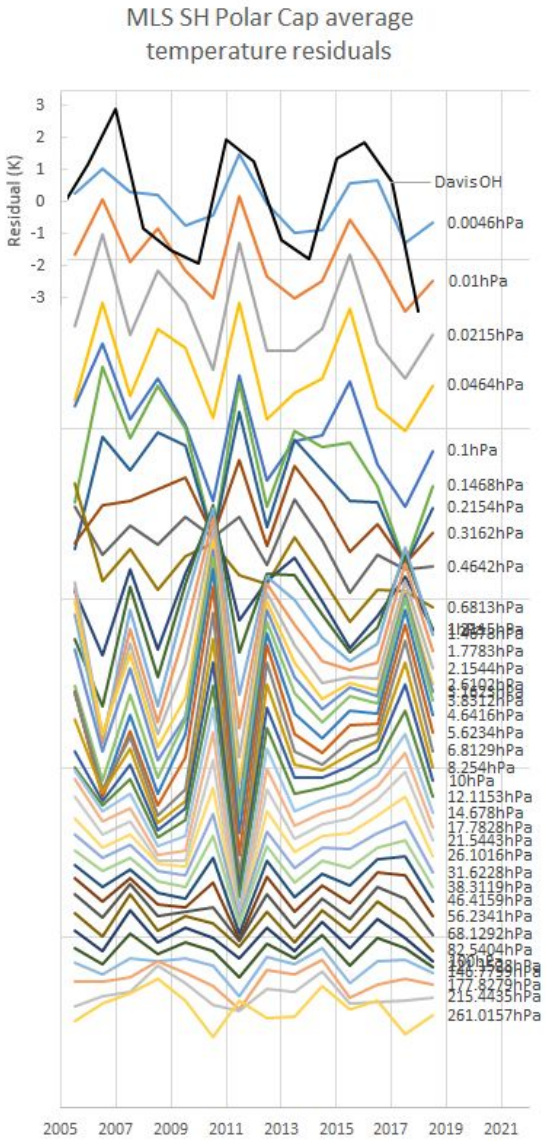


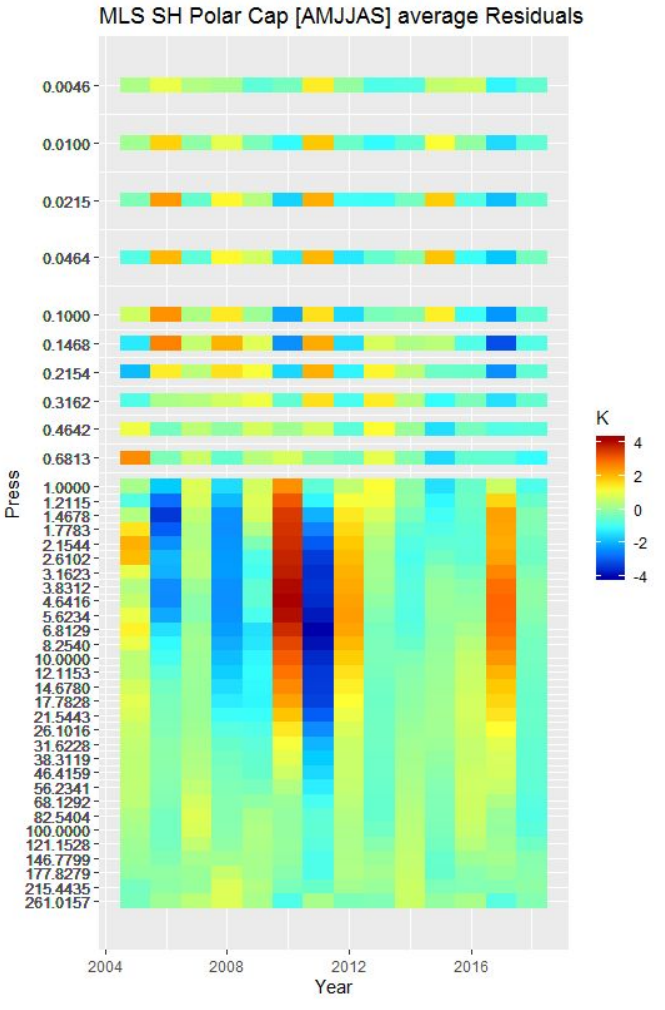

Full correlation plots for some additional levels are also provided below for your reference, but note that the selected levels do in general capture the correlation patterns throughout the atmosphere profile.

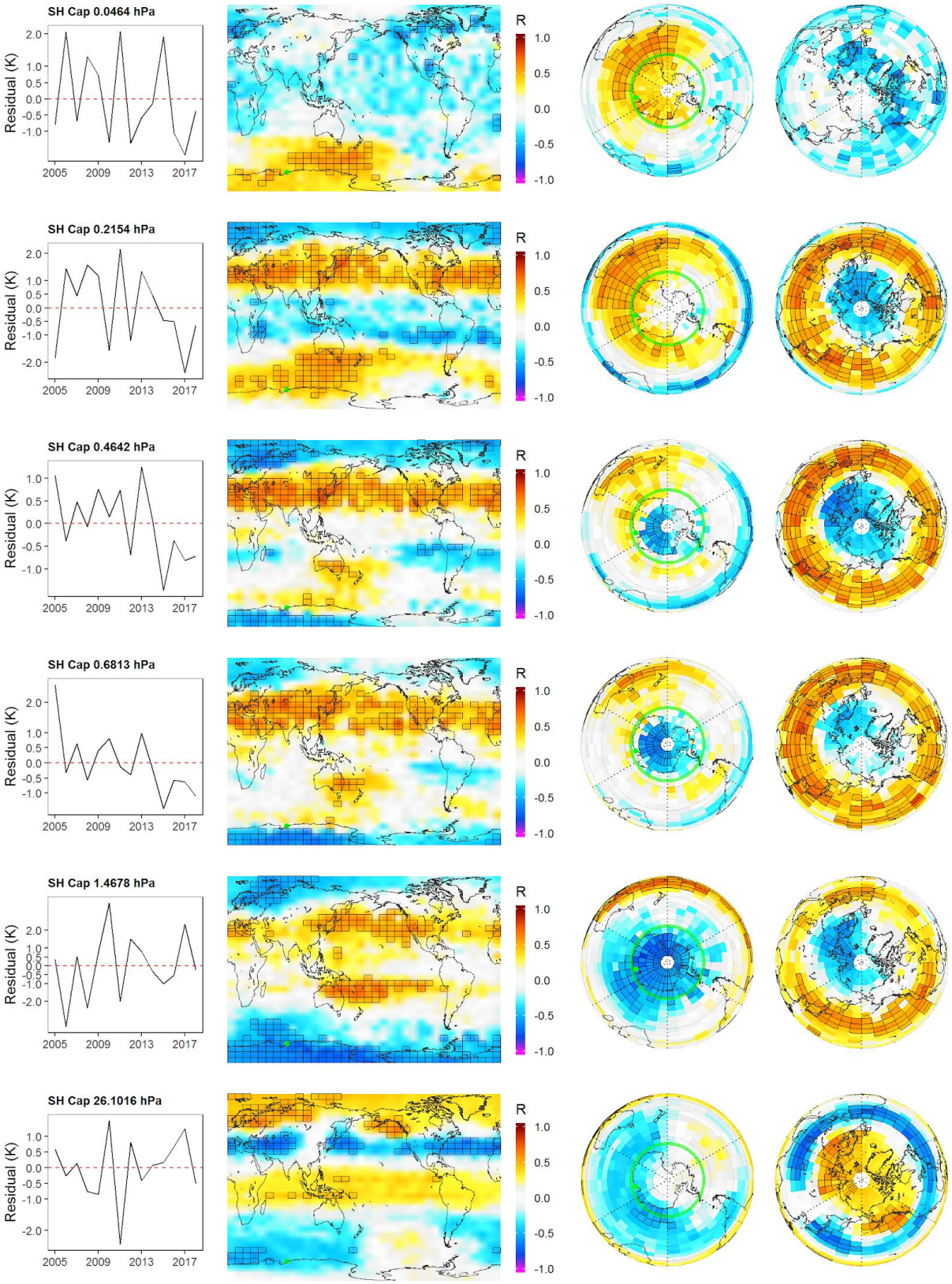

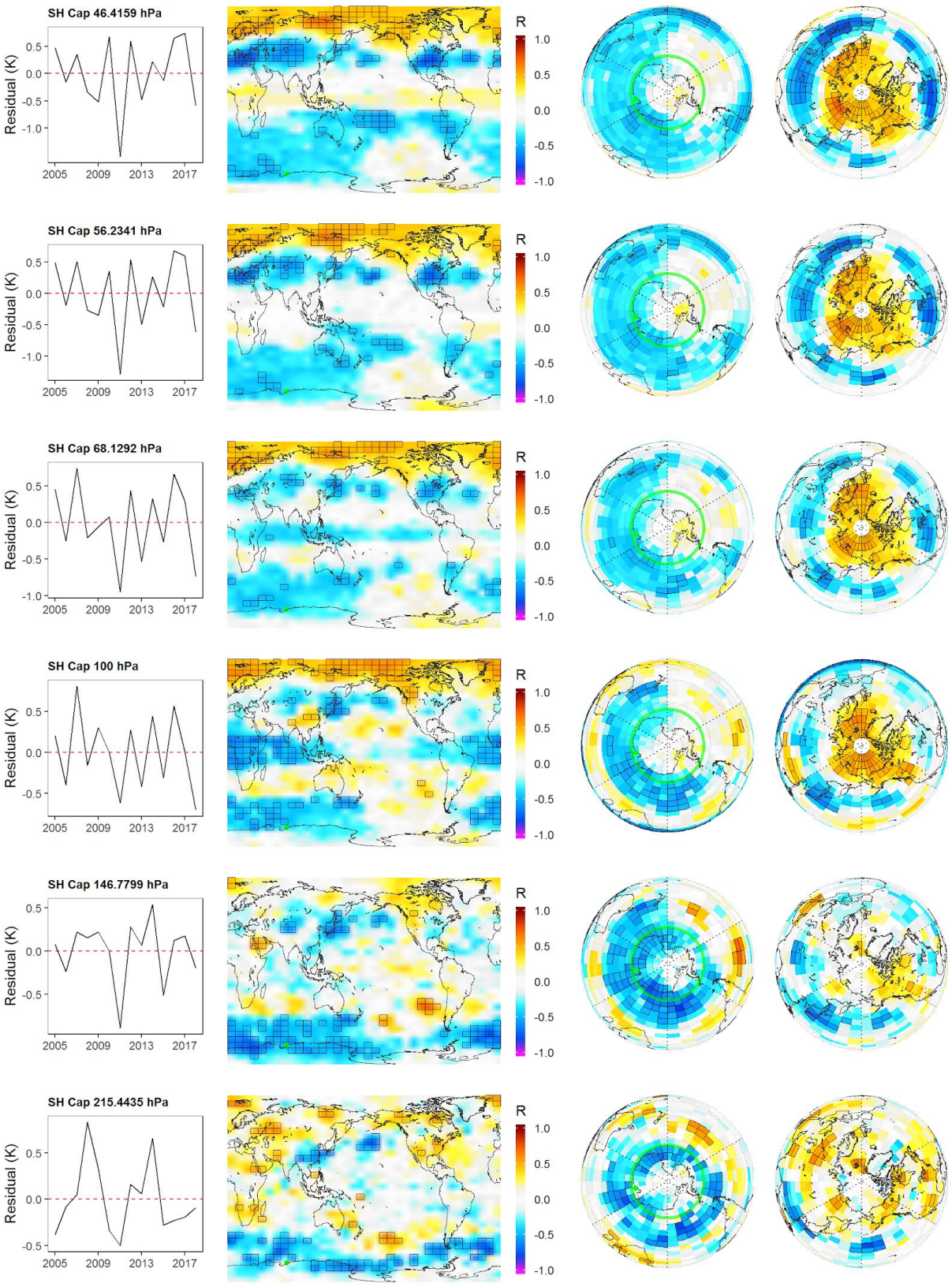
SH Cap 46.4159 hPa
SH Cap 56.2341 hPa
SH Cap 68.1292 hPa
SH Cap 100 hPa
SH Cap 146.7799 hPa
SH Cap 215.4435 hPa
Residual (K)
2005
2009
2013
2017
R
1.0
0.5
0.0
-0.5
-1.0

4) Fig.3 and Fig.4: Please give time series as in the left hand panel in Fig.2.

Figures 3 and 4 are *composites* of 5° x 10° (latitude x longitude) or 36 x 36 grid cells corresponding to the cold, mid and warm years of the Davis detrended QQO signal shown in Fig 1(b). As composites the series are accumulated by the Davis detrended temperature, not by time.

We have tried several variants of the significance hatching on these plots to the boxing applied on Fig 2 but this is too heavy with the smaller grid cells in ERA5. We prefer the original although we have modified the point density (see examples below). Again, we will work with editors to optimise this.

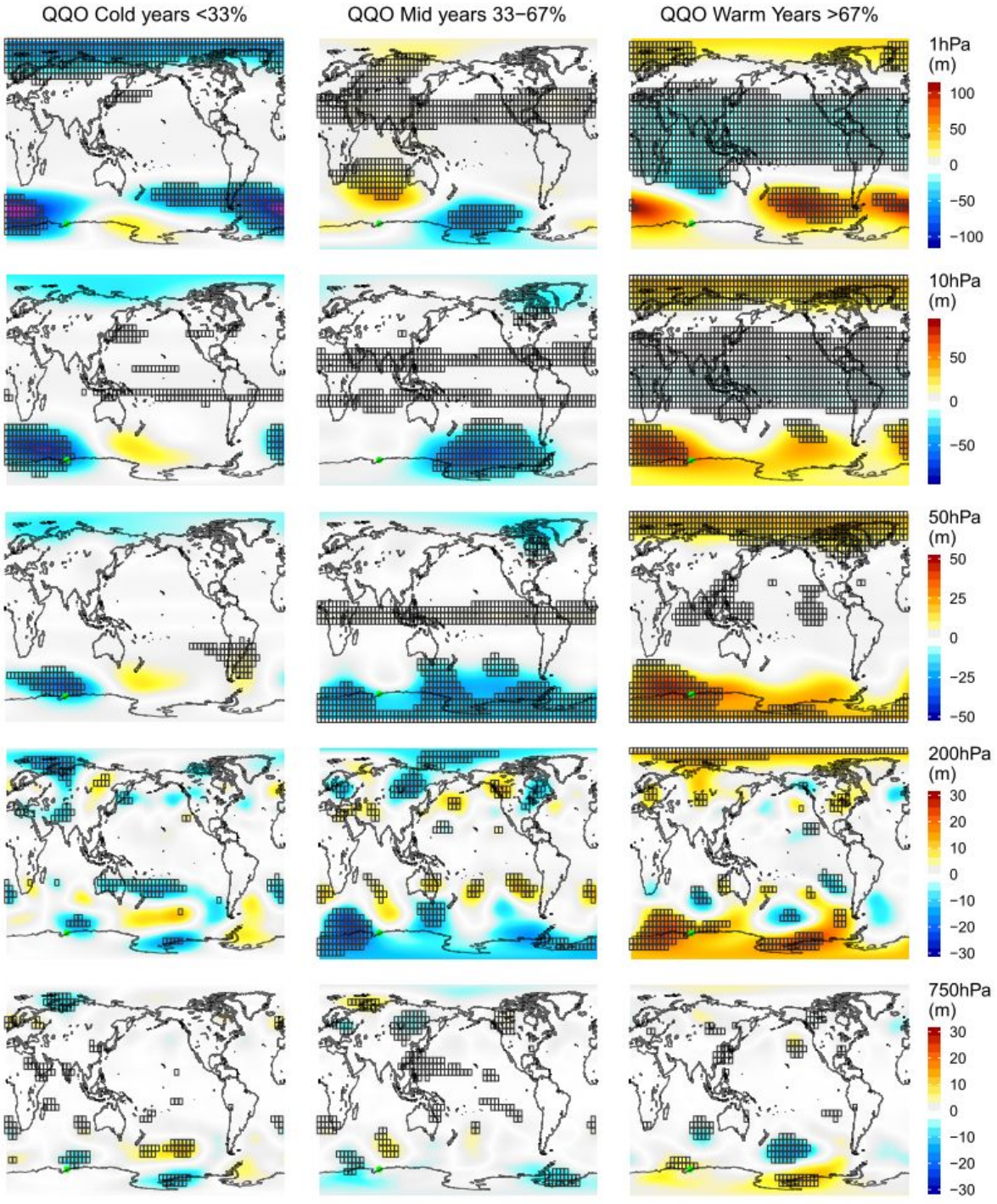

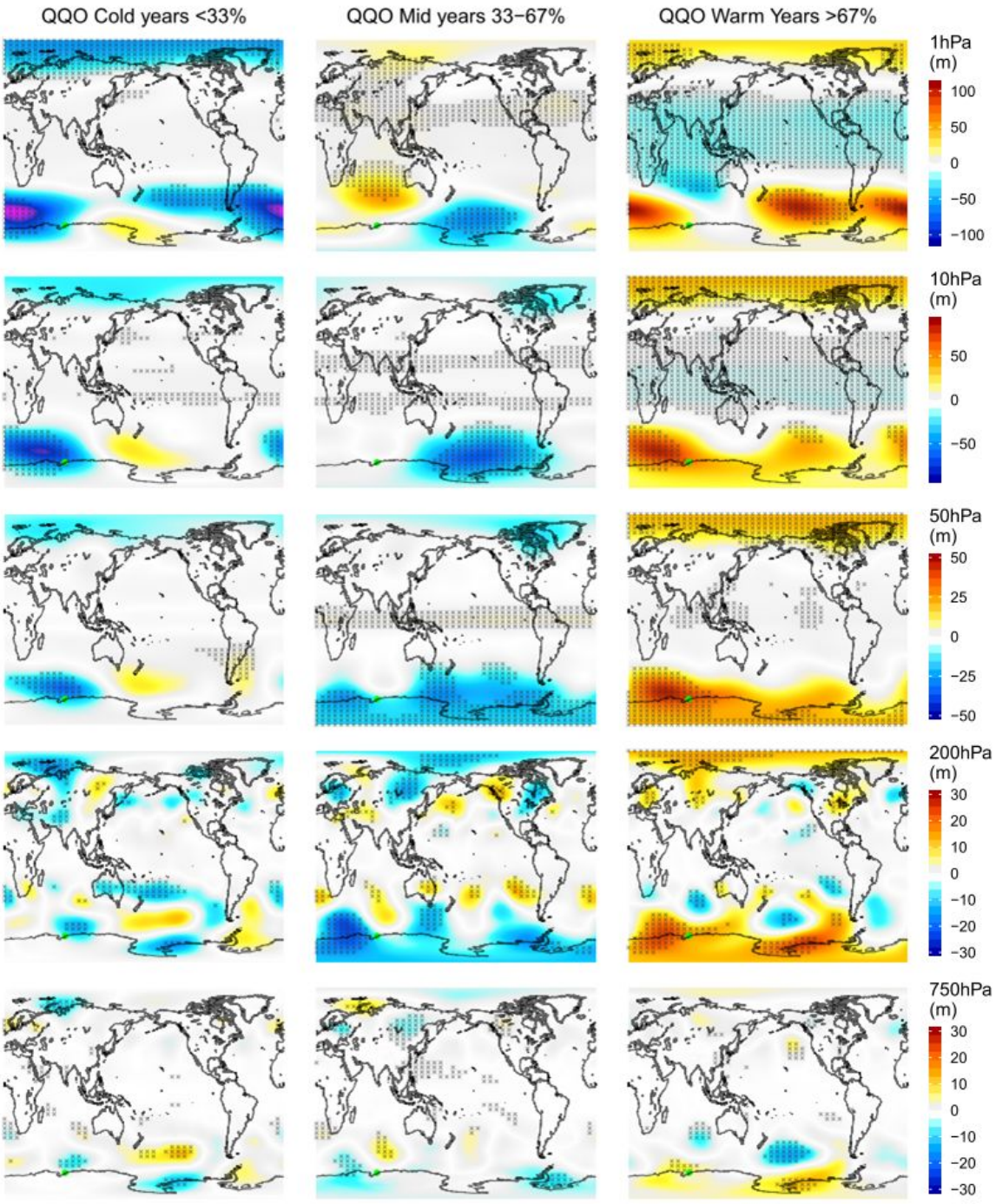
QQO Cold years <33%
QQO Mid years 33−67%
QQO Warm Years >67%
1hPa
(m)
100
50
0
−50
−100
10hPa
(m)
50
0
−50
50hPa
(m)
50
25
0
−25
−50
200hPa
(m)
30
20
10
0
−10
−20
−30
750hPa
(m)
30
20
10
0
−10
−20
−30

5) Fig.5: Please give a time series for SST (near to Davis)!

The correlation analysis in Fig 5a does not show, and we do not claim, a significant correlation of the Davis OH QQO signal with SST in the vicinity of Davis (region C). Instead, we note in the text that the "strongest and most consistent patterns of anti-correlation (QQO warmest for below average SST) for the two epochs occur at mid-latitudes in the south-western Pacific Ocean (to the south of Australia and New Zealand, region D), in the south-western Atlantic Ocean (near the east coast of South America), and in the west-central Indian Ocean (to the west of Madagascar, region B). Significant positive correlation is also seen at mid-latitudes south of Africa (region A), and for the longer-term Davis data set, in the south-eastern Pacific Ocean."

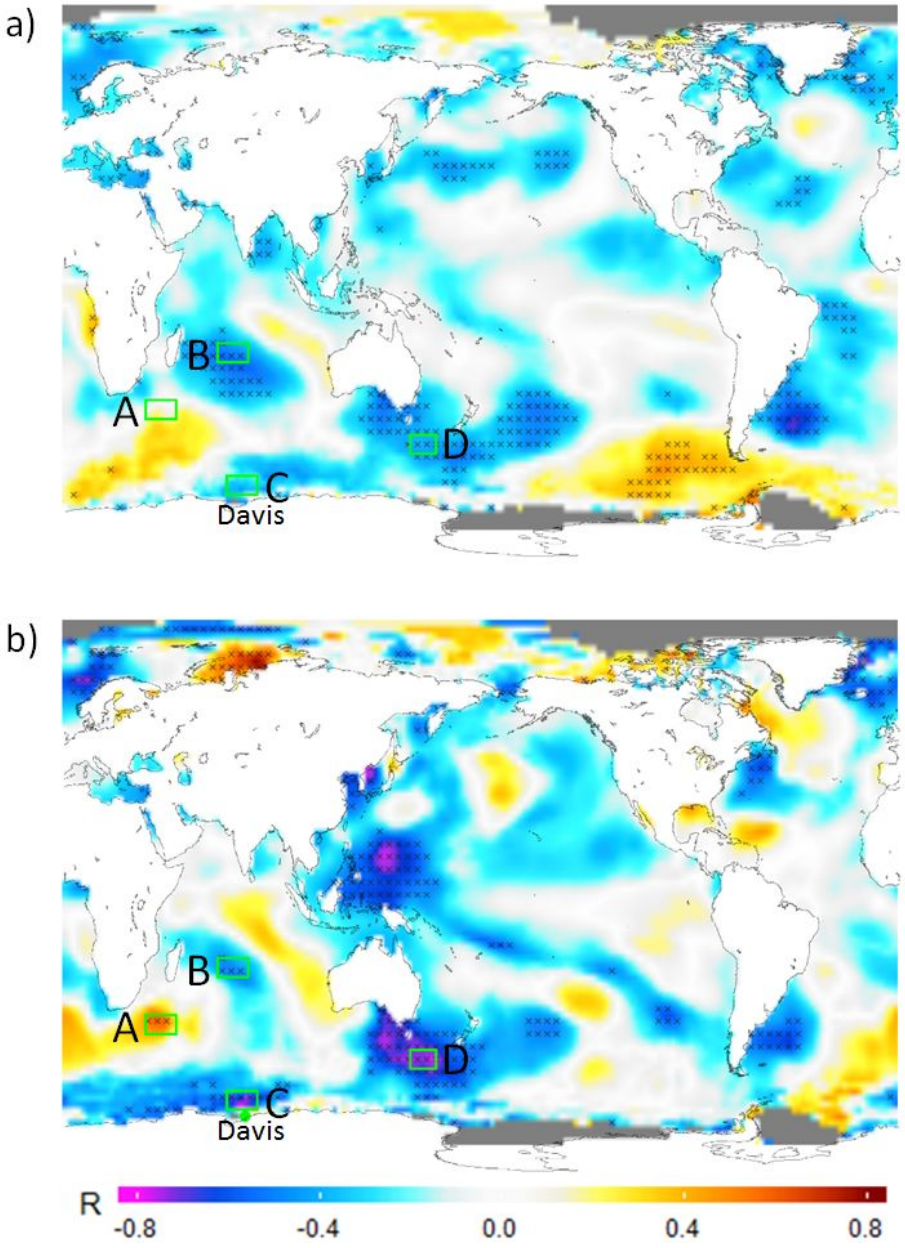


We have plotted below timeseries of SST anomaly compared to the Davis OH residuals and Aura/MLS residuals for the mean within the green bounding boxes A,B,C, and D above.

Correlation coefficients for Davis (Dav) and Aura/MLS (MLS) are provided in the legend text. This figure shows the positive correlation with region A and the negative correlation with region D

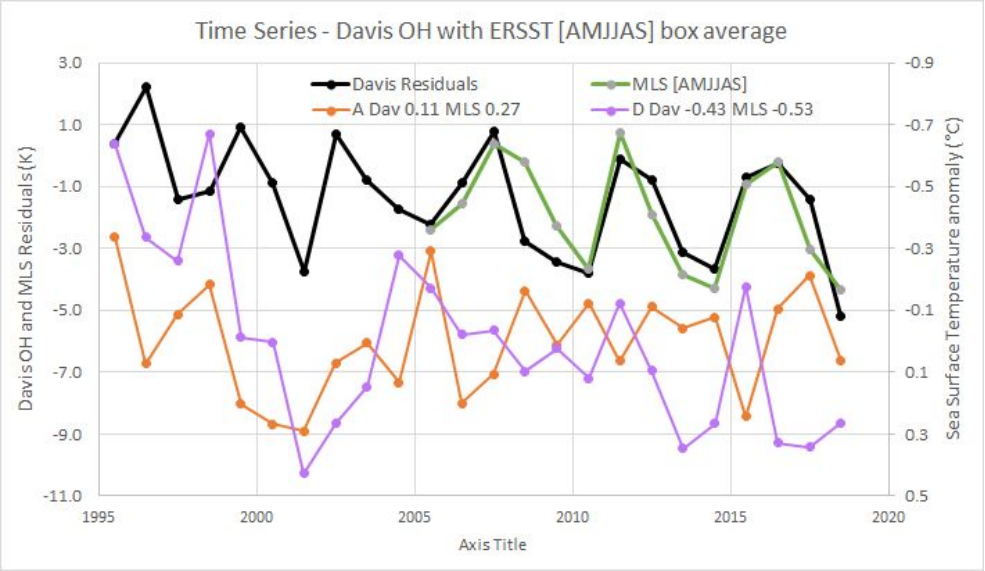


This figure shows the negative correlations with regions B and the vicinity of Davis region C. Note that the latter is largely sea-ice during the AMJJAS months.

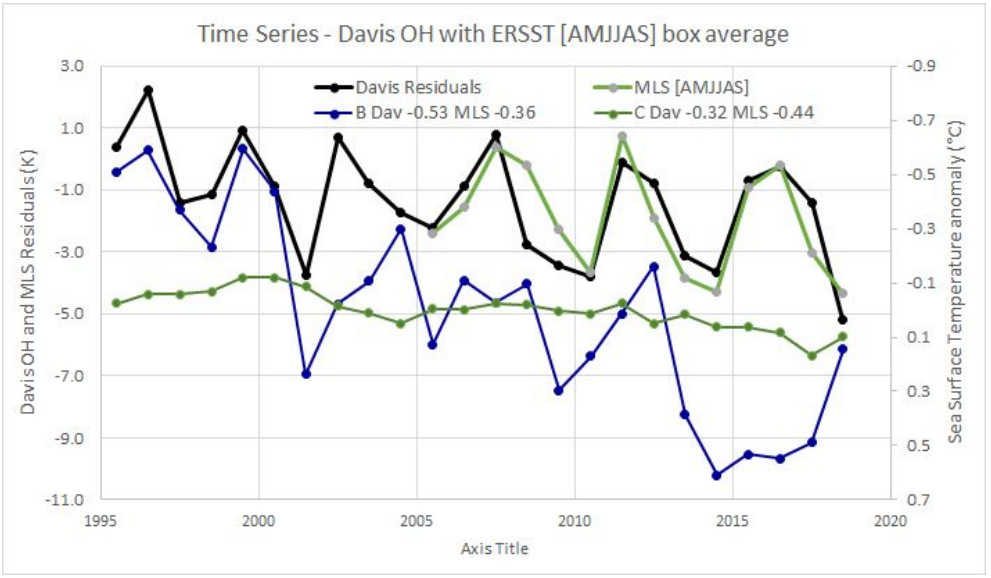

6) Fig. 6: Please give time series!

Figure 6 has been modified to improve significance plotting and time-series of the two regions of significant correlation (identified as A and B in figure 6a have been provided below.

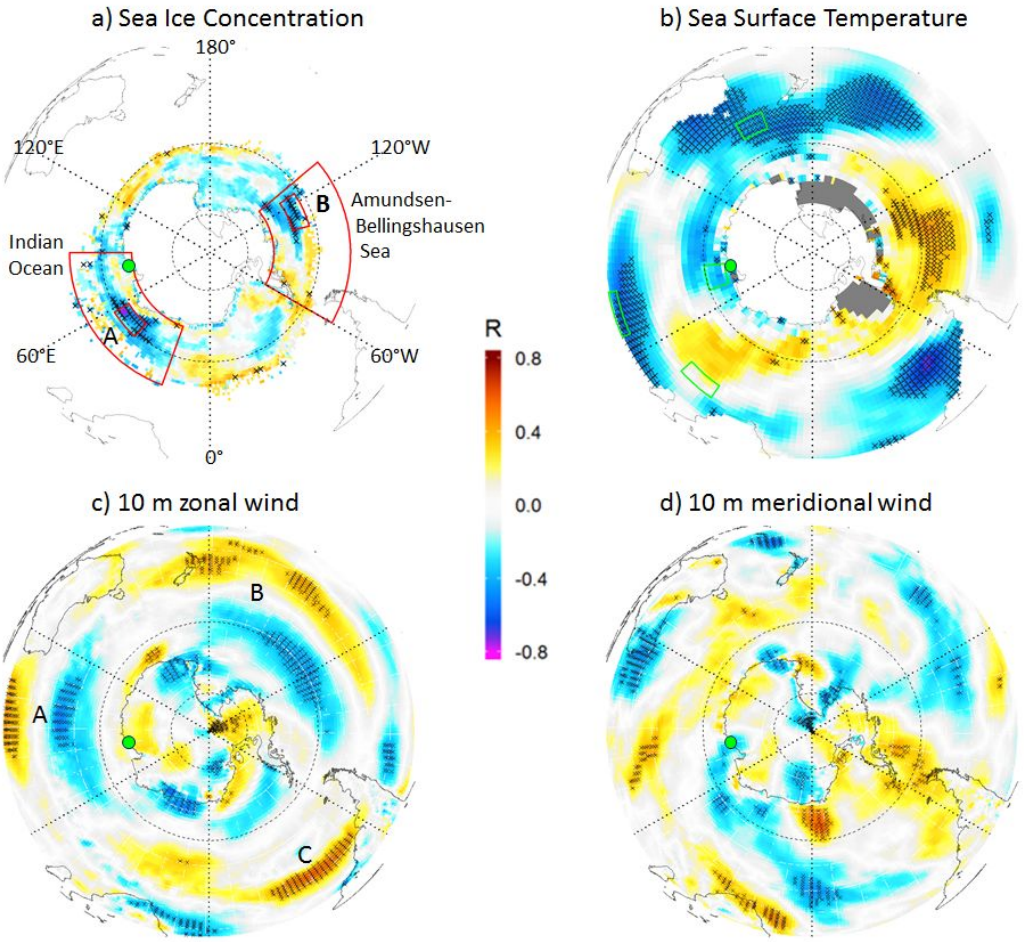


Time series for A and B regions of maximum anticorrelation are provided below (correlation coefficients provided in the legend). Note the inverse sea ice cover axis.

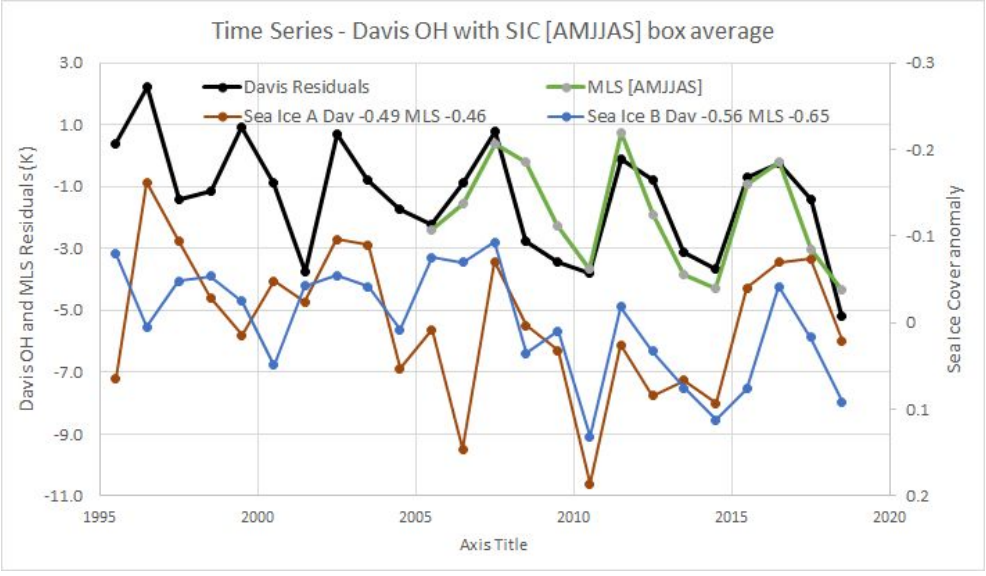

7) Section 4.1: I understand that the authors are interested in showing a conection between SST and sea ice, and the upper atmosphere QQO. However, Sect.4.1 is not really suitable for this. The correlations discussed are marginal or non-existent (L387: R = -0.09 is not a correlation). The text refers to many literature papers that one would need to read in order to understand the text. Finally, correlation of a parameter below the tropopause with one above the tropopause is generally a delicate business, as is, for instance, indicated by Fig.3, 4. Altogether, a much mor extended analysis would be needed, as the authors state by themselves. As this is beyond the scope of this paper, I recommend to summarize this Section in a few sentences or omit it, at all.

We have moved this section to Section 4.4 to provide better flow in the discussion. We have also added text to better describe the motivation for this section. It is not that we are interested in showing a connection but rather, we note that there are regions in the sea ice zone that are significantly correlated with the Davis QQO variation (regions A and B below) that appear to have a wave-2 structure. We propose that both the upper mesosphere and sea ice may be responding to a common driver and suggest that possibly the meridional winds could drive both observations ie “a persistent northward (southward) flow on one side of a circulation anomaly could increase (decrease) sea ice due to the associated flow of relatively cold (warm) air from higher (lower) latitudes and expansion compaction) of the ice edge.

As shown in Fig 6a, specific regions of significant correlation between the Davis OH temperature record and sea ice concentration occur (regions A and B below). On this map, we have added values for the local maxima and minima of the correlation coefficient where these values are significant. ie region A -0.49 and region B -0.56 (see response to item 6 above) The maximum anti-correlation is -0.61 at 55.5°E, 61.5°S (within region A, marked with purple dot)

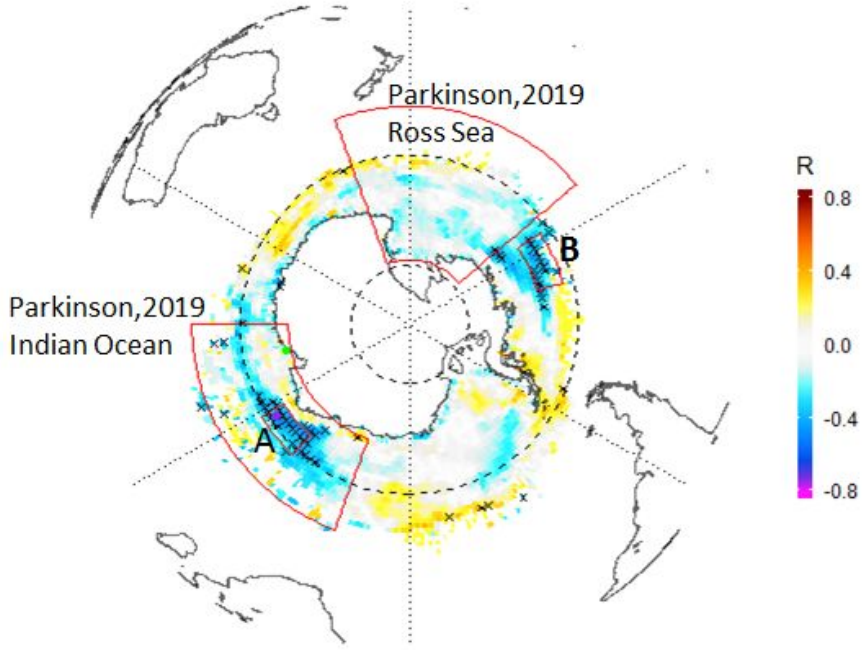

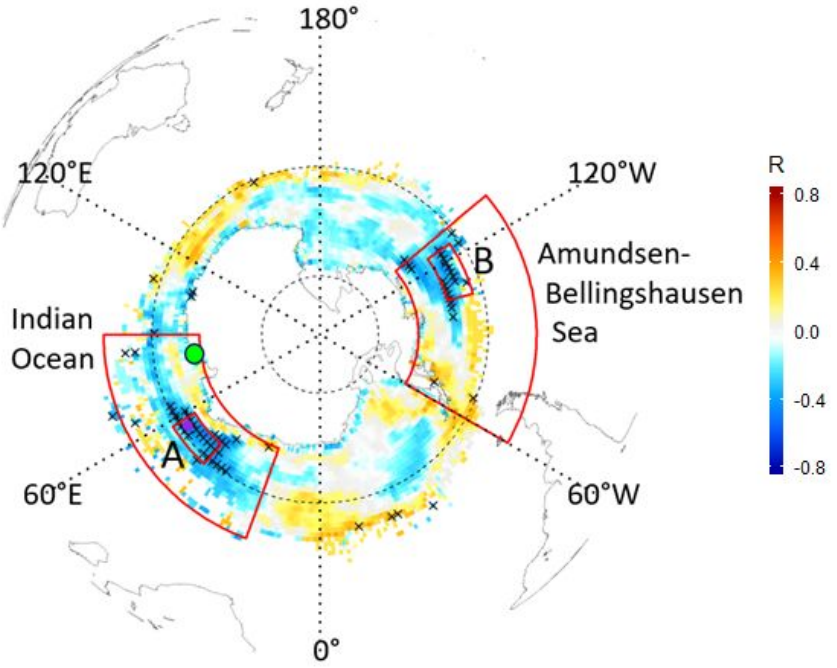


The correlation given at L387 the reviewer is referring to (R = -0.09), is the coefficient of the correlation between the time series of sea ice anomaly for a large sector of the Ross Sea region from Parkinson et al. (2019) and the Davis OH residual. We have compared with Parkinson et al (2019) because this reference provides a recent assessment of sea ice trends in various sectors of Antarctica.From the plot above it is clear that the Ross Sea region is not well correlated compared to regions A and B. Instead of the Ross Sea region, we now compare with the Amundsen-Bellingshausen sea region used by Parkinson (2019). The correlation is more negative (R=-0.24) but not significant. We have restated the sentence starting at L386 to better convey that there is no significant correlation for this particular region.

8) Section 4.3, L444pp: Obviously, the data of Dyrland and of Espy are Northern Hemisphere data. How does this compare to your SH results? Can you give a picture?

The table below shows a comparison of the Dyrland et al. (2010), and Espy et al. (2003) values to the results obtained here. As noted in the comment, the data in Dyrland et al. (2010) are from the NH (78 N), but the data in Espy et al. (2003) are from the SH (~68 S). Northward wind is positive; at both poles, poleward flow results in warmer temperatures. Figure 3 in Espy et al. (2003) and Figure 3 in Dryland et al (2010) show correlation plots similar to Figure 7(b) in this work. A reference to earlier work by Garcia and Solomon (1985) has been added in response to a comment from referee 2.

| Reference | Location | Cofficient of linear regression (temperature to meridional wind) (K/m·s$^{-1}$) (Northward wind is positive; at both poles, poleward flow results in warmer temperatures) | Correlation coefficient |
|---|---|---|---|
| Espy *et al*. (2003) (Fig. 3) | Rothera (67.6°S, 61.8°W) | -0.71 | -0.61 |
| Dyrland *et al*. (2010) (Fig. 3) | Longyearbyen(78°N, 16°E) | +0.50 | 0.71 |
| This work | | | |
| OH(6-2) T_Residual | Davis (68°S, 16°E) | -0.70 ± 0.25 | -0.56 |
| MLS T(0.0464 Pa) Residual | Davis (68°S, 16°E) | -0.89 ± 0.24 | -0.73 |
| SABER T_VER Residual | Davis (68°S, 16°E) | -0.96 ± 0.24 | -0.71 |

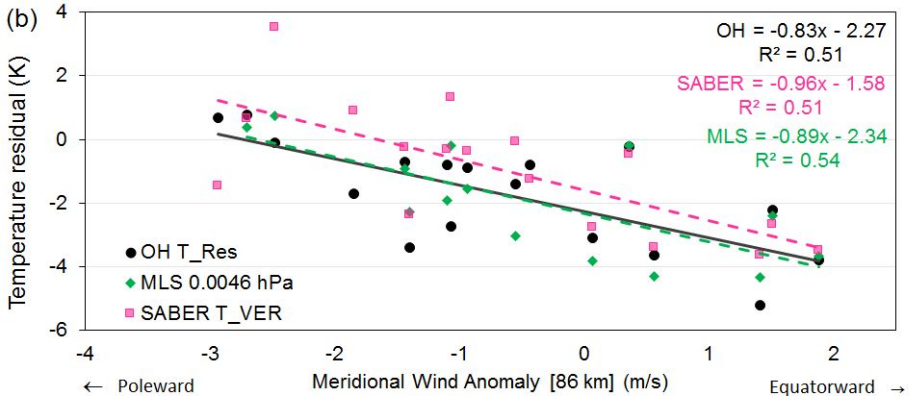


9) Section 4.4: CO is an important parameter, and its analysis is interesting. However, the correlation $R^2$ = 0.13 at 14 datapoints is barely significant.

The square of the correlation coefficient was incorrectly stated as 0.13; it should be 0.19 (as rounded to 2 significant figures) and thus explaining 19% of the variance.

10) L483: Do you mean concentrations or mixing ratios in the text and figures?

As noted at L473 and the caption to Figure 8 and 9, we use CO mixing ratios, with units in ppmv (parts per million by volume). We have clarified the reference to CO at L483 in terms of mixing ratio.

11) Fig.9a, L493pp: I could detect the “crosses of significance” only if I used a strong magnifying glas.

We have improved Fig 9 so that a magnifying glass is no longer required to detect the crosses of significance. The correlation scale is common and applies to all panels so only one scale is now shown.

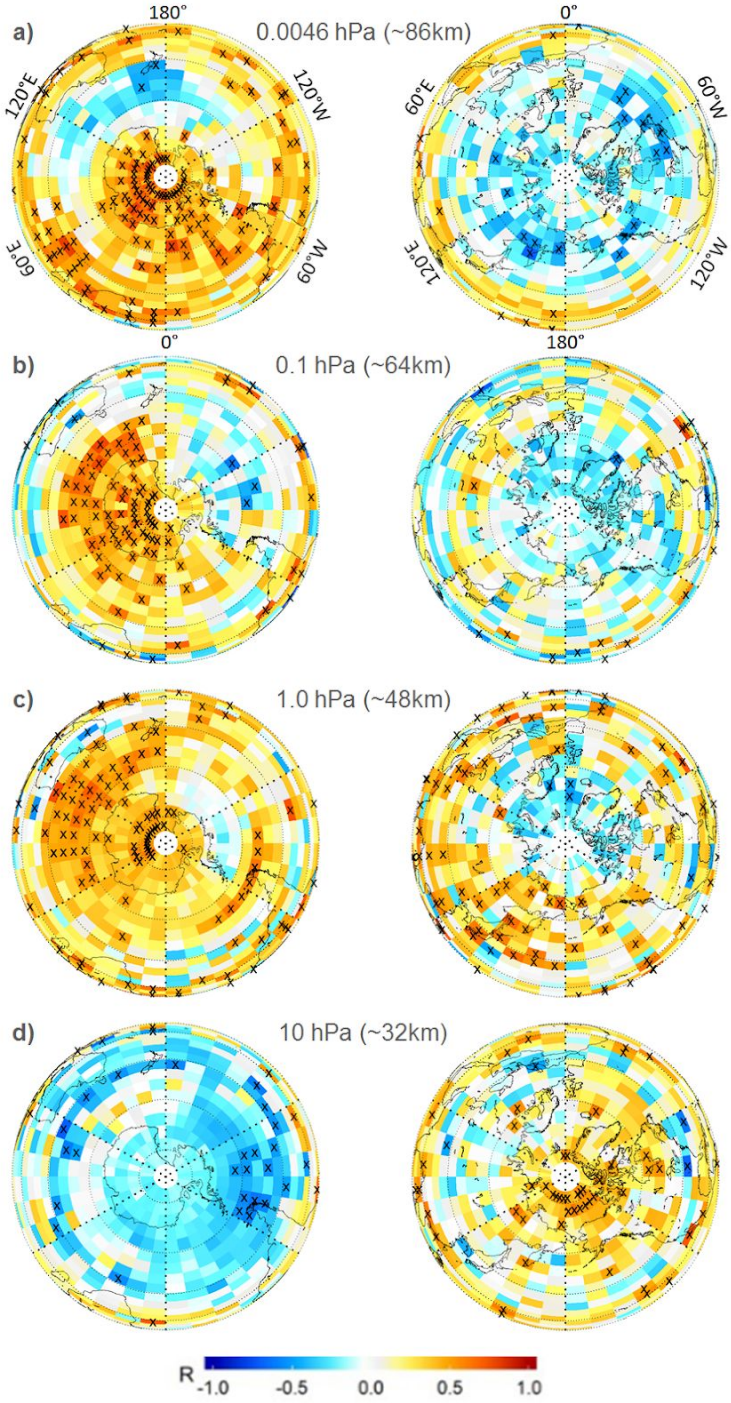


Figure 9

12) Sect.4.5; Lines 507, 510: If you omit two or four data points from a series of fourteen, the resulting conclusions are very dubious. Please phrase more cautiously!

Section 4.5 has been substantially modified to *'suggest'* the phase and amplitude relationships between summer and winter NH and SH QQO variation given the data set only spans 14 years. We can only base our interpretation on the data available but believe it is worthwhile examining the SH/NH and winter/summer seasonal comparison. The

observations drawn from this comparison that the QQO amplitude appears to be larger in summer than in winter (in both hemispheres), and that the NH (summer) is the opposite phase to the SH we dont believe are overly dubious.

13) Lines 529, 530: Apparently, WACCM does not detect your QQO, either! Why then show this Section 4.6?

As we state in section 4.6 “Our interest here is to see if the model physics produces a QQO response in the mesosphere” and have added “particularly as Offermann et al. (2015) had noted that the CESM-WACCM model showed low-frequency variability in temperatures on 3-6 year timescales over Middle Europe”

If WACCM did show a statistically significant QQO it could be explored and understood through the model mechanism. The fact that it shows a sporadic or not statistically significant response implies a limitation of the model. We have added further text to refer to time-period spectra for each ensemble at three pressure levels - these spectra are shown as Fig. S8 in the Supplementary Material.

14) L 610-612: This is a misunderstanding: The periods cited are from the Duffin oscil- lator which is a non-linear oscillator in the ocean. However,the oscillations discussed by Offermann et al., 2015, are intrinsic in the atmosphere! These authors state that their results are not in contradiction to other authors who reported solar cycle harmon- ics. They note, however, that it is difficult to disentangle these two types (Section 6.2, last paragraph in that paper).

Lines 610-612 refer to the association by Offermann et al (2015) of the periods they found in their data with similar periods found in GLOTI data and the NAO index. The only point we wish to make here is that the QQO found in the Davis data has similarity to the periods reported by Offermann et al (2015). We have rephrased the sentences referring to Offermann et al.(2015) in an attempt to clarify the point.

15) Summary, L 626pp: Please state clearly, that the Davis data are winter data, and that summer values are lacking. Fig.10 shows that there may be large differences!

We have specified ‘winter average’ throughout the summary and conclusions section to make this point clear. In general, the fact that the Davis data are winter measurements is stated explicitly in the Abstract, Introduction, Data sets (section 2.1) and with reference to the months [AMJJAS] for comparison with Aura/MLS, SABER and other data sets. Section 3 and in the discussion in section 4.

Minor Comments

1) Line 38: relationship is suggesting

Changed to ‘suggests’

2) L 50: French et al., 2020

Corrected all occurrences referring to Part 1 of the paper.

3) L 80 : including high

removed ‘at’ as suggested

4) Fig.3 – 5 : Please indicate location of Davis.

Davis location has been added to Figs 3-5

5) Fig.8: Please give error bars.

Error bars have been added to Fig 8

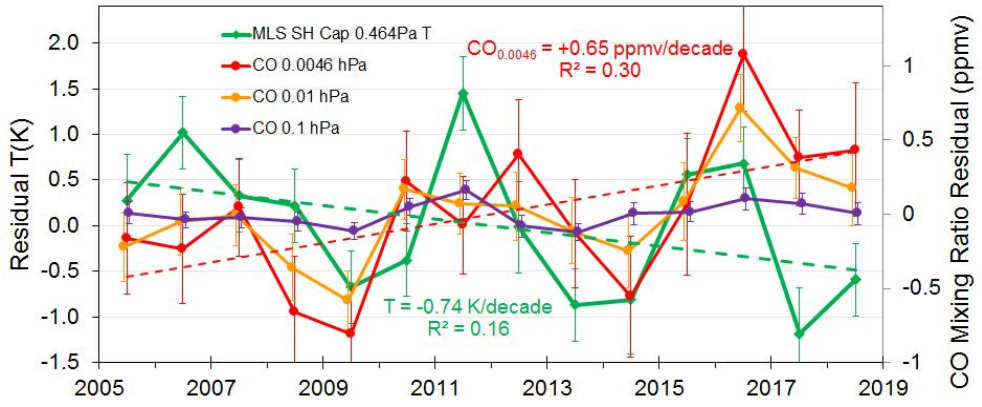


6) Fig. 10: Please give error bars. Orange and red lines difficult to distinguish!

Added error bars, modified trend line colors and separated SH from NH to improve visibility. Corrected NH winter trend value.

New

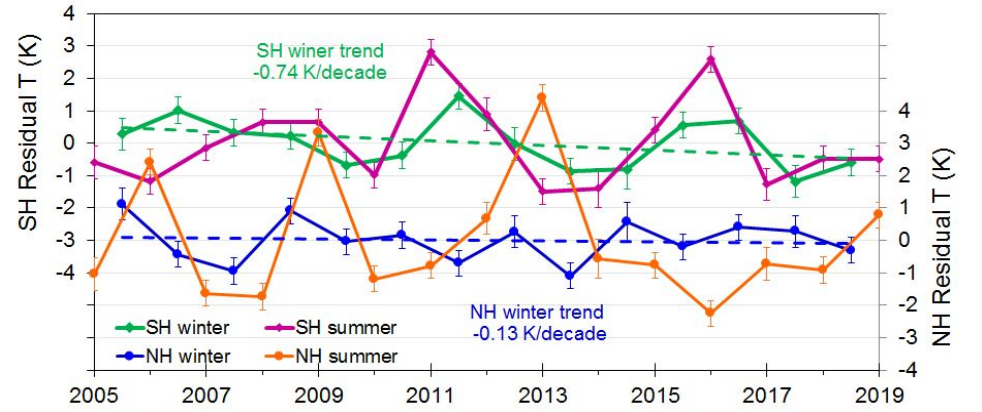


Old

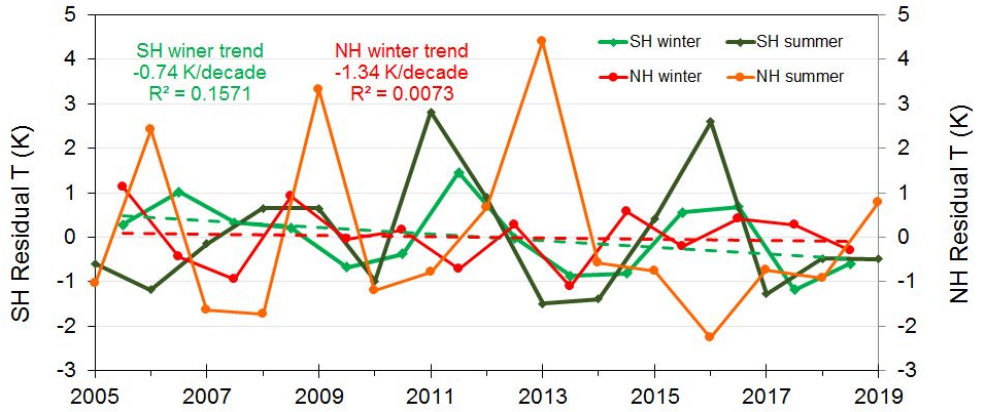

# Response to RC2

Review of "Analysis of 24 years of mesopause region OH rotational temperature 1 observations at Davis, Antarctica. Part 2: Evidence of a quasi-2 quadrennial oscillation (QQO) in the polar mesosphere" by French et al.

This manuscript reports on the detection of a quasi-quadrennial oscillation detected in the SH polar winter OH nightglow, MLS and SABER temperatures. The feature is characterized after the removal of the solar signal and a linear trend as described in Part 1 of the study. The signal has a counterpart in the NH according to MLS data. The authors suggest a relationship between the temperature QQO and the changes in the mesospheric meridional winds and the corresponding changes in downwelling through adiabatic cooling and heating. The authors also show a significant correlation with the SST and provide an explanation of the connection with the mesospheric QQO through a changing GW filtering by modulated PWs.

I found the paper interesting in general and well written, the methodology used is convincing, and the results are new. Therefore, I think it is in principle suitable for publication in ACP. However, I must admit that I sometimes got lost when reading the discussion in Sect. 4. There are several places where it is not clear to me what the authors want to state. There are cases where mechanisms that are clearly not connected to the feature (for example, due to their time-scale) are even described in detail. The discussion should be more concise in order to make the reading more fluent and the reasoning more understandable. It should provide briefer but still comprehensive information only on mechanisms that may potentially be connected to the mesospheric QQO. Also, the authors should try to use a more cautious wording because they only suggest the origin of the feature through reasonable connections but do not provide a solid proof. In summary, in order to improve the paper, I urge the authors to re-write and significantly shorten section 4. Besides taking into account the suggestions listed below, I think the paper would that way be ready for publication in ACP.

We thank the Reviewer RC2 for your considered and helpful review. We have revised and re-organised the discussion in section 4 to hopefully improve the flow and comprehension of our study and the discussion. Please find specific responses to your review below. References to figures and sections are as per the reviewed manuscript, but be aware figure order and sections have been rearranged in the revised manuscript.

Comments:

L19 "peak-to-peak" amplitude

Added as suggested

L27 suggesting -> suggests

Corrected

L27 That the authors have found a correlation between the QQO and the CO vertical transport does not necessarily mean that a "substantial part of the QQO is the result of adiabatic heating and cooling driven by the meridional flow" but just that the QQO is plausibly linked, at least, to the

change in meridional flow. Please, provide some quantification proving such substantial contribution or re-write the sentence.

'Plausibly linked' is a better term to describe the relationship. Thank you. We will use that. We have added the correlation coefficients for the OH temperature and radar derived meridional wind at 86 km (from Fig 7) and from the CO correlations in Fig 8. The text in this section has been re-written and now reads …

"We find a significant anti-correlation between the QQO temperature and the meridional wind at 86 km altitude measured by a medium frequency spaced antenna radar at Davis (R2 ~ 0.516; poleward flow associated with warmer temperatures at ~0.83±0.21 K/ms-1). The QQO signal is also marginally correlated with vertical transport as determined from evaluation of carbon monoxide (CO) concentrations in the mesosphere (R2 ~ 0.18 at 0.73±0.45 K/ppbvCO). Together this relationship suggests that the QQO is plausibly linked to adiabatic heating and cooling driven by the meridional flow.

L30 In case it is not confirmed by modelling, please, replace 'suggest a tidal or planetary wave influence in' by 'is consistent with tidal or planetary waves influencing'

Modified sentence as suggested.

L32: 'potentially' -> 'plausibly'

Modified as suggested.

L40, insert comma after Antarctica

Inserted comma.

L78. Close parenthesis

Parenthesis closed.

L147 'Retrieved' might be ambiguous in this context. Do you mean 'selected'?

Changed wording to 'selected'.

L148 Did you select both daytime and nighttime MLS profiles? If so, did you check mean biases with respect to nighttime only profiles?

Yes, both daytime and nighttime profiles were selected as there are only ~2 profiles per day, however for our high latitude winter comparison the vast majority of the samples are night-time profiles. The latest version of the Aura/MLS data quality document (https://mls.jpl.nasa.gov/data/v4-2_data_quality_document.pdf) does not raise temperature biases between the ascending and descending passes as an issue over the recommended pressure level range.

There is a small diurnal temperature variation in the upper atmosphere (largely ozone heating). We have measured the diurnal variation to be <2K in the Davis OH temperatures.

Xu et al., 2010 (Jiyao Xu, A. K. Smith, Guoying Jiang and Wei Yuan. "Seasonal variation of the Hough modes of the diurnal component of ozone heating evaluated from Aura Microwave Limb Sounder observations" JGR, VOL. 115, D10110, doi:10.1029/2009JD013179, 2010) report on the diurnal variation in MLS temperatures due to ozone heating throughout the atmosphere which shows a minimum in the mesopause region (their Fig 2.) with the comment that "at 90 km, not all of the absorbed solar energy immediately appears as heat in the atmosphere. Substantial portions of the

incident solar energy are stored as chemical potential energy (i.e., as photodissociation products or other reactant species) and released as heat during exothermic reactions, which can take place during day or night."

L153 The selection of this altitude is somehow artificial. The OH-layer altitude changes with time. Explain using SABER data the year-to-year change of this altitude and its effect on MLS data. Also explain the relationship between the QQO in temperature and the QQO in altitude.

The selection of the 0.00464hPa native MLS pressure level as an appropriate representation of an OH equivalent temperature for comparison with the Davis measurements is detailed in Part 1 of this study. This was also a reviewer concern in Part 1 and the following is paraphrased from the response provided.

In selecting the 0.0046hPa level we compared the Davis OH winter average anomaly with MLS [AMJJAS average] anomaly over a range of altitude and pressure levels. (see plots below, the first are altitude ranges, the second pressure levels, both temperatures and the anomaly are shown).

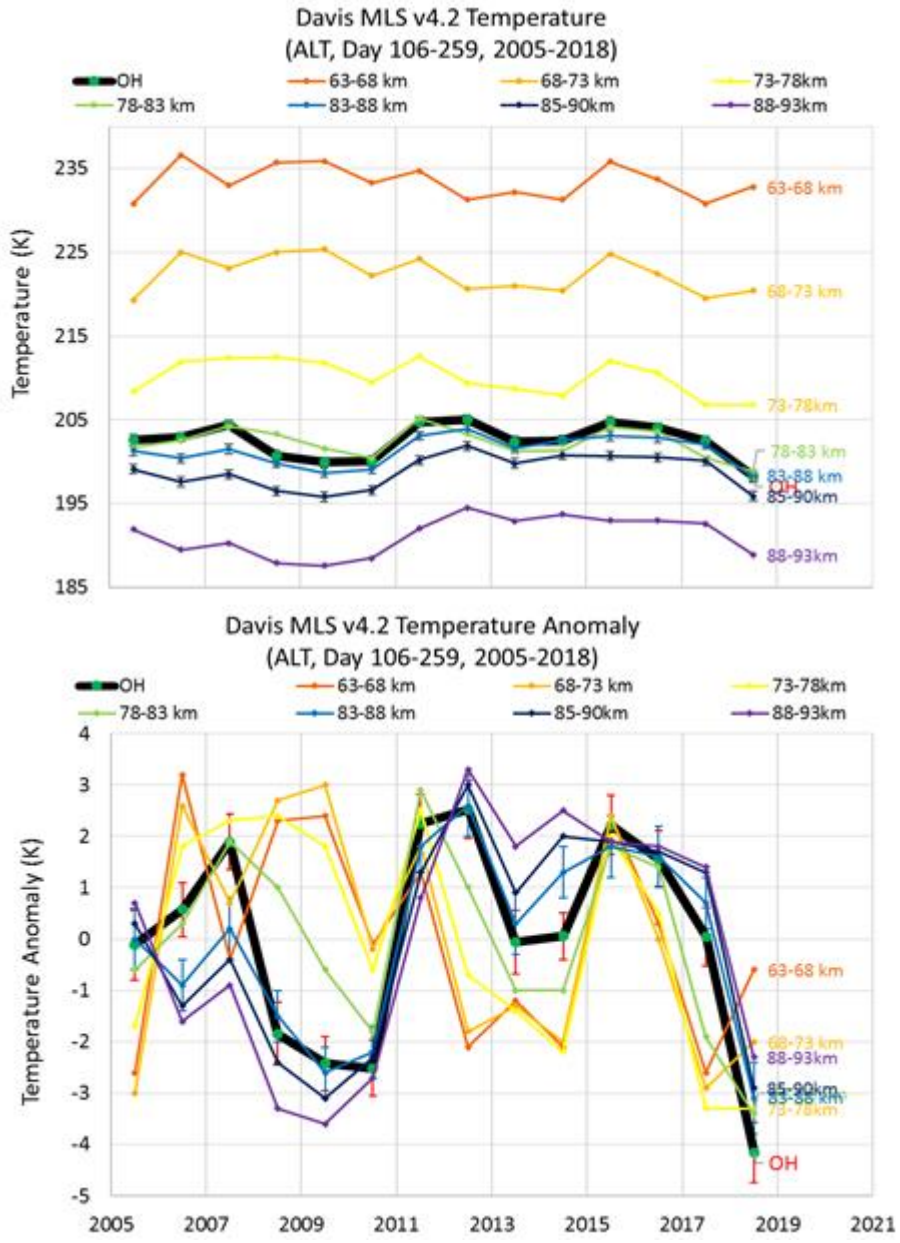

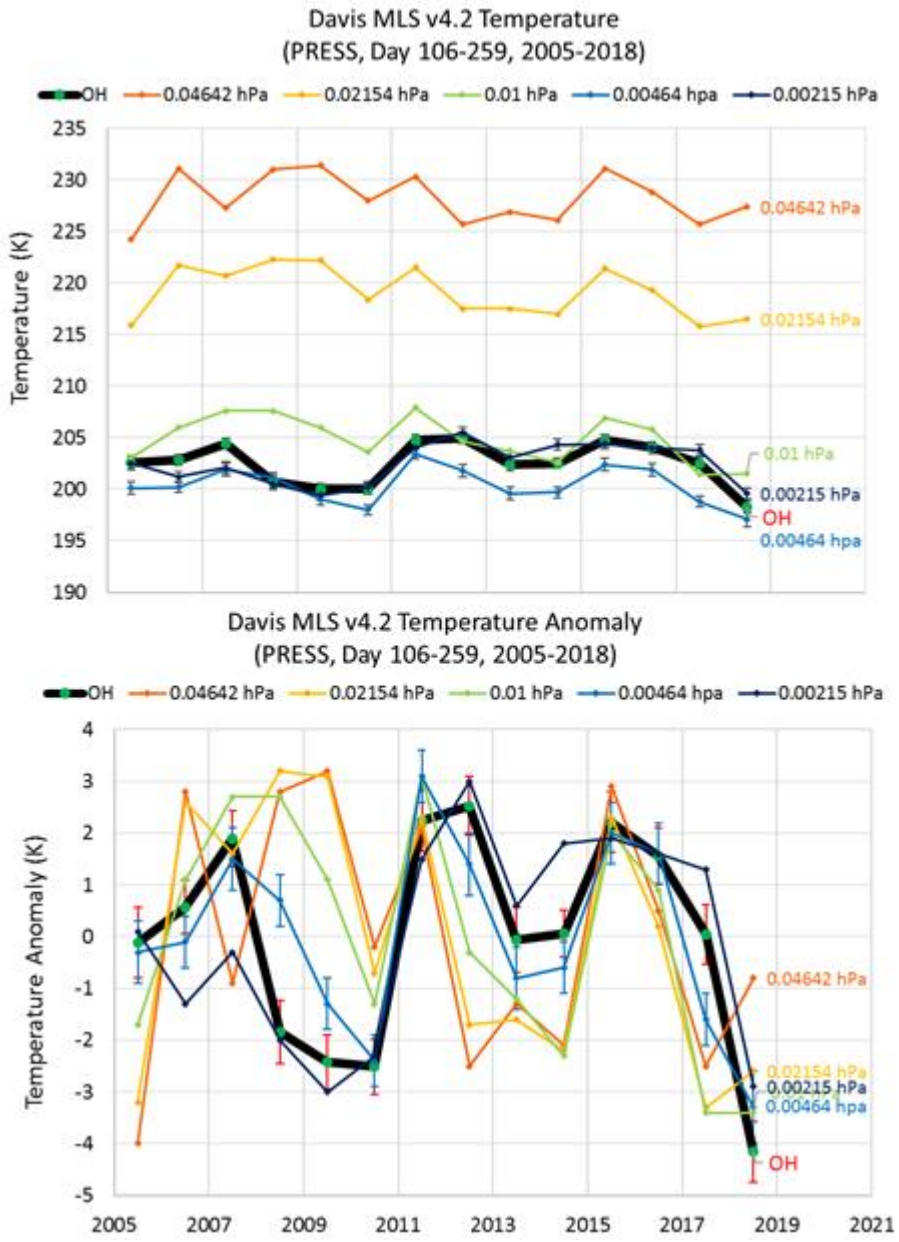


Altitude ranges 78-83km, 83-88km and 85-90km and pressure ranges 0.00215hPa and 0.00464hPa are all in reasonable agreement (<5K in absolute terms) with the OH temperatures, but we know there are biases with MLS (see French and Mulligan, 2010), and we know that the Davis OH temperatures are ~2 K high using LWR transition probabilities compared to those computed with the experimentally measured transition probability ratios determined in French et al., 2000.

We have previously reported, and routinely compare our measured OH temperatures with both Aura/MLS and SABER profiles. In particular, French and Mulligan, 2010 examined biases between Davis OH temperatures and both Aura/MLS and SABER. A significant limitation of SABER for comparisons with Davis observations is the yaw cycle sampling of the satellite. Comparable observations over Davis are confined to two intervals (day-of-year 75–140 and 196–262) and days prior to 106 and after 259 are outside the OH winter averaging interval. Therefore only days 106-140 and 195-259 are comparable and a large part of the winter months is not sampled. As a consequence SABER winter averages do not fit the OH observations at Davis as well as MLS.

In any case for this study, these biases are removed by comparing anomalies. We calculate the Chi-Square goodness of fit parameter between the OH winter average anomaly with the Aura/MLS anomalies. The 0.0046hPa pressure level yields the smallest chi-sqr (14.8) compared to a layer centred on the traditional 87km altitude level (85-90km chisqr=18.8).

This difference is small, but we prefer the pressure level comparison because we agree that the geometrical altitude of the layer varies. Since the hydroxyl layer position is primarily controlled by collisional quenching with $O_2$ and $N_2$ on the bottom-side of the layer, and reaction with atomic oxygen on the top-side of the layer it is the concentration (density) of the reacting species that governs the layer position. Therefore it is reasonable to compare with MLS pressure (proportional to density) levels than on geometrical altitude levels.

With regard to the change of altitude determined by SABER. We have examined the variation in OH layer height over this period in Part 1 of this study (acp-2019-1001; Figure 7 and related text). The overall trend is not significant, the mean winter VER peak altitude is 85.6 km and the standard deviation is 0.32 km, bearing in mind that the OH temperatures are integrated over the 8km FWHM of the layer shape, and for Aura/MLS the FWHM of the averaging kernel at this height is approximately 15 km.

The Figure below shows a comparison of SABER VER (altitude of peak) and corresponding pressure value (mb) for the years 2002-2018 (day 106 – 259 of each year) at Davis Station. The OH peak occurs at pressures in the range 0.00255 hPa to 0.003 hPa ($2.55x10^{-3}$ - $3.0x10^{-3}$ Pa). This value lies between two of the Aura MLS levels (0.00464 hPa and 0.00215 hPa) on which the averaging kernels are centered and is in excellent agreement with the Davis MLS 4.2 Temperature PRES plot (page 4 above). An inverse relationship between altitude and pressure at the OH peak is clearly evident, and justifies the selection of a pressure level comparison for OH temperatures over an altitude level.

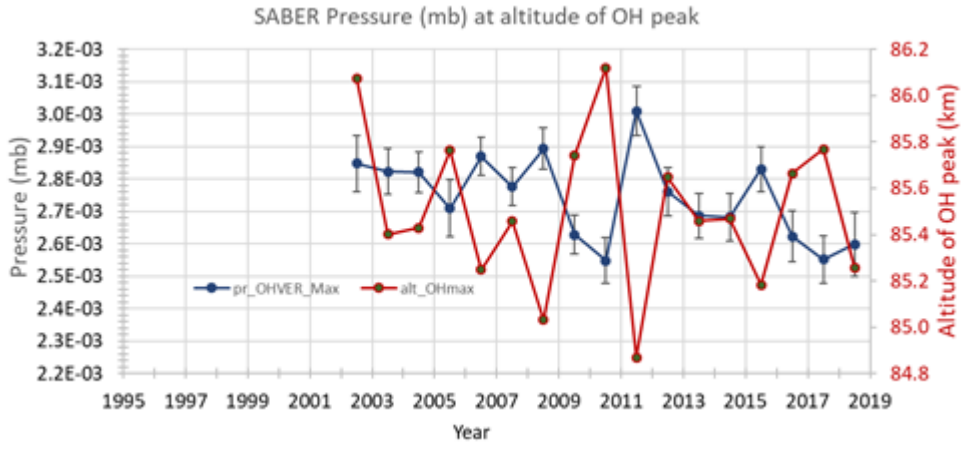


In a global context, we can also examine the altitude (or pressure) of OH peak as a function of latitude, the figure below shows the variation of the altitude of the OH peak as a function of latitude and day-of-year for the year 2005 from SABER data. The overall pattern shown here is repeated year after year with only minor changes in detail.

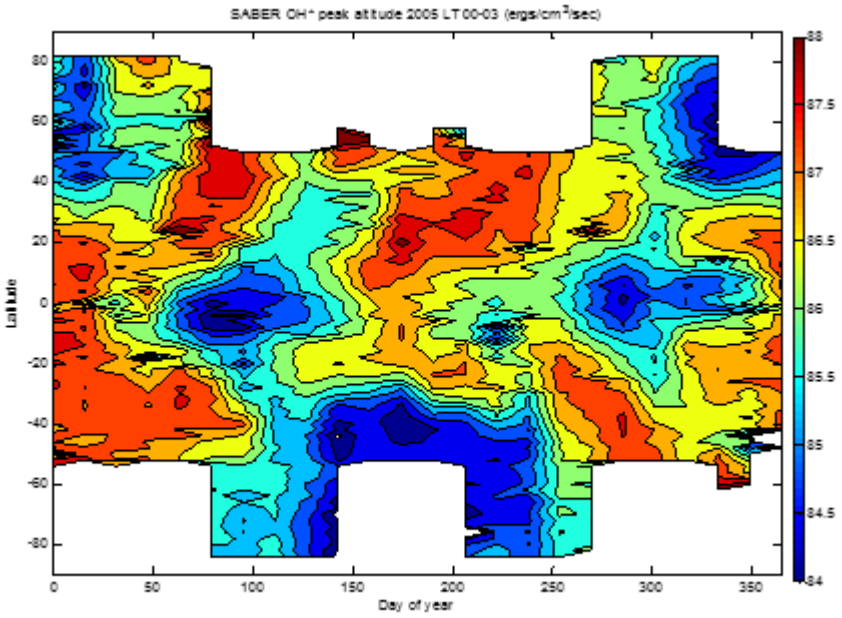


Based on the two figures above, the MLS averaging kernel centered on 0.00464 hPa would appear to be a good representative for the temperature of the OH layer.

The relationship between pressure and geopotential height (GPH) is examined below using the MLS data set. Global decreases in GPH anomaly (between ~110 to 240 metres/decade) at the 0.0046 hPa pressure level are consistent with a contraction of the underlying atmosphere and also consistent with the SABER trend in OH mean winter layer altitude for Davis shown in Fig 7. (200metres/decade) and discussed in the text in part 1 of this study.

MLS slope of fit to residual geopotential height at 0.0046 hPa

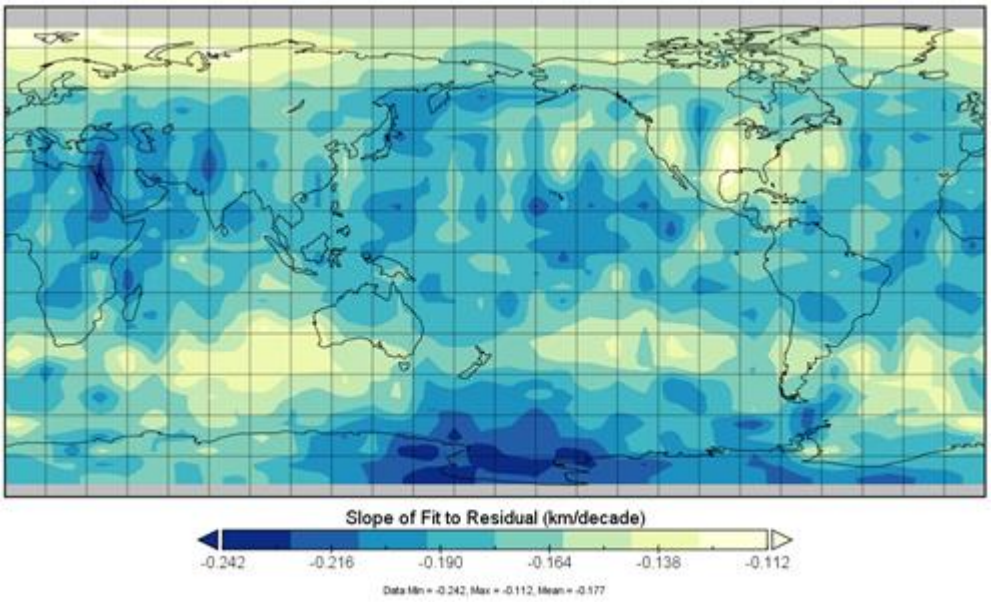

L184 What is the error in temperature due to a 1km-vertical shift?

The precise answer to this question depends on the vertical temperature profile and the OH volume emission rate vertical profile at the time of the measurement. (The OH-equivalent temperature (T_VER) is determined from a SABER temperature profile weighted with the volume emission rate profile (VER) measured simultaneously.) Using a typical temperature profile at Davis in the middle of the observing season, a 1 km -vertical shift in the OH-layer at 87 km would result in a temperature error of less than 1 K (added to the manuscript). This study uses long-term averages however and we note from above that the standard deviation in emission peak altitude for mean winter profiles is ~320 metres (over 16 years).

L190 Your figure 2b shows that the seasonal variation of the QQO is significant, further, its year-to-year change is quite important. Indeed, according to the colour lines in Fig.1b, the large 2011 residual temperature seems to be influenced by the lack of measurements during doys 141-195, with lower temperatures. This suggests that, due to a potential sampling bias, comparing SABER data with the ground-based OH dataset shown in Fig.1a, that includes doys 141-195, might be misleading. Also there should be a bias in the derived trend and solar term due to that fact. I suggest to compare just with results from ground-based OH using only the coincident days, or at least FMA+ASO data in Fig. 1b, even if this needs from another figure. This may lead to a better SABER and Davis OH agreement. Indeed, I was expecting a better agreement than with MLS, given that SABER takes into account potential variations of the layer altitude.

Figure 2b) does not show any seasonal variation in the QQO. This is the MLS polar cap average for the months AMJJAS at 0.00464hPa. We assume you are actually referring to figure 1b).

Figure 1b) shows the variation in detrended Davis OH temperatures for the intervals FMA, MJJ and ASO compared to the winter mean [AMJJAS]. This is *not* SABER data which has the missing days 141-195 due to the yaw cycle *every* year (not just 2011) .

The comparison with SABER data in Fig 1a) is provided only to demonstrate that the QQO pattern exists in the SABER OH-equivalent temperatures in the vicinity of Davis. We have stated that the SABER data exclude days 141-195 from the winter averaging window (*every year*; L197) and so do not believe the comparison is misleading.

The derived solar response and long-term trend from SABER OH equivalent temperatures in the vicinity of Davis is reported and discussed in part 1 of this study (acp-2019-1001). We have also previously compared Davis-OH and SABER temperatures in French and Mulligan (2010). The focus of this manuscript is to explore the QQO feature and the SABER temperatures provided in Fig 1a serve only to support the existence of a QQO pattern in winter average temperatures. We are aware that the yaw cycle data gap in SABER observations may yield a bias in the direct comparison with OH temperatures, but this is not a study of satellite biases.

L190. I wouldn't say that not observing from 21 May to 14 July means that 'SABER samples the same days'. Please, correct.

Modified sentence to read “Thus only days 106-140 and 196-259 are comparable between SABER and Davis-OH over the winter interval and days 141 - 195 (21 May to 14 July) are excluded.”

L193 What trend and solar terms do OH data provide when not using doys 141-195?

The terms are :

Davis OH (1995-2018)
L = -1.68±0.68 K/decade (-0.26 > L > -3.09 K/decade 95% confidence)
S = 4.11±1.35 K/100sfu (6.9 > S > 1.31 K/100sfu 95% confidence)
if days 141-195 are omitted from each year (1995-2018) and

Davis OH (2002-2018)
L = -0.912±1.16 K/decade (1.58 > L > -3.40 K/decade 95% confidence)
S = 5.40±3.03 K/100sfu (9.55 > S > 1.25 K/100sfu 95% confidence)
if days 141-195 are omitted from each year (2002-2018) to compare with the SABER trends in the vicinity of Davis.

SABER OH-equivalent T_VER (2002-2018)
L = -0.76±1.06 K/decade (1.52 > L > -3.03 K/decade 95% confidence)
S = 3.38±1.87 K/100sfu (7.39 > S > -0.63 K/100sfu 95% confidence)
for SABER T_VER within 500km of Davis (given yaw cycle excludes days 141-195)

This comparison is of interest for the trend assessment in Part 1 of this study but is not particularly relevant to the discussion of the QQO in this part.

L197. According to a sentence written four lines above this one, the SABER T_VER trend is -0.77K/decade. This sounds contradictory with the -0.13 K/year mentioned in L197.

Line 194 is the result of the solar cycle and linear trend model fit, whereas line 197 is the trend in the raw temperatures (i.,e., no solar component removed) in order to compare directly with the trend in the VER peak height. Edited the sentence to make this clear.

L198 This anti-correlation has a strong seasonal dependency, being significant in late autumn and very small in early spring for their case (e.g., Garcia-Comas et al., 2017) this. It is therefore not surprising that you get only slight anti-correlation when mixing temperatures for the two intervals doy 75-140 and 196-

See response to L262 below and Figure of the anti-correlation for days 106-140 plus days 196-259 (top plot), days 106-140 only (middle plot) and days 196-259 only (lower plot). Days prior to day 106, and after day 259 are not considered because they are outside the observing season at Davis station.

L208 End sentence with a dot.

corrected

L250 Is this MLS temperature also?

Yes, this correlates the Aura/MLS polar cap mean temperature (indicated by the green ring in Fig 2b) with each MLS grid box, on several pressure levels. The sentence has been modified slightly to explicitly state this.

L262 What happens to the temperature-altitude anti-correlation if you separate these two intervals? This should also help to answer my previous comment on the effect of OH altitude variation on temperature.

The temperature-altitude anti-correlation for SABER DoY 106-140 is -4.6 ± 1.4 K/km and is significant at the 95% level (R2 = 0.43), whereas the corresponding value for SABER DoY 196-259 is -3.2 ± 1.3 K/km and is also significant at the 95% level (R2 = 0.29). In view of the difference between the two intervals, we calculated the solar and linear terms as in the case of the Davis OH data.

**Summary of trends from SABER T_OH-equivalent (2002-2018) at Davis**

| | DOY 106-140, 196-259 | Significant at 95% | DOY 106-140 only | Significant at 95% | DOY 196-259 only | Significant at 95% |
|---|---|---|---|---|---|---|
| Solar term, *S* | 3.4 ± 1.8 K/100 sfu | No | 6.2 ± 2.3 K/100 sfu | Yes | 1.2 ± 2.3 K/100 sfu | No |
| Linear trend, *L* | -0.77 ± 1.05 K/decade | No | -0.9 ± 1.3 K/decade | No | -0.1 ± 1.3 K/decade | No |

Again, this comparison is of interest for the trend assessment in Part 1 of this study but is not particularly relevant to the discussion of the QQO in this part.

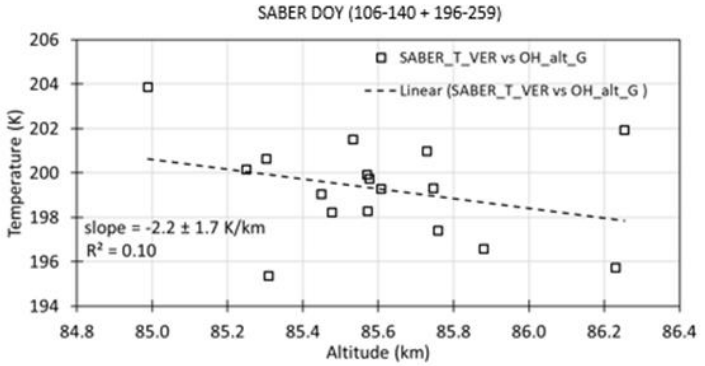


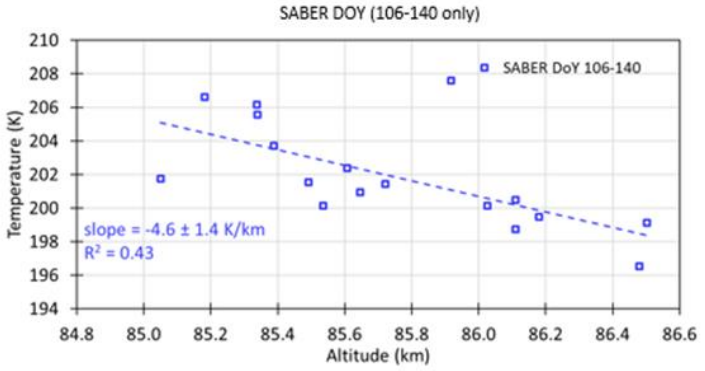


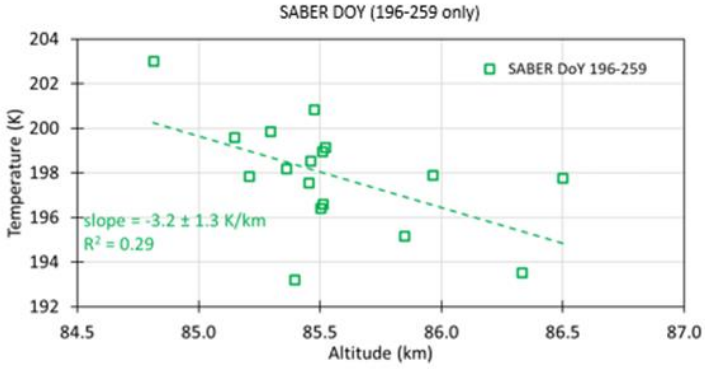

L260 Why the detrended OH temperature is compared with the GPH anomaly instead of the detrended GPH?

These are GPH composites, binned by the detrended Davis OH temperature into warm, mid and cold years, not time correlations. ie the detrended temperatures are only used to define the composite bins. The linear trend in the GPH does not affect the wave pattern observed in the results.

L294 Perhaps, this is more like a WN1 + WN2 structure. The WN2 is more clearly seen at 50hPa.

Agreed, it certainly appears as a WN2 pattern in the warm years meridional wind but more WN1 like in the cold and intermediate years. Modified this sentence to make this point.

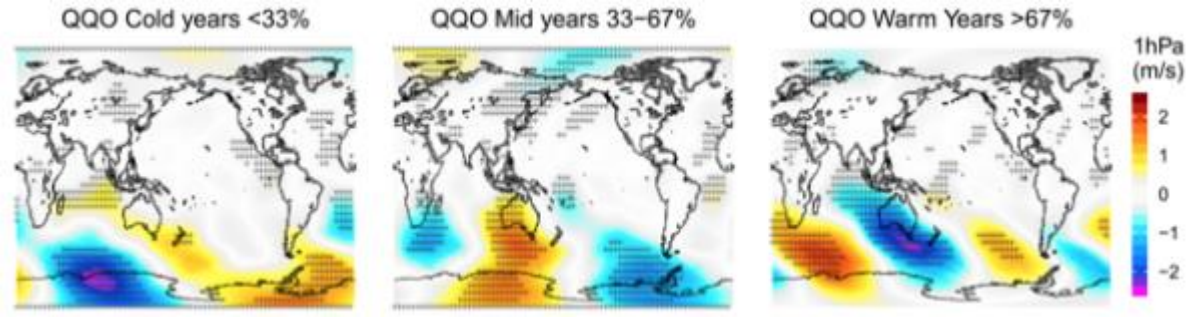


L308 I do not think the feature is a wave-3 structure but more a wave-2. Note that the apparent wave-3 is due to the equirectangular projection.

Agreed, zonal wind at 10 hPa is not a wave 3. Corrected to wave-2.

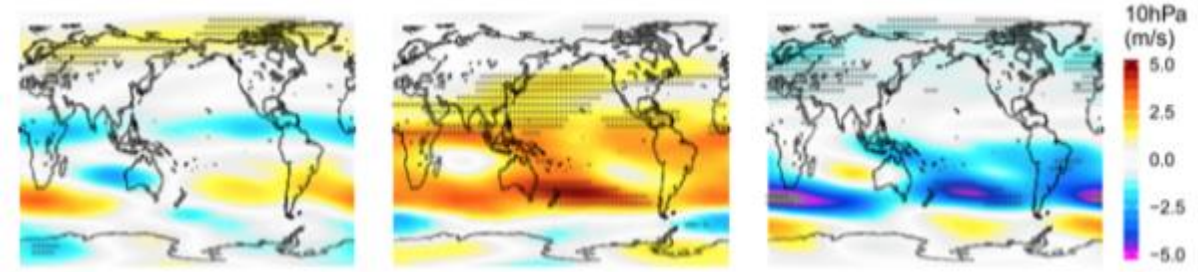


L347 Do you mean 10m meridional and zonal winds?

Yes 10 m or 'near-surface' - as described in that sentence.

L350 I do not see a clear correlation between sea ice and the OH QQO, except for mesoscale areas. The QQO is however more clearly correlated with the SST in Fig.6b or the winds in Figs 6c-6d. That the sea ice concentration should be related to the SST and the winds seems not really big news. Then, what is the additional information from OH-QQO and the sea ice correlation here? If it is difficult to provide a satisfactory answer, I would suggest changing the title of section 4.1 to "SST and winds", suppressing Fig.6a and the long discussion below on the sea ice QQO (L376-L386).

We have added time series for the correlation between the regions of maximum anti-correlation between Davis-OH and the sea-ice cover to the supplementary material (see figures below). Region A has a correlation coefficient -0.49 with Davis and -0.46 with MLS. Region B has a correlation coefficient -0.56 with Davis and -0.65 with MLS.

We do not see sea ice cover as a potential source of the mesospheric QQO. "Correlation does not imply causation". Rather, we note that there are regions that are significantly correlated with the Davis QQO variation (regions A and B below) that appear to have a wave-2 structure and suggest

that possibly the meridional winds could drive both observations ie “a  persistent  northward (southward) flow on one side of a circulation anomaly could increase (decrease) sea ice due to the associated flow of relatively cold (warm) air from higher (lower) latitudes and expansion compaction) of the ice edge.”

This section on correlations with sea ice cover has been revised, suppressed, moved from section 4.1 to 4.4 and renamed “Relationship with SST and Antarctic sea ice”.

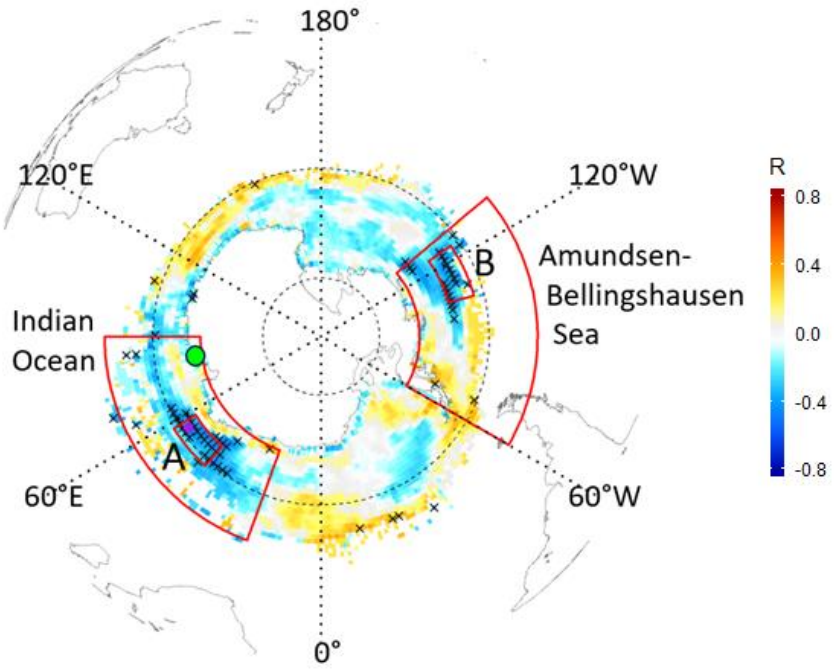


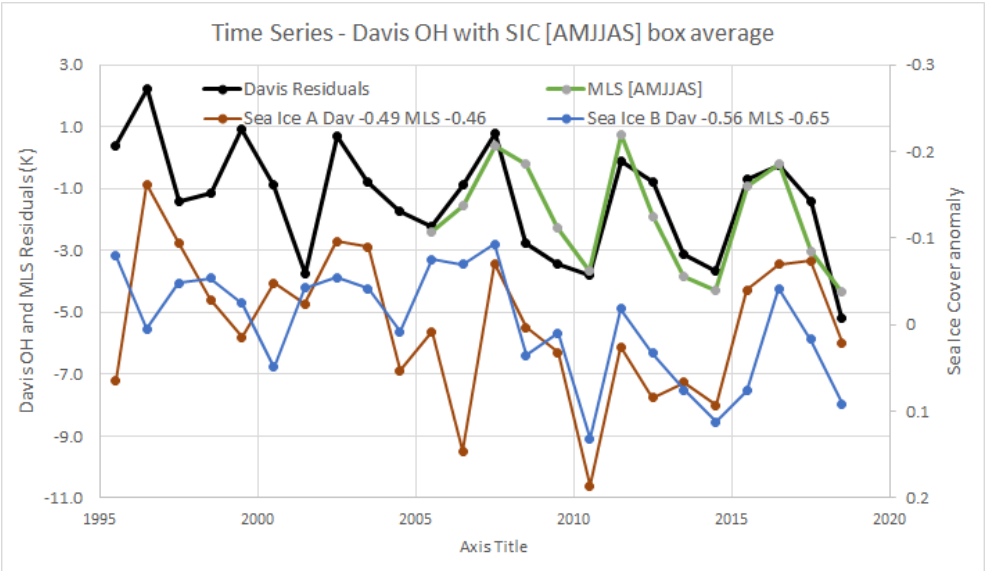


L359 Do you mean cyclonic circulation anomalies? Note that you show correlations in Figure 6 and not winds.

Inserted ‘anomalies’

L366 I think the reasoning is in general correct but what the authors show here is a strong connection between the QQO and the SST and also links to the surface circulation. The phenomenon where the origin resides cannot be determined from this type of analysis.

Agreed, we only suggest “this could hint as to the origin” and provide a plausible possibility to explore with other analyses.

L369 Again, unless I missed something, I do not understand the interest of mentioning the sea ice in this work unless the authors see it as a potential source of their OH QQO. Please, provide a more convincing argument or suppress.

See response to L350 above.

L385 QQO temperature signal at what level?

Generally speaking the QQO in the upper mesosphere. We have shown the QQO detected at Davis is correlated with the SH polar cap between 0.0046 hPa, down to 0.1hPa. We have added “in the upper mesosphere” to the sentence to clarify.

L405 colder 'mesospheric' temperatures

Inserted ‘mesospheric’.

L414-426 I do not really understand the need for this discussion. Even if the tides are affected by the QBO, there is no impact of QBO-ENSO on OH QQO. Could you please extend on the point here?

We find distinctly different wave patterns in the ERA5 geopotential and meridional wind anomalies during warm and cold years of the QQO so some factor is modifying the behaviour of these parameters on a QQO timescale. Is this possibly tides or planetary waves ?. This discussion makes the point that interaction between tides with the QBO and ENSO can have an impact at inter-annual timescales as reported by Baldwin et al (2019) and Liu (2016). Is a similar interaction occurring to produce these different wave patterns on a QQO timescale?. The discussion merely poses this as a possibility by corollary with the QBO and ENSO interaction.

L415 Not particularly but only in the cold years.

We see a SH wave-1 structure in the composite cold years, but also possible in the mid years. However, have removed the word ‘particularly’

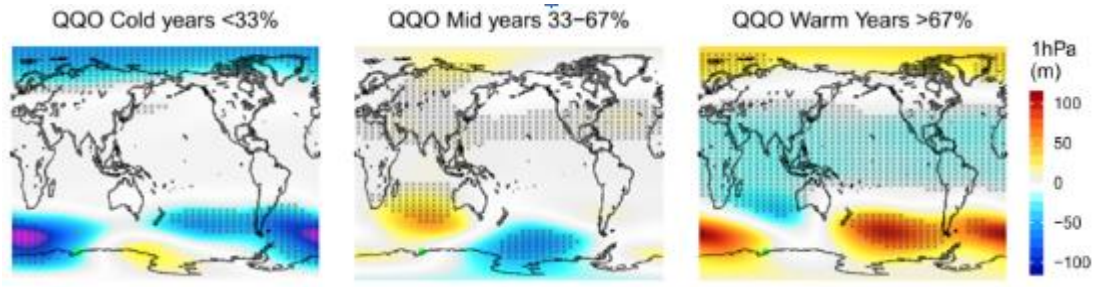


L423 'longitudinal' wave patterns

Inserted ‘longitudinal’.

Figure 7a. Is that really detrended OH T, as the x-axis title states? Please, write also in the caption "zonal mean meridional wind anomaly". Also, this figure is somehow redundant with Fig. 1. Winds could be overplotted there.

No, they are residual temperatures as stated in the caption. Thank you for picking that up, the y-axis title has been corrected. The meridional wind anomaly is that measured at Davis it is *not* a zonal mean. Thanks for the suggestion, we agree the figure is somewhat replicated from figure 1 but with the addition of the mean meridional winds. The winds could be added as a separate panel in fig 1 but we prefer to keep this separated as the radar winds are not introduced until the discussion in section 4.2.

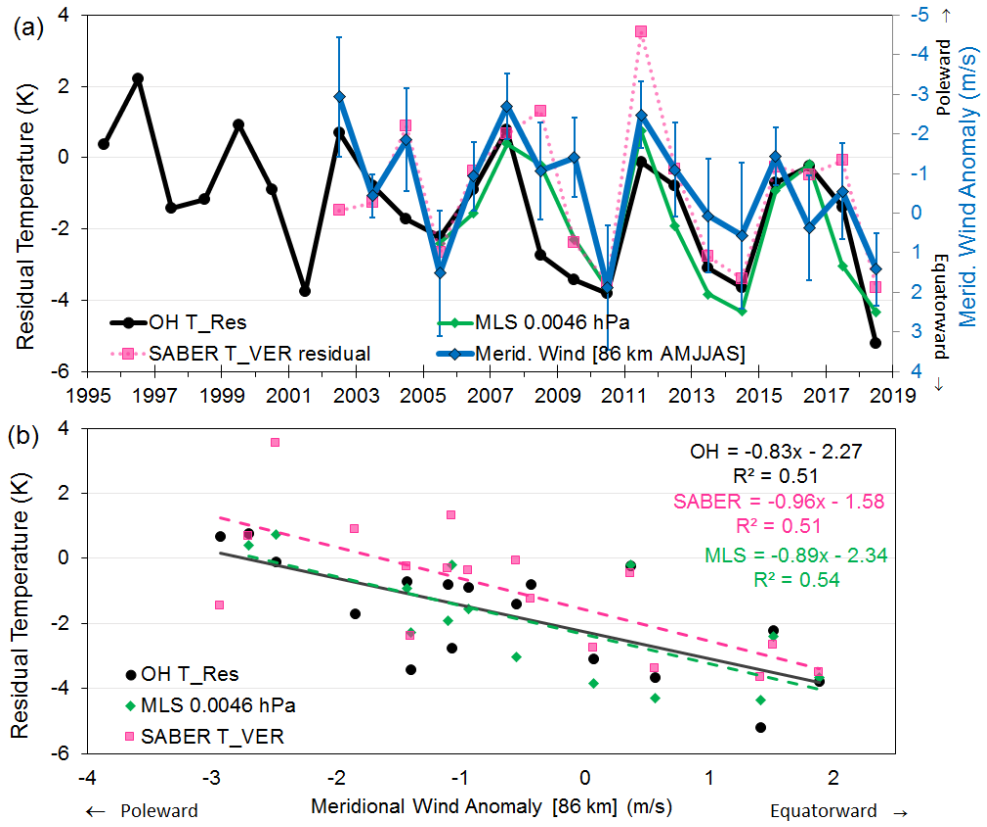


Figure 7b. I think Fig. 7b is not needed. The correlation is clearly seen in Fig. 7a. Remove Fig 7b or, at least, move it to the supplement.

Figure 7b provides the regression coefficients and $R^2$ values for the meridional wind to OH, Aura/MLS and SABER temperatures referred to in the text. As the relationship of the OH temperature QQO to the meridional wind has the most significant correlation ($R^2$ 0.51) of the factors compared this is a key finding in the investigation and we prefer to keep this figure (time-series and slope of the relationship) in the manuscript.

L439 Do you mean the background 'meridional' wind?

Inserted ‘meridional’.

L438-442 I think it is well known that the mesospheric poleward circulation is connected to downwelling and adiabatic heating below 100km. I do not think the references credited by the authors are the first ones showing that.

We agree with the comment. These references are selected because they are among the first to report observing the effect in OH temperatures, which are the data in which the QQO was identified initially in this study. We have added a reference to the earlier work of Garcia and Solomon (1985).

L444 'the adiabatic action of the residual meridional circulation' sounds confusing and may be misinterpreted

The sentence has been modified to avoid possible confusion. “and the long-term linear trend is due to ~~the adiabatic action of the residual~~ meridional circulation.”

L452-L454 Please, remove this sentence. It is not necessary to provide the sources and the sinks of CO. Just knowing that it is a dynamical tracer due to its long lifetime, particularly, during polar winter, is enough.

The sentence has been removed.

L464 I find the anti-correlation between temperature and the CO trends interesting. This might be out of the scope of this paper and not worth to mention in the paper but: What are the errors of the CO measurements? Is the instrumental drift characterized? Can the authors provide a link for the trend anti-correlation? Perhaps CO2 increase?

Uncertainties in the CO measurements are of the order of 0.3-0.4 ppmv at 0.00464hPa and 0.05-0.07 ppmv at 0.1 hPa. Error bars have been added to figure 8 as shown below.

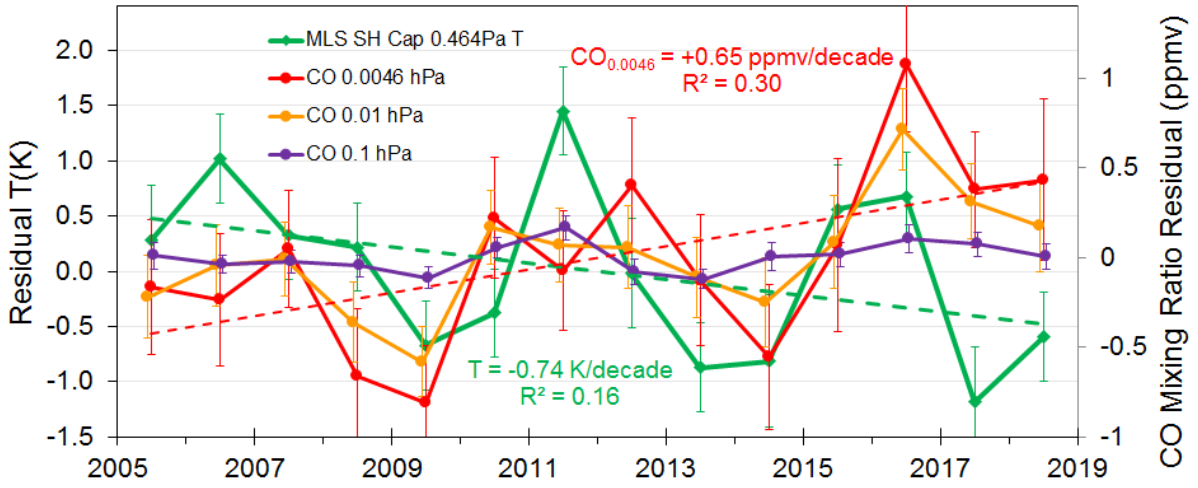


Instrumental drift and calibration is addressed by the Aur/MLS science team (https://mls.jpl.nasa.gov/products/co_product.php) but is beyond the scope of this work. There are both dynamical and chemical factors that could contribute to the trend in CO. Perhaps there are trends in the large scale upwelling and downwelling via meridional flow that occur over the polar caps and, as you suggest perhaps the trend is associated with $CO_2$ increases. This deserves further study, but is outside of this manuscript aims.

L473 Would the correlation be better if the CO detrended data were used? Given the nature of the link between CO and T QQOs that the authors are providing, does it make sense to provide 8 maps with projections for selected altitudes instead of just one plot with a lat-z cross section? On the other hand, if the QQO is clearly exhibited in the SH polar cap average (see Fig. 2 and Fig 3), why the correlation with T and CO QQO is not ubiquitous south of 65S?

The correlation coefficient with detrended CO and Temperatures is described on L463. We have considered a Lat vs Z plot but this necessarily requires zonal averages whereas Fig 9 shows that the patterns are zonally asymmetric. These levels and the plot format are provided so that they can be compared directly to the plots in Fig 2,3 and 4 (mesosphere levels). With regard to the polar cap we describe in the text “temperature and CO are significantly positively correlated over most of

Antarctica, which is consistent with Fig. 8 and our hypothesis that the QQO temperature variation is an adiabatic response (i.e. increased (decreased) temperature is associated with increased (decreased) CO concentration due to descent (ascent)). This general positive correlation over Antarctica is also seen for CO at 0.1 hPa (Fig. 9b) and is apparent though less clear for CO at 1 hPa (Fig. 9c)."

L495 Temperatures at what pressure level?

inserted "(the 0.0046hPa pressure level)"

L498-500 I would not call that "somewhat smaller". There is a very weak QQO in the NH winter.

We have modified this section substantially and the sentence now reads "we see little evidence of a QQO variation in the NH winter (blue line with linear fit)" referring to Fig 10 (below)

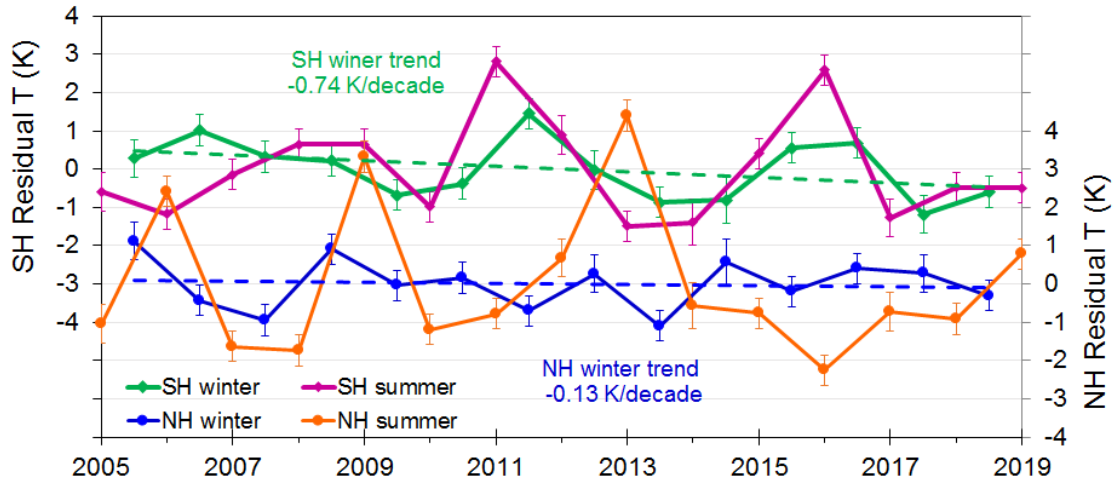


Section 4.5 Why is this section called "inter-hemispheric coupling"? Certainly, Figure 10 shows NH and SH residual temperatures but their connection is not discussed at all.

We have modified the section heading to Hemispheric comparison as your point is correct.

L530 If that is the case, why the QQO is largest during the SH summer?

We do not have measurements over the summer to confirm the Aura/MLS observation of a larger QQO in the summer months [ONDJFM] in Fig 10. We do state "We have attempted to examine the seasonal variability of the QQO signal by dividing averages into intervals FMA, MJJ, ASO (also plotted in Fig 1b). While these shorter term averages obviously suffer from greater uncertainty, there is a suggestion that the QQO is strongest over the winter months MJJ, mid-range in ASO and less apparent in the FMA interval."

Davis is not near the GW hot spot of the Antarctic Peninsula and we also comment from L543 "Gravity wave energy is generally weak in summer but in winter, gravity waves have large amplitudes and are distributed around the polar vortex in the upper stratosphere and mesosphere. The wave energy is not zonally uniformly distributed but is concentrated on the leeward side of the Southern Andes and Antarctic Peninsula. Energy propagation extends several thousand kilometres eastwards which explains the gravity wave distribution around the polar vortex in winter."

L544 Please, state this is true for SH.

That this refers to the SH is stated in the preceding sentence on L543.

L550-554 I do not think that results from Sato et al. (2012) (showing a close to annular structure around the Arctic edge, with maximum values over the Antarctic Peninsula) are well reproduced by Fig. 2a and 2b (showing more or less homogeneous correlations over the Arctic and a lack of correlation over the Peninsula).

The polar projection plots of the SH at 0.01 hPa (not 0.1 hPa as stated in the original manuscript) and 0.0046 hPa shown in Figure 2(c) in this work show a striking resemblance to the pattern in the SH winter months shown in Sato et al. (2012).

Compare the polar projection plots of June, July, August and September from Figure 2 of Sato et al. (2012) shown below with Figure 2(b) at 0.01 hPa and above from this work (also shown below). Please note that the Sato et al. (2012) plots have longitude 0° at the top of each projection plot, while the SH in Figure 2 of this work have 180° at the top of each projection plot. (This is corrected in the revised manuscript)

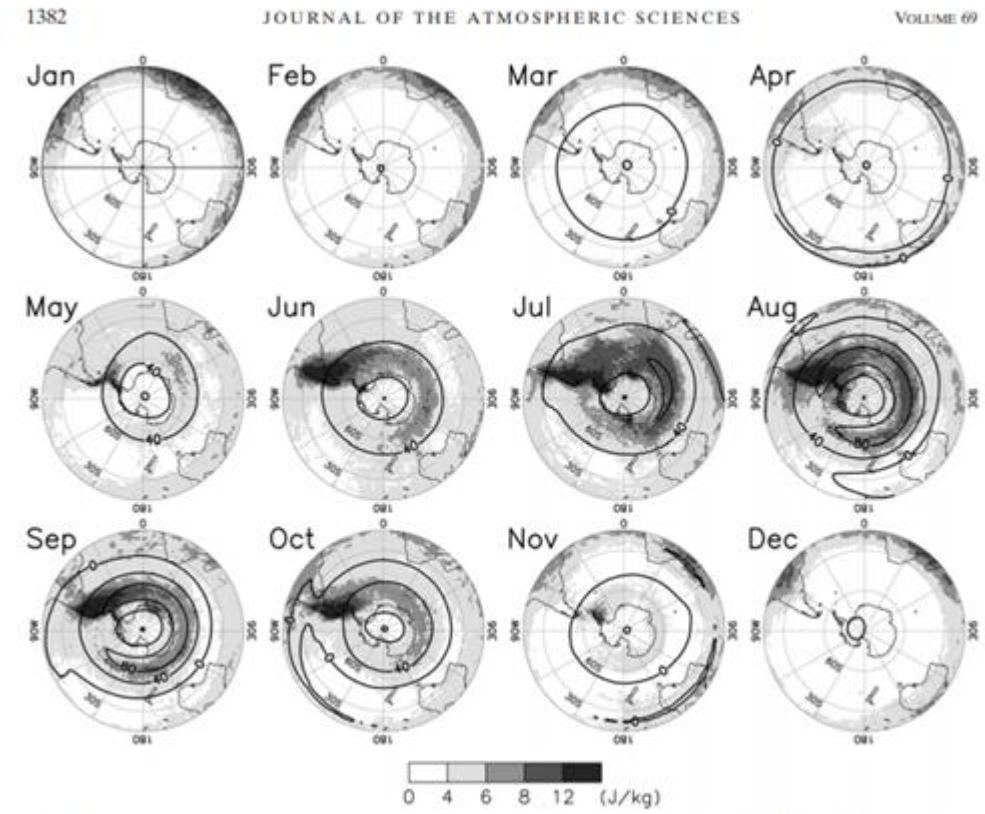


FIG. 2. Polar stereo projection maps of gravity wave potential energy (shading) in the SH for each month at 10 hPa. Monthly mean zonal winds are shown by thick contours at an interval of 40 m s$^{-1}$.

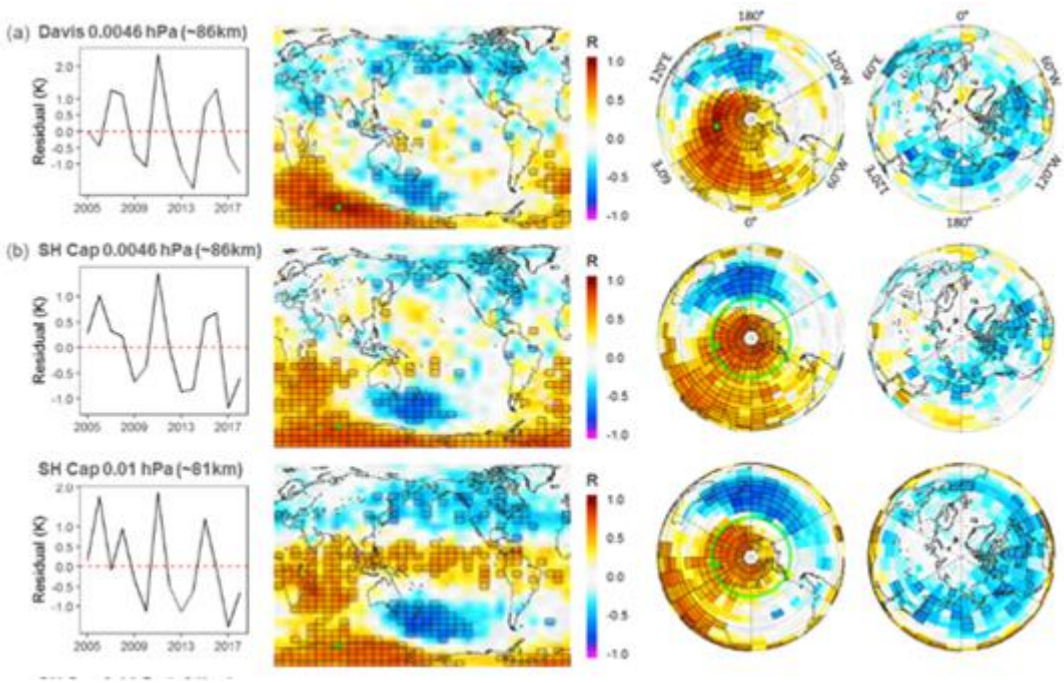


P554-558 Could the authors provide some conclusion after these sentences and make clear the relationship with their work?

A concluding sentence has been added to the text after these sentences. “The results of Sato et al. (2012), together with the focussing of GWs into the polar night wind reported by Wright et al. (2016, 2017) suggests GWs as a plausible explanation for the asymmetry in the polar projection plots of the QQO correlation coefficient at 0.01 hPa and above. “

L562-570 The vertical and latitudinal structure of Zhang et al.'s TO is similar to the QBO. However, the authors showed no correlation of their QQO with the QBO. Then, why this discussion of that TO if the four-year oscillation is not even discussed in Zhang et al.? Please, clarify the interest of this discussion or remove. Please, also note that, even if Zhang et al. showed no evidence of the four-year oscillation at 45 km, they did at 85km.

As the referee has noted, Zhang et al. (2017) found evidence of a four year oscillation at 85 km in their analysis. This is stated explicitly in the second sentence of the paragraph, which is the reason that we include it in our discussion. Since we have found evidence of the QQO at different altitudes, we note that Zhang et al. (2017) also found a four-year oscillation at 25 km. Zhang et al. (2017) do not discuss the 4-year oscillation (as we state), presumably because it has a much lower amplitude than the periods on which they focus. We make mention of the three-year oscillation simply because Zhang et al. (2017) suggest that it may arise from a modulation of the QBO by the semiannual oscillation. This struck us as interesting, and we included it here for that reason. We examined our data for evidence of a similar explanation for the QQO, but we did not find any evidence of it (and so we do not not include it here).

L570-572 From the discussion in the previous section, I thought that the authors were suggesting that mesospheric QQO was related to orographic GWs.

The previous section entitled “Gravity wave interaction” noted the similarity of the pattern of GW potential energy at 10 hPa in Fig 2. of Sato et al. (2012) with the polar cap correlation plots of

Aura/MLS temperature (at 0.01 hPa (and above)) with the QQO. This was interpreted as a possible clue to the origin of the QQO without being specific about the period. The section entitled "Mechanisms for a 4-year cycle" discusses reports which include references to periods in the vicinity of a 4-year cycle.

L573-575 Did Liu et al. find any QQO in their GW potential energy at the equator. Figure 2b shows a QQO there at e.g. 81km

Liu et al. (2017) do not refer to a QQO component in their results.

L579-585 That a changing eddy diffusion is not needed anymore to explain SABER CO2 trends has nothing to do with its potential link with a QQO.

The three sentences dealing with this point have been removed.

L594 Replace the fist two dots by a comma

replaced as advised

L596 Offermann et al. note in their introduction periods ranging from around 2 yrs to 11 yrs. What periods do the authors refer to in this sentence? All of them?

This sentence has been modified to focus on periods at 3.4 and 5.5 years that are closest to the QQO.

L623-624 If the polar cap also shows a QQO of similar amplitude and in phase with Davis (as you write in the next sentence, it is obvious that the Davis QQO is positively correlated with the polar cap QQO. Please, re-write.

The first point (L620-621) notes that the OH-layer equivalent temperatures of both Aura/MLS and SABER in the vicinity of the station (within 500km) agree with the Davis OH temperature QQO in amplitude, period and phase.

The following point (L622-624) notes that the Davis QQO signal is positively correlated with the Aura/MLS 0.0046 hPa level temperature field large over a large part of the polar cap and southern Indian ocean (and where it is anti-correlated in the Southern Ocean).

both points have been re-written to make this distinction clearer and the negative correlation with the NH identified as a separate point.

L631 extends vertically "at least" from the mesopause

Added text as suggested

L646 Would a significant variability in atmospheric tides be actually expected at this high polar latitudes?

No, good point, tidal variability would not be expected to be significant (tides less that 2K) but potentially their interactions with longer term oscillatory modes is responsible for the different wave patterns seen during warm and cold years of the QQO. We suggest only a potential role. See also response to L414-426.

L653-655 I do not think the authors prove this connection to be "most likely".

This point is modified to the word 'possibly' and merged with the previous point.

L669-672 Is the Davis QQO anti-correlated with the NLC boundary latitude reported by Russell et al.?

NLC data from Russell et al., 2014 are for the NH and span 2005-2011. Their fig 4 shows the NLC occurrence frequency anomaly for these years in 5° latitude bands and fig 5 the corresponding MLS and SABER [MJJA] temperatures. From our Fig 10 (see below), MLS NH summer [AMJJAS] averages show warm years in 2006 and 2009 and cold years in 2007-08 and 2010-11 when we would expect increased NLC occurrence. There is an indication of an NLC increase in 2007-08 and 2011 in their fig 4 panels h and i for the high latitude bands but the variation is small. The difficulty with the temperature/NLC correlations at high latitude are nicely explained in their summary "As latitude increases, the cloud frequency increase weakens significantly, and in high polar latitudes, the cloud frequency remains roughly constant over the 10 years examined here. This is expected because under highly saturated conditions, i.e., when temperature is far below the frost point, the cloud frequency is close to 100%, so there is no room for further increases, and the temperature control of cloud frequency no longer holds."

The low latitude boundary anomaly is provided in their fig 7 (reproduced right) and in summary "The results show a statistically significant increase in the number of PMCs each season in the latitude range 40°N–55°N for the 10 year period examined. Increases in cloud frequency appear to be driven by the corresponding temperature decreases over the same time period. During this time, solar activity decreased from an active to a quiet period, which might have been partially responsible for the temperature decrease over this time period." There is possible evidence of a QQO in the SABER data, but generally not enough data to be definitive.

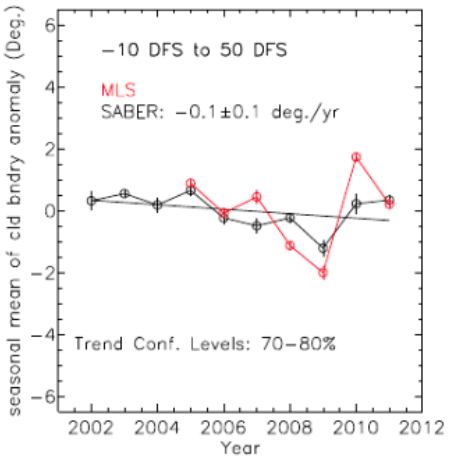


**Figure 7.** Interannual variability of the PMC low-latitude boundary anomaly (in degrees) from its 10 year average. The anomaly is first calculated on a daily basis, and then, a seasonal average is obtained for each year. The seasonal length used here is from −10 DFS to 50 DFS when PMCs are widespread enough to cover all longitudes. The error bars are the standard error of the mean. The results show a slightly negative but statistically insignificant change in the low-latitude PMC boundary over the 10 year period used in this study.

Fig 2 caption. I think the caption for b) is not correct. If "as for a)", shouldn't it be just "correlation of the SH polar cap average", without "0.0046hPa"?

a) correlates the **0.0046hPa grid box temperature over Davis** with the MLS temperature field
b) correlates the **0.0046hPa polar cap average temperature** with the MLS temperature field

both show the same plot layout of time-series and projection maps (which was the As for a) reference). We have removed the "As for a)" and specified the correlation in b) explicitly in the figure caption.

L921 What green circle?

The green circle on the SH projection map at 0.0046hPa which indicates the polar cap averaging region. It has been made a bit thicker for visibility. Figure 2 has been redone.

Figure 6. Please, indicate the maximum and minimum values in the legend of the color scale for the lower panels. Are the two color scales the same? If the answer is yes, just keep one of them. If the answer is no, use the same color scale for the four panels.

Figure 6 has been redone with the same color scale for all panels.

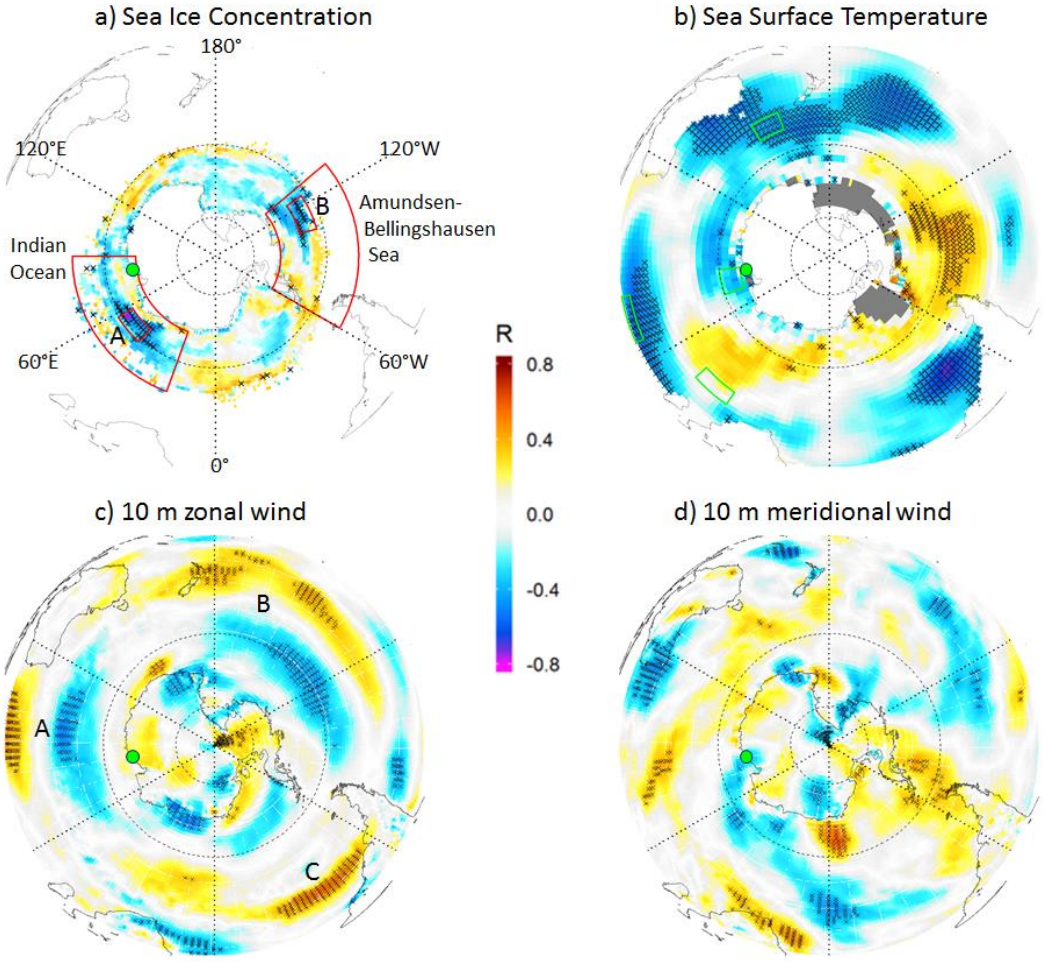


Figure 10. Please, use the same scale for both the NH and the SH residuals. Otherwise, they are not easily compared.

Figure 10 has been reformatted so the SH and NH scales are the same, but offset 3k to separate the time series.

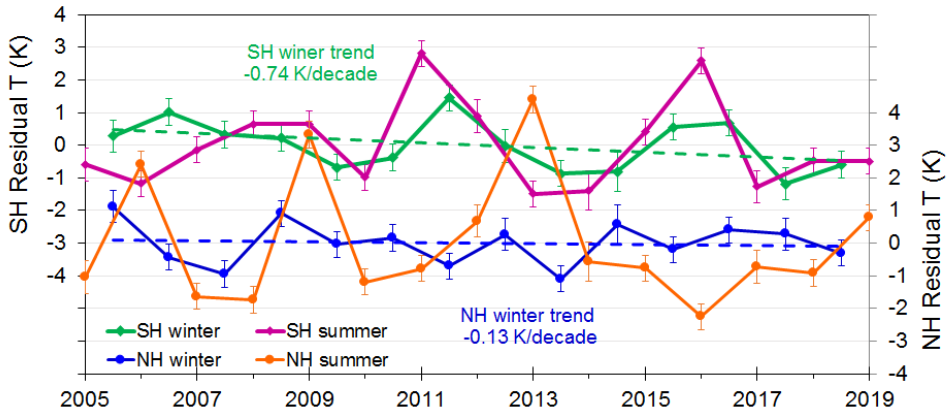

# Analysis of 24 years of mesopause region OH rotational temperature observations at Davis, Antarctica. Part 2: Evidence of a quasi-quadrennial oscillation (QQO) in the polar mesosphere.

W. John R. French[1], Andrew R. Klekociuk[1,2] and Frank J. Mulligan[3]

[1]Australian Antarctic Division, 203 Channel Hwy, Kingston, Tasmania, 7050, Australia
[2]Department of Physics, University of Adelaide, Adelaide, 5005, Australia
[3]Maynooth University, Maynooth, Co. Kildare, Ireland

*Correspondence to:* W. John R. French (john.french@aad.gov.au)

# Abstract

Observational evidence of a quasi-quadrennial oscillation (QQO) in the polar mesosphere is presented based on the analysis of 24 years of hydroxyl (OH) nightglow rotational temperatures derived from scanning spectrometer observations above Davis Research Station, Antarctica (68°S, 78°E). After removal of long term trend and solar cycle responses, the residual winter mean temperature variability contains an oscillation over an approximately 3.5 - 4.5 year cycle with a peak-to-peak amplitude of 3 - 4 K. Here we investigate this QQO feature in the context of the global temperature, pressure, wind and surface fields using the Aura/MLS and TIMED/SABER satellite data, ERA5 reanalysis and the Extended-Reconstructed Sea Surface Temperature (ERSST) and Optimum-Interpolation (OISST) ally Interpolated sea ice concentration data sets. We find a significant anti-correlation (R2^2 ~ 0.516; poleward flow associated with warmer temperatures at ~0.83 K/ms-1) between the QQO temperature and the meridional wind at 86 km altitude measured by a medium frequency spaced antenna radar at Davis (R2 ~ 0.516; poleward flow associated with warmer temperatures at ~0.83±0.21 K/ms-1). The QQO signal is also marginally correlated with vertical transport as determined from evaluation of carbon monoxide (CO) concentrations in the mesosphere (R2 ~ 0.18 at 0.73±0.45 K/ppbvCO). Together this relationship suggestssuggesting that a substantial part of the QQO is plausibly linked to the result of adiabatic heating and cooling driven by the meridional flow. The presence of quasi-stationary or persistent patterns in the ERA5 data geopotential anomaly and the meridional wind anomaly data during warm and cold phases of the QQO is consistent with tidal or planetary waves influencingsuggests a tidal or planetary wave influence in its formation, which may act on the filtering of gravity waves to drive an adiabatic response in the mesosphere. The QQO signal plausibly potentially

**Commented [1]:** R^2 =0.51 from Fig 7b for OHT and radar meridional winds

arises from an ocean-atmosphere response, and appears to have a signature in Antarctic sea ice extent.

## 1. Introduction

In Part 1 of this study (French et al., 2020) we quantify the solar cycle and long term trend in 24 years of hydroxyl (OH) rotational temperature measurements from Davis Research Station, Antarctica, and observed that the winter mean residual temperatures revealed a periodic oscillation over an approximately 4 year cycle with amplitude of 3-4 K. While periodic oscillations occur on many timescales in the atmosphere from minutes to years (gravity waves, tides, planetary waves, seasonal variations, quasi-biennial oscillation (QBO), El Nino Southern Oscillation (ENSO), Pacific Decadal Oscillation (PDO), solar cycle), the approximately 4-year period of this quasi-quadrennial oscillation (QQO) is unusual in terms of weather and climate modes. Here we seek to characterize the features and extent of the observed behavior and to examine correlation and composites with several atmospheric parameters which might suggest a possible mechanism for the phenomenon.

References to quasi-quadrennial variability in Earth's climate system have previously been reported by Jiang et al. (1995) who found both quasi-quadrennial (52 month) and quasi-biennial (24 and 28 months) oscillation modes in equatorial (4° N - 4° S) sea surface temperature (SST) and 10 m zonal wind fields over the 1950 - 1990 interval. They found the variation consistent with a "devils staircase" interaction between the annual cycle and ENSO. Liu and Duan (2018) use principal oscillation pattern analysis over the 1979 - 2013 era to also identify a QQO (48 months) in global SST anomaly which is dominant in the equatorial Pacific Ocean region. Liu and Xue (2010) investigated the relationship between ENSO and the Antarctic Oscillation (AAO) index with empirical

orthogonal function analysis in sea level pressure anomalies from 1951 - 2002. They concluded that ENSO plays a key role in the phase transition of AAO at the quasi-quadrennial timescale. Pisoft et al. (2011) point out that the quasi-quadrennial oscillations that have been reported are almost always associated with the ENSO phenomenon and variations in sea surface temperatures or the wind field over equatorial areas. Pisoft et al. (2011) applied a 2-dimensional wavelet transform technique to changes in 500 hPa temperature fields in two 50-year reanalysis datasets (ERA-40 and NCEP-NCAR) and established the presence of a distinct QQO and a quasi-decadal oscillation in addition to the annual and semi-annual cycles. Their analysis showed that the QQO is present in at least 15 of 50 years in both reanalysis datasets not only in the equatorial zone (30° S to 30° N), but also over a significant area of the globe including ~~at~~ high latitudes. Both reanalysis datasets showed relatively high QQO wavelet power north of the Bellinghausen and Amundsen Seas, over the Bering~~Bearing~~ Sea and over North America (north of ~45° N). A region of relatively high wavelet power was detected north of the Mawson and Davis seas near Antarctica in ERA-40 only.

There are relatively few reports of observations of multi-year variability in the mesosphere and higher altitudes, and as far as we are aware, the existence of a QQO in the high latitude mesopause region as discussed here has not previously been reported. Offermann et al. (2015) reported multi-annual temperature oscillations in Central Europe detected in SABER data during the period 2002 - 2012, which were reproduced in simulations by the Hamburg Model of the Neutral and Ionized Atmosphere (HAMMONIA chemistry climate model (Schmidt et al., 2006) and the Community Earth System Model - Whole Atmosphere Community Climate Model (CESM-WACCM); Marsh et al., 2013) models. Periods of 2.4 - 2.2 years, 3.4 and 5.5 years were present in the SABER data over a range of altitudes from 18 to 110 km. Perminov et al. (2018) reported statistically

significant periods of OH* temperature variations at 3 years and 4.1 years (with amplitudes of 1.3 ± 0.2 K and 0.6 ± 0.2 K respectively) from a Lomb-Scargle analysis of 17-years (2000 - 2016) at Zvenigorod, Russia. Reid et al. (2014) detected significant periodicities at 4.1 years in O($^1$S) emission intensity and ~ 3-year in the OH emission intensities by performing Lomb-Scargle analysis of a 15 year series of observations at Adelaide, Australia. However, Perminov et al. (2018) and Reid et al. (2014) do not offer causes of these periodicities.

The outline of this paper is as follows. In section 2 we review the Davis OH rotational temperature measurements (described in Part 1 of this study) and the derived residual temperatures which contain the QQO feature. In section 3 we explore correlation and composite analyses of the QQO signal using satellite and meteorological reanalysis datasets. Discussion of the results, summary and conclusions drawn are given in Sections 4 and 5. Additional figures are presented in the supplementary material.

As for Part 1 we use the following terminology for the analysed temperature series. From the measured temperatures and their nightly, monthly, seasonal or winter means, *temperature anomalies* are produced by subtracting the climatological mean or monthly mean (we fit a solar cycle and linear long-term trend to the anomalies), *residual temperatures* additionally have the solar cycle component subtracted and *detrended temperatures* have both the solar cycle component and the long term linear trend subtracted.

## 2. Data Sets

### 2.1 OH(6-2) rotational temperatures.

Scanning spectrometer observations of the OH airglow (6-2) band have been made at Davis station, Antarctica (68.6° S, 78.0° E) for each winter season over the last 24 years (1995-2018) to provide a time-series of rotational temperatures (a layer weighted proxy of atmospheric temperatures near 87 km altitude). The solar cycle and long term linear trend in this temperature series are examined in Part 1 of this study (French et al., 2020). Fitting a solar cycle (using 10.7 cm solar flux) and linear long term trend model to the winter mean temperature anomalies (nightly mean temperatures averaged over day-of-year 106 to 259 with mean climatology subtracted) yields a solar cycle response coefficient $S$ of 4.30 ± 1.02 K/100 sfu (95% confidence limits 2.2 K/100 sfu < $S$ < 6.4 K/100 sfu) and a long term linear trend $L$ of -1.20 ± 0.51 K/decade (95% confidence limits -0.14 K/decade < $L$ < -2.26 K/decade). However, only 58% ($R^2$) of the year-to-year variability is described by this model (see Fig. 3 of Part 1). Residual temperatures (solar component removed) are shown in Fig. 1a and the detrended temperatures (solar component and long-term linear fit removed) in Fig 1b. The QQO signal is apparent, with a peak-peak amplitude of 3-4 K. A sinusoid fit to the residual temperatures is provided as a guide and has a peak-to-peak amplitude of 3.0±0.7 K and a period of 4.2±0.1 years. A wavelet analysis of the residual time-series shown in Fig. 1c reveals an oscillation period increasing from ~3.5 years in 2000 to 4.5 years in 2013.

We have attempted to examine the seasonal variability of the QQO signal by dividing averages into intervals FMA, MJJ, ASO (also plotted in Fig 1b). While these shorter term averages obviously suffer from greater uncertainty, there is a suggestion that the QQO is strongest over the winter months MJJ, mid-range in ASO and less apparent in the FMA interval.

## 2.2 Aura/MLS temperature profiles.

Long-term temperature data for the mesopause region are available from two satellite instruments; the Microwave Limb Sounder on the Aura satellite (Aura/MLS) and the Sounding of the Atmosphere using Broadband Emission Radiometry (SABER) instrument on the Thermosphere Ionosphere Mesosphere Energetics Dynamics (TIMED) satellite. Hydroxyl layer equivalent temperature measurements from these instruments are overlaid on Fig 1a.

Aura/MLS temperatures are derived from observations of thermal microwave emissions near the oxygen spectral lines of $O_2$ (118 GHz) and $O^{18}O$ (234 GHz). The instrument scans the Earth's limb every 24.7 s and the retrieval algorithm (for version v4.2 level 2 used here) produces useful temperature profiles on a fixed vertical pressure grid from 316 hPa (~8 km) to 0.001 hPa (~97 km) over the latitude range 82° S - 82° N with about 14 orbits per day. The along-track resolution is typically 165 km through the stratosphere to 220 km at the top of the mesosphere. The vertical resolution is defined by the full width at half maximum of the averaging kernels and varies from 5.3 km at 316 hPa to 9 km at 0.1 hPa and up to 15 km at 0.001 hPa (Schwartz et al., 2008). We also use profiles of carbon monoxide (CO) mixing ratio, which are scientifically useful between 215 hPa to 0.0046 hPa and have similar vertical and horizontal resolution to the temperature measurements.

For comparison with the Davis OH temperatures we selected ~~retrieved~~ Aura/MLS profiles acquired within 500 km of Davis station (about 60 coincident samples per month) between 2005 (Aura launched in July 2004) and 2018, applied selection criteria according to the quality control recommendations described in Livesey et al. (2018) and averaged over the winter months April to September (AMJJAS; similar to the averaging period for the Davis winter mean) at the native Aura/MLS retrieval pressure level of 0.00464 hPa ~~(0.46 Pa)~~. The 0.00464 hPa pressure level statistically provides the best chi-squared fit,

comparing temperature anomalies of Aura/MLS to the Davis anomalies, and are in good agreement in absolute ~~temperature~~ terms~~, and in the correlation of variability,~~ to the OH(6-2) temperatures we derive using Langhoff et al. (1986) transition probabilities (see discussion in Part 1; French et al., 2020). The Aura/MLS AMJJAS mean temperature residuals are overlaid in Fig. 1a (green line from 2005); the solar cycle component is removed in the same way as for the OH data. For comparison, regression values for Aura/MLS (2005 – 2018) are 3.4 ± 2.3 K/100 sfu for the solar term and -1.3 ± 1.2 K/decade for the long term trend (but neither term is significant at the 95% level; $R^2$ = 0.2). If the solar response coefficient derived for the 24 years of OH measurements is used to compute residuals, the Aura/MLS long term linear trend becomes -1.4 ± 1.1 K/decade ($R^2$ = 0.12). The Aura/MLS measurements show very good agreement with the OH measurements, both in terms of the long term linear fit to the residuals, and in the magnitude and pattern of the QQO feature over its last 3 cycles.

2.3 TIMED/SABER profiles

The SABER instrument measures Earth limb emission profiles over the 1.27 – 17 µm spectral range from the TIMED satellite, which was launched in December 2001 into a circular orbit at 625 km altitude and 74° inclination to the equator (Russell III et al., 1999). The satellite undergoes a yaw cycle every 60 days, alternating coverage of latitude bands 54° S to 82° N and 82° S to 54° N, and precessing slowly to complete 24 h local time over the yaw interval. Temperature is retrieved over an altitude range of 10 – 105 km, with a vertical resolution of about 2 km, and along-~~-~~track resolution of 400 km from 15 µm and 4.3 µm carbon dioxide ($CO_2$) emissions (Mertens et al., 2003). Generally, errors in the retrieved temperatures in the mesopause region are estimated to be in the range ±1.5 – 5 K (García-Comas et al., 2008).

SABER also measures a volume emission rate (VER) from a radiometer sensitive over the 1.56 – 1.72 µm spectral range (OH-B channel) which includes mostly the OH(4-2) and OH(5-3) bands. SABER v2.0 Level 2B data are used in this study. We use a Gaussian fit to the VER to derive weighted average OH layer equivalent temperatures (T_VER; as for French and Mulligan, 2010). While the VER layer weighting function is not explicitly a vibrational level 6 profile but a combination of the 4 and 5 vibrational levels from the OH-B channel, the difference from the v'=6 profile in terms of peak altitude is not expected to be greater than 1 km, compared to the ~8 km full- width at half maximum (FWHM) of the layer (McDade, 1991; von Savigny et al., 2012). The resulting temperature offset well less than 1K.

As for Aura/MLS we average all SABER profiles within 500 km radius of Davis station that fall within the winter averaging window. Due to the satellite yaw cycle this limits SABER observations to two intervals day-of-year 75 – 140 and 196 – 262 and the days prior to 106 and after 259 are rejected as outside the OH winter interval. Thus, only days 106-140 and 196-259 are comparable between SABER and Davis-OH over the winter interval and ~~Essentially, SABER samples the same as the OH observations except~~ days 141 - 195 (21 May to 14 July) are excluded. As for the OH temperatures and Aura/MLS, a fit of solar cycle (F10.7) and linear trend terms is made. ~~to remove the solar cycle component~~. Regression values for SABER for 2002 - 2018 are 3.4 ± 1.8 K/100 sfu for the solar term and -0.77 ± 1.05 K/decade for the long term trend using this model. Neither term is statistically significant at the 95% level ($R^2$ = 0.22). The solar term is significant at the 90% level.

Both the OH-peak altitude and the OH T_VER (ignoring the solar term) show slightly negative trends over the period 2002 - 2018 (-0.02 ± 0.02 km/year $R^2$ = 0.09 and -0.13 ± 0.11 K/year $R^2$ = 0.09 respectively) but they are not statistically significant. Plots of

the OH peak altitude and OH T_VER time series and the anti-correlation relationship are provided in Fig. S1 of the supplementary material. There is a slight anti-correlation between OH-peak altitude and T_VER (-2.2 ± 1.7 K/km, $R^2$ = 0.1), but once again, the value is not statistically significant. ~~Plots of the OH peak altitude and OH T_VER time series and the anti-correlation relationship are provided in Fig. S1 of the supplementary material.~~

The derived SABER residual mean temperatures are also plotted in Fig. 1a (pink dotted line) for years 2002 - 2018. Given that the yaw cycle excludes days 141-195 from the winter averaging in these data, in general the SABER residual temperatures also reproduce the QQO variation, except 2011 appears to be anomalously warm (by ~3 K). The OH peak altitude derived from the SABER OH_VER profile also shows an anomalously low layer altitude for 2011 (lowest winter mean altitude in the 2002 - 2018 year record, see Fig S1).

## 2.4 ECMWF/ERA5

As discussed in the introduction, reported oscillations on a quasi-quadrennial scale have almost always been associated with ENSO and its interactions in near-surface equatorial pressure, wind and sea surface temperature fields. To investigate the possible connection to the Antarctic mesopause QQO observation we perform correlation and composite analyses using the European Centre for Medium Range Weather Forecasting (ECMWF) ERA5 reanalysis products (Copernicus Climate Change Service, 2017; https://apps.ecmwf.int/data-catalogues/era5/?class=ea). These include global monthly average geopotential height and wind components provided on 37 pressure levels (surface to 1 hPa) at 0.25° x 0.25° grid point resolution.

### 2.5 ERSST and OISST

Sea surface temperatures (SST) used in this study are from the National Oceanic and Atmospheric Administration (NOAA) Extended Reconstructed Sea Surface Temperature (ERSST v5; https://www.ncdc.noaa.gov/data-access/marineocean-data/extended-reconstructed-sea-surface-temperature-ersst-v5) monthly dataset derived from the International Comprehensive Ocean–Atmosphere Dataset (ICOADS). These are available globally extending from January 1854 to the present at 2° x 2° grid resolution with spatial completeness enhanced using statistical methods (Huang et al., 2017).

For sea ice cover, we also use the NOAA Optimum Interpolation Sea Surface Temperature (OISST) V2 product, available as monthly means on a 1° global grid using in situ and satellite SSTs plus SSTs simulated by sea-ice cover. (Reynolds et al., 2002; https://www.esrl.noaa.gov/psd/data/ gridded/data.noaa.oisst.v2.html )

## 3. Features of the QQO

The spatial extent of the QQO signal observed at Davis is explored with the Aura/MLS dataset for the 2005 - 2018 interval of concurrent observations. These data are averaged into 5° x 10° (latitude x longitude) grid cells. In Fig. 2a~~)~~ we correlate the Aura/MLS AMJJAS temperature residual time series for the grid cell over Davis (14 years; time series plotted in the left hand panel) with each grid cell of the Aura/MLS AMJJAS temperature residual at 0.0046 hPa. The 3 map panels show correlation ~~(*R*)~~ coefficient (R) in equi-rectangular, Southern Hemisphere (SH) and Northern Hemisphere (NH) projections. The correlation colour scale is common to all maps and crossed grid cells~~hashed areas~~ show significance at the 90% level. The Davis QQO signal shows a significant positive correlation with a large part of the east Antarctic and southern Indian

Ocean sectors and significant anti-correlation in the Southern Ocean near New Zealand. In the NH summer, there is a general region of negative correlation at mid- to high-latitudes, indicating that the QQO has opposite phases in the two hemispheres. We return to compare the ~~examine phase~~ response between ~~the~~ hemispheres in Section 4.5.

Extending this analysis, Fig. 2b shows the correlation between the mean Aura/MLS temperature of the polar cap (65° S - 85° S), which has a variation similar to that shown in Fig. 2a for Davis (left hand panel), with Aura/MLS temperatures for each grid box on a range of ~~different~~ pressure levels representative of the mesopause region, mesosphere, stratopause region and stratosphere. It is apparent that the QQO signal observed at Davis extends over the majority of the polar cap, and through most of the mesosphere down to at least the 0.1 hPa level with similar amplitude (3 - 4 K peak-to-peak) and phase. Significant anti-correlation of the QQO signal then occurs in the upper stratosphere (pressure range 1 - 10 hPa) in the polar cap and Southern Ocean, while a significant positive correlation occurs in the region of the subtropical jets at 10 hPa. Time-series of Aura/MLS [AMJJAS] polar cap (65-85°S) averages at additional pressure levels are provided in Fig. S2 in the supplementary material to complement the selected levels in Fig 2b and detail the transition in wave pattern from mesosphere to stratosphere.

We further examine the Davis QQO signal using correlation and composite analysis with the ECMWF/ERA5 reanalysis data and NOAA/ERSST v5 data described above. Figure 3 shows the composites of the ERA5 geopotential height anomaly (with respect to the 1995-2018 climatology) averaged over AMJJAS for the 33$^{rd}$ percentile ('cold' years), the 67$^{th}$ percentile ('warm' years) and the remaining 'mid' years (between the 33$^{rd}$ and 67$^{th}$ percentiles) of the *detrended* Davis hydroxyl temperature winter average QQO signal at pressure levels of 750, 200, 50, 10 and 1 hPa. The first two pressure levels are globally generally within the troposphere, and the other levels are generally within the stratosphere.

The ‘cold’ years (threshold -0.99 K) and their detrended temperature values (in parenthesis) are: 1997 (-1.166), 2001 (-3.039), 2005 (-1.023), 2008 (-1.188), 2009 (-1.738), 2010 (-1.998), 2014 (-1.381), 2018 (-2.451). The ‘warm’ years (threshold 1.24 K) and their detrended temperature values (in parenthesis) are: 1996 (2.325), 1999 (1.399), 2002 (1.523), 2007 (2.210), 2011 (1.796), 2012 (1.241), 2015 (1.688), 2016 (2.287). The cold (warm) years are shown by the blue (red) dots in Fig. 1b. Composite maps for meridional and zonal wind anomalies at these pressure levels are provided for comparison in Figs. 4 and S3~~2~~ (supplementary), respectively. The hatching used in these figures to indicate significance is set at the 90% level based on a two-tailed Student’s T-test assuming normally distributed statistics.

Examining Fig. 3, it is seen that cold years are associated with a small significant region of negative geopotential height anomaly to the north-east of Davis at 750 hPa, which expands and appears to shift equatorward and westward at higher altitudes (lower pressures). A similarly placed, though more extensive region of significant positive geopotential height anomaly is seen in the composites for the warm years, and generally the mid- to high-latitude regions of significant anomalies appear to have opposite signs between the composites for the cold and warm years. Note that in the northern high-latitudes there are regions of negative geopotential height anomaly in the cold year composites, and similarly placed positive anomalies for the warm year composites, although these are not significant in all cases. The intermediate composites provide some contrasts with the cold and warm year composites. For the intermediate years at and below the 50 hPa level, there are negative anomalies in the southern polar cap and mid-latitudes that are similarly located to positive anomalies for the warm years. However at 10 hPa and 1 hPa, the main negative feature at southern high latitudes in the intermediate composites is in the southern Pacific Ocean towards the Antarctic coasts.

In Fig. 4, the 50, 10 and 1 hPa levels show large-scale patterns in mid- and high-latitudes of the SH. For the cold year composite, there is a region of negative (poleward) anomalous flow south of Australia towards Antarctica at 50 hPa that extends further poleward and westward towards and over Davis in the upper levels. At 1 hPa in the cold years, the pattern generally has a zonal wave-1 structure, which is also seen in the cold year geopotential height anomaly composite at this level (top left panel of Fig. 3). The warm year meridional wind composite (right panels of Fig. 4) appears to show a pattern that has a wave-2 structure in the upper levels, with a general orientation north west to south east at 1 hPa. In the region near Davis, the meridional wind anomaly is equatorward in the upper levels for the warm years. The intermediate years provide a contrast between the cold and warm years in the meridional wind, with regions that show opposite sign in some of the regions common with either the cold or warm year composites. For example, at 1 hPa near Australia, the meridional wind anomaly is positive (equatorward) for the intermediate years and negative (poleward) for the warm years, whereas near the Antarctic Peninsula, the wind anomaly is positive in the cold years and negative in the intermediate years. The zonal wind composites (provided in supplementary Fig. S3~~2~~) also show contrasting patterns between the cold, intermediate and warm year averages, particularly in the upper levels. Here regions of significant anomalies tend to extend into the tropics and NH. At 10 hPa the SH patterns tend to show a wave-2~~3~~ structure in the cold and warm years.

Overall there are geographical regions showing some clear anti-phase relationships between the cold and warm years in the ERA5 composites (i.e. statistically significant and of opposite sign), but the intermediate years also show significant patterns suggesting that there may not be one clear driver for any association with the mesopause region temperatures. Some intermediate years are close to the cold or warm threshold, but varying the threshold did not significantly alter the patterns in the composites. We also produced

composite maps using ERA5 temperatures (not shown). While able to span more years than are ~~that~~ possible with Aura/MLS temperatures, the ERA5 composites for the 1 hPa and 10 hPa levels were qualitatively consistent with the correlation maps shown in the lower two rows of panels in Fig. 2b.

Figure 5 presents correlation maps of both the Davis OH residual winter average QQO signal (24 years; a) and Aura/MLS 0.0046hPa polar cap [AMJJAS] residual QQO signal (14 years; b) against ERSST v5 anomalies (evaluated with respect to the 1995-2018 climatology). The strongest and most consistent patterns of anti-correlation (QQO warmest for below average SST) for the two epochs occur at mid-latitudes in the south-western Pacific Ocean (to the south of Australia and New Zealand; region marked 'D'), in the south-western Atlantic Ocean (near the east coast of South America), and in the west-central Indian Ocean (to the west of Madagascar; region marked 'B'). Significant positive correlation is also seen at mid-latitudes south of Africa (region marked 'A'), and for the longer-term Davis data set, in the south-eastern Pacific Ocean. Time series of SST anomalies in regions A, B, C and D are provided in Fig S4 in the supplementary material. The correlation maps generally show a dipole-like pattern in the Indian Ocean (although the positive correlation in the east-central Indian Ocean is not significant), and weak or no correlation in the central Pacific Ocean where ENSO SST anomalies tend to be located. Comparing with the 500 hPa air temperature analysis of Pisoft et al. (2011), their Fig. 3 shows regions of high wavelet power in the QQO timescale at mid- and high southern latitudes for the ERA-40 reanalysis that bear some similarity to the location of regions of high correlation in Fig. 5a.

# 4. Discussion

~~4.1 Antarctic sea ice~~

~~On the basis of the SST patterns apparent in Fig. 5, we examined the possibility of a QQO signal in Antarctic sea ice concentration using the NOAA Optimum Interpolation SST (OI SST) dataset version 2 (Reynolds et al., 2002). As can be seen in Fig. 6a, there are regions of significant negative correlation between the Davis OH residual temperature time series and OI SST sea ice concentration towards the Antarctic coast between 30° E and 60° E (south east of Africa, region marked 'A' R = -0.49), and also centered on 120° W (in the Amundsen Sea, region marked 'B'; R = -0.56). The maximum anti-correlation is -0.61 at 55.5°E, 61.5°S (within region A, marked with a purple dot). These regions tend to lie to the south of regions where the SST is positively correlated with the Davis OH temperature residuals (Fig. 6b), consistent with warm (cold) SSTs having reducing (increasing) sea ice concentration. A link between sea ice concentration and meridional and zonal wind could be expected if persistent near-surface circulation anomalies are related to the mesospheric QQO. For example, a persistent northward (southward) flow on one side of a circulation anomaly could increase (decrease) sea ice due to the associated flow of relatively cold (warm) air from higher (lower) latitudes and expansion (compaction) of the ice edge (e.g. Fig. 3 of Turner et al., 2016). Both the zonal and meridional near-surface (10 m) wind components (Fig. 6c and 6d) show regions of negative correlation with the Davis OH temperature QQO at the Antarctic coast near 30 - 60 ° E where the pattern in Fig. 6a is significant, but these correlations are generally weak and of relatively small area. There areis also regions ofa weak and not significant positive correlation around much of the equatorward edge of the sea ice zone.~~

**Commented [2]:** I think move this section after 4.4 CO but this will require re-order of the figures too.

**Commented [3]:** AK to add a few introductory sentences about sea ice and recent variability (e.g. gradual increase up to 2015, then sudden drop, appearance of some long term variability)

Further equatorward from the Antarctic coast, Fig. 6c and 6d show correlation patterns (marked 'A', 'B' and 'C' on Fig. 6c) that are suggestive of cyclonic (anticyclonic) circulation anomalies under warm (cold) QQO phases. These features appear to be consistent with the extent of negative (cyclonic) and positive (anti-cyclonic) geopotential height anomalies at 200 hPa and 750 hPa in the warm and cold composites of Fig. 3, respectively (also marked 'A','B' and 'C' on Fig 3. bottom right panel). Intriguingly, the features appear close to the 'gatekeeper' circulation features in the southern Indian Ocean (SIO), south west Pacific Ocean (SWP) and south west Atlantic Ocean (SWA), respectively, identified by Turney et al. (2015) as having a strong influence on Antarctic surface temperatures (see their Fig. 4). This could hint as to the origin of the QQO forcing as residing with a tropical interaction with the mid- and high latitude SH circulation, particularly in the wave-3 near-surface features of the southern high latitudes (Raphael, 2004) which potentially also influences surface conditions including sea ice. Furthermore, we note that Turney et al. (2015) in their Fig. 9 show periodicities in South Pole temperatures in the 4 – 6 year period in recent decades that appear to be associated with the variations in pressure in the SIO and SWP regions.

Figure 4c of Parkinson (2019) shows the annual time series of Antarctic sea ice extent in the Indian Ocean sector (20° E – 90° E) which spans the general region of negative correlation at eastern longitudes in Fig. 6a (red box marked as 'Indian Ocean'). While there is evidence for an anti-correlation of this sea ice time series with the Davis OH temperature residuals (Fig. S43; $R^2$ = 0.26, p = 0.001), it is not consistent for all years (e.g. 1999). Parkinson (2019) also provides a sea ice time series for the Ross sea region (160° E – 130° W), which covers part of the region of significant negative correlation in Fig. 6a (red box marked as 'Ross Sea'), but also a more extensive region to the east. There is a weak but

**Commented [4]:** I have added this region to fig 6a plot

~~not significant negative correlation between this specific time series and the Davis OH temperature residual ($R$ = -0.09) is not significant.~~

~~Overall, further investigation of sea ice variability in connection with a QQO signature is suggested, particularly as the annual time series of Antarctic sea ice extent presented in Fig. 1c of Parkinson (2019) appears to show 4 – 6 year variability, at least since the early 1990s, which generally appears anti-correlated with the QQO temperature signal.~~

4.1~~2~~ QBO and ENSO relationships to the QQO

Residual variability in the Davis OH data set has been previously investigated by French and Klekociuk (2011) using indices for planetary wave activity (derived by zonal Fourier decomposition of the 10 hPa geopotential height at 67.5° S from the NCEP-DOE reanalysis, polar vortex intensity (PVI based on the zonal wind anomaly at 10 hPa), 30 hPa standardized QBO and the Southern Annular Mode (SAM; calculated as the difference between the normalized monthly mean sea level pressure at 45° S and 65° S). No statistically significant correlations were found with the PVI, QBO or SAM indices over the entire data set (then extending 1995 - 2010); however, there was clear evidence of planetary wave modes identified in the 10 hPa NCEP reanalysis data penetrating to OH layer heights at different times in the series. Over the shorter time series, the QQO was not readily apparent in that study.

In a study of the SH summer mesosphere responses to ENSO, Li et al. (2016) suggest that constructive interference of ENSO and QBO could lead to stronger stratospheric westward zonal wind anomalies at SH high-latitudes in November and December thereby causing early breakdown of the SH stratospheric polar vortex during warm ENSO events in the westward phase of the QBO. This would in turn lead to greater SH mesospheric eastward gravity wave (GW) forcing and much colder mesospheric polar

temperatures. The opposite effect would occur during cold ENSO events in the eastward QBO phase leading to warmer mesospheric polar temperatures. We have re-examined the QBO and ENSO indexes as likely candidates for a possible source of the observed QQO. However, comparing both 30 hPa and 10 hPa Singapore QBO data (https://www.geo.fu-berlin.de/en/met/ag/strat/produkte/qbo/) and the Multivariate ENSO index (MEIv2) (https://www.esrl.noaa.gov/psd/enso/mei/) yields no significant correlation to the QQO variation. Time series plots are available in the Figs. S5~~4~~ and S6~~5~~ of the supplementary material.

The clear presence of patterns in the ERA5 composite data in Fig. 3 (wave-1 structure at 1 hPa, ~~particularly~~ in the cold years), and Fig. 4 (wave-2 structure at 1 hPa in the warm years) suggests that non-migrating tides or stationary planetary waves may have some part to play in the formation of the QQO. Baldwin et al. (2019) reported strong inter-annual variability in the amplitude of the diurnal migrating tide (DW1) observed in SABER temperature data, which appears to be related to the stratospheric QBO. Liu (2016) notes that the modulation of tides by the QBO and ENSO can have an impact at inter-annual timescales in a review of the influence of low atmosphere forcing on variability of the space environment. The absence of a direct correlation between the QQO and the QBO (or ENSO), together with the presence of distinctly different longitudinal wave patterns in the ERA5 geopotential and meridional wind anomalies during warm and cold years of the QQO, provide a tantalizing picture of the complexity of the mechanisms that influence the upper atmosphere.

### 4.2~~3~~ Relationship with Mesospheric Zonal and Meridional Winds

To further explore the origin of the QQO temperature variation, we examined the AMJJAS mean meridional and zonal winds measured by the medium frequency spaced

antenna (MFSA) radar, co-located at Davis (Murphy et al., 2012). Correlations between the Davis OH and SABER residual temperatures (compared over the common satellite era 2002-2018) and the MFSA meridional wind at 86 km both yield $R^2$ values of 0.51 as shown in Fig. 6~~7~~. The Aura/MLS correlation $R^2$ is 0.54 over the shorter time span (2005-2018). The correlation between mesopause region temperature and the meridional wind is such that higher (lower) temperatures correspond to poleward (equatorward) flow over the site. The regression coefficients are -0.83±0.21 K/ms-1 (Davis OH), -0.89±0.24 K/ms-1 (SABER) and -0.96±0.24 K/ms-1 (Aura/MLS). There is no significant correlation with the zonal wind.

Garcia and Solomon (1985), Dyrland et al. (2010) and Espy et al. (2003) have reported a similar relation between temperature and the background meridional wind in the mesosphere. Espy et al. (2003) derive -0.71 K/ms-1 R2 = 0.37 (Rothera 68°S, 62°W) and Dyrland et al. (2010) +0.51 K/ms-1 R2 = 0.50 (Longyearbyen 78°N, 16°E; note opposite sign for poleward flow in NH). The relationship is ~~, which they~~ explained in terms of adiabatic processes whereby poleward circulation leads to convergence and downwelling and therefore adiabatic heating, while equatorward circulation is symptomatic of upwelling and cooling. The correlation suggests that at least part of the temperature variation at Davis after removal of the seasonal cycle, the solar cycle response, and the long-term linear trend is due to ~~the adiabatic action of the residual~~ meridional circulation. This hypothesis is supported by the Aura/MLS polar cap correlation plots which show the highest correlation in the region of the SH polar cap, but only down to an altitude of ~64 km (0.1 hPa).

## 4.3~~4~~ CO as a tracer of vertical transport

Additional evidence supporting the association between temperature and large-scale adiabatic processes over the polar cap was obtained by examining the concentration

of CO using Aura/MLS measurements. The primary source of CO in the upper stratosphere and mesosphere is photolysis of $CO_2$, while production via oxidation of methane occurs throughout the middle atmosphere (Brasseur and Solomon, 2005; Lee et al., 2018). The long lifetime (> 1 month) of CO makes it a useful tracer for vertical and meridional transport, particularly during the polar winter when there is a lack of photolysis over the polar cap. Figure 7~~8~~ shows a general positive correlation between the time series of the SH polar cap winter residual temperature at 0.0046 hPa and CO mixing ratio at levels between 0.0046 hPa and 0.1 hPa using Aura/MLS data. Here we have used the same gridding and averaging as for Fig. 2, and obtain the residual by subtracting the seasonal cycle and a fitted solar cycle response for each grid box before forming averages over the polar cap. The linear correlation coefficient at 0.0046 hPa between the temperature and CO time series is 0.11, which increases to 0.43 ($R^2$ = 0.18) on removal of the linear trends from both time series (-0.74 K/decade in temperature and +0.65 ppmv/decade or ~+0.4% per decade). Similar values of $R^2$ are observed down to the 10 hPa level on removal of linear trends. The positive correlation is consistent with CO being transported into (out of) the polar cap by convergence (divergence) of air masses which cause adiabatic warming (cooling) in the process. As there is a strong positive vertical gradient in CO in the upper mesosphere (Lee et al., 2018), we suggest that the largest contribution to changes in CO in Fig. 7~~8~~ is from vertical transport, rather than from horizontal transport. Below the 0.1 hPa pressure level, the correlations diminish.

Figure 8~~9~~ shows the spatial correlation between the polar cap QQO temperature signal at 0.0046 hPa and the CO residual mixing ratio at four pressure levels. In Fig. 8~~9~~a, temperature and CO are significantly positively correlated over most of Antarctica, which is consistent with Fig. 7~~8~~ and our hypothesis that the QQO temperature variation is an adiabatic response (i.e. increased (decreased) temperature is associated with increased

(decreased) CO mixing ratio ~~concentration~~ due to descent (ascent)). This general positive correlation over Antarctica is also seen for CO at 0.1 hPa (Fig. 8~~9~~b) and is apparent though less clear for CO at 1 hPa (Fig. 8~~9~~c). There are also regions of significant positive correlation to the south east of Madagascar and near the southern tip of South America that are consistent with the regions of significant positive correlation in Fig. 2b. Note however that the region of significant negative correlation in Fig. 2b south of New Zealand also shows negative correlation in Fig. 8~~9~~a, albeit mostly not significant. This suggests that temperature and CO mixing ratio are in opposing phases in this region, unlike the in-phase response over Antarctica. The implication here is that the response in the sub-New Zealand region does not tally with an adiabatic response. In the NH, there are generally no large scale significant patterns of correlation. However it can be seen, particularly in Fig. 8~~9~~a, that there are regions of significant correlation between the SH polar temperature and CO over northern mid- to high-latitudes, which have negative correlation in Fig. 2b. This suggests that the QQO in the NH summer is in the opposite phase to the QQO in the SH winter, and that the forcing of temperature is consistent with an adiabatic response.

## 4.4 Relationship with SST and Antarctic sea ice

On the basis of the SST patterns apparent in Fig. 5, we examined the possibility of a response~~QQO signal~~ in Antarctic sea ice concentration from a QQO signal. We do not suggest that the upper mesosphere is responding to changes in sea ice, but rather that both the upper mesosphere and sea ice may be responding to a common driver. Our motivation here was two-fold. Firstly, a near-surface QQO forcing might be expected to couple to sea ice through modification of oceanic and atmospheric heat flux and circulation (for example, promotion of sea ice formation due to cooling or surface divergence). Secondly, the Antarctic average sea ice extent since at least the 1990s shows an indication of variability

**Commented [5]:** I think move this section after 4.4 CO but this will require re-order of the figures too.

**Commented [6]:** AK to add a few introductory sentences about sea ice and recent variability (e.g. gradual increase up to 2015, then sudden drop, appearance of some long term variability)

on a timescale of 4-6 years (e.g. Fig. 2c of Parkinson, 2019). We~~For this we using~~ obtained the areal sea ice concentration from the NOAA Optimum Interpolation SST (OI-SST) dataset version 2 (Reynolds et al., 2002). As can be seen in Fig. 9a, there are regions of significant negative correlation between the Davis OH residual temperature time series and OI-SST sea ice concentration towards the Antarctic coast between 30° E and 60° E (south east of Africa, region marked 'A' R = -0.49), and also centered on 120° W (in the Amundsen Sea, region marked 'B'; R = -0.56). The maximum anti-correlation is -0.61 at 55.5°E, 61.5°S (within region A, marked with a purple dot). These regions tend to lie to the south of regions where the SST is positively correlated with the Davis OH temperature residuals (Fig. 9b), consistent with warm (cold) SSTs having reducing (increasing) sea ice concentration. A link between sea ice concentration and meridional and zonal wind could be expected if persistent near-surface circulation anomalies are related to the mesospheric QQO. For example, a persistent northward (southward) flow on one side of a circulation anomaly could increase (decrease) sea ice due to the associated flow of relatively cold (warm) air from higher (lower) latitudes and expansion (compaction) of the ice edge (e.g. Fig. 3 of Turner et al., 2016). Both the zonal and meridional near-surface (10 m) wind components (Fig. 9c and 9d) show regions of negative correlation with the Davis OH temperature QQO at the Antarctic coast near 30 - 60 ° E where the pattern in Fig. 9a is significant, but these correlations are generally weak and of relatively small area. There are also regions of weak and not significant positive correlation around much of the equatorward edge of the sea ice zone.

Further equatorward from the Antarctic coast, Fig. 9c and 9d show correlation patterns (marked 'A', 'B' and 'C' on Fig. 9c) that are suggestive of cyclonic (anticyclonic) circulation under warm (cold) QQO phases. These features appear to be consistent with the extent of negative (cyclonic) and positive (anti-cyclonic) geopotential height anomalies at

200 hPa and 750 hPa in the warm and cold composites of Fig. 3, respectively (also marked 'A','B' and 'C' on Fig 3. bottom right panel). Intriguingly, the features appear close to the 'gatekeeper' circulation features in the southern Indian Ocean (SIO), south-west Pacific Ocean (SWP) and south-west Atlantic Ocean (SWA), respectively, identified by Turney et al. (2015) as having a strong influence on Antarctic surface temperatures (see their Fig. 4). This could hint as to the origin of the QQO forcing as residing with a tropical interaction with the mid- and high latitude SH circulation, particularly in the wave-3 near-surface features of the southern high latitudes (Raphael, 2004) which potentially also influences surface conditions including sea ice. Furthermore, we note that Turney et al. (2015) in their Fig. 9 show periodicities in South Pole temperatures in the 4 – 6 year period in recent decades that appear to be associated with the variations in pressure in the SIO and SWP regions.

Figure 4c of Parkinson (2019) shows the annual time series of Antarctic sea ice extent in the Indian Ocean sector (20° E – 90° E) which spans the general region of negative correlation at eastern longitudes in Fig. 9a (red box marked as 'Indian Ocean'). While there is evidence for an anti-correlation of this sea ice time series with the Davis OH temperature residuals (Fig. S7; R = -0.51, R2 = 0.26, p = 0.001), it is not consistent for all years (e.g. 1999). Parkinson (2019) also provides a sea ice time series for the Amundsen-Bellingshausen~~Ross~~ sea region (130~~6~~° W~~E~~ – 6~~13~~0° W; red box marked as 'Amundsen-Bellingshausen Sea'), which covers part of the region of significant negative correlation in Fig. 9a (marked 'B'), but also a more extensive region to the east towards the Antarctic Peninsula where the correlation is positive. For this region, t~~T~~here is an overall weak and~~but~~ not significant negative correlation between this specific time series and the Davis OH temperature residual (R = -0.24~~09~~, R2 = 0.06, p=0.25)~~ is not significant~~.

**Commented [7]:** is that number correct?

**Commented [8R7]:** Its S4 the 3 was crossed out as a tracked changed edit, but then the whole section was cut and pasted to section 4.4. It has retained all the tracked changes as new text.

**Commented [9]:** Changed to Amundsen-Bellingshausen sea region (130W-60W). AK will evaluate correlation for the new region. Fig 6a needs updating for the new region.

**Commented [10]:** I have added this region to fig 6a plot

FOverall, further investigation of sea ice variability in connection with a QQO signature is suggested, particularly as the annual time series of Antarctic sea ice extent presented in Fig. 2c of Parkinson (2019) appears to show 4 - 6 year variability, at least since the early 1990s, which generally appears anti-correlated with the QQO signal that we obtain fortemperature signal in the upper mesosphere.

4.5 HInterhemispheric coupling comparison

Returning to the phase response of the QQO signal between the hemispheres, we performed a similar analysis to that shown in Fig. 2 but using average temperatures (at the 0.0046hPa pressure level what pressure level) across the Arctic polar cap (65° N to 85° N) in winter months October to March (ONDJFM) and summer months (AMJJAS). We compare the time series in Fig. 10, together with SH polar cap winter (green line with linear fit) and summer (purple line) time seriesand winter time series (green line with linear fit). First, we see little evidence of a QQO variation in the NH winter (blue line with linear fit), suggesting that the mechanism that drives the QQO in the SH winter is not as strong, or absent, in the NH winter. that the in winter, the NH response (bluered line with linear fit) has a somewhat smaller smaller amplitude than in the SH (green line with linear fit) and a less clear QQO variation. In summer For the SH summer (dark green line), the response is generally in-phase with the SH winter, except in years 2005-2008 but of considerably greater amplitude than the winter season. . In addition, the amplitude of the SH summer response is larger than for the SH winter. For the NH summer (orange line), a QQO response is apparent with similar amplitude to the SH summer but the response is in an approximately opposite phase to the SH winter (except for years 2005-2006), but with similar amplitude to the SH summer. Our QQO signal for the NH summer polar cap shown

in Fig. 10 is consistent with temperatures for 2002 - 2010 NH summers shown in Fig. 5 of Russell et al. (2014) poleward of 60° N using TIMED/SABER and Aura/MLS data.

4.6 Comparison with CESM-WACCM

Following on from Offermann et al. (2015), we examined simulations produced from a version of CESM-WACCM for phase 1 of Chemistry-Climate Model Initiative (CCMI-1; ~~(~~Morgenstern et al., 2017~~)~~), specifically the CESM1 WACCM model which includes both interactive atmospheric chemistry and interactive ocean physics to provide a self-consistent simulation of climate. Our interest here is to see if the model physics produces a QQO response in the mesosphere, particularly as Offermann et al. (2015) had noted that the CESM-WACCM model showed low-frequency variability in temperatures on 3-6 year timescales over Middle Europe. We obtained 3 ensemble members from the REF-C2 simulation of the model spanning 1955-2100. The REF-C2 simulation follows particular scenarios for interactive chemistry involving ozone depleting substances and radiative forcing (the WMO A1 and RCP 6.0 scenarios, respectively; Morgenstern et al., 2017), with a repeating synthetic solar cycle beyond 2010. SH polar cap (65° S - 85° S) temperatures were averaged over AMJJAS for pressure levels of 0.01 Pa (~105 km altitude), 0.5 Pa (~85 km) and 0.15 hPa (~60 km), and Morlet wavelet analysis (Torrence and Compo, 1998) was applied to the individual ensemble members. While a solar-cycle (10 - 11 year period) signal was detected with better than 95% confidence ~~at each pressure level~~ for all ensemble members near and above the 0.01 hPa level, ~~,~~ no periodicity in the 3 - 6 year range exceeded the 95% confidence limit in the mean spectrum for any member. We do note however, that particular ensemble members showed power that was significant at the 95% confidence limit in the 2-3 year period range in certain epochs (Fig. S8~~Sx~~ of Supplementary Material) and in some cases in the 4-5 year period range. We therefore

**Commented [11]:** Need to add in a new figure in Supplementary Material for the wavelet results.

cannot rule out that the model does not reproduce the QQO signal, but the significance and amplitude of any signal over recent decades of the historical period in the Antarctic mesopause region appears less than in our observations.

4.7 Gravity wave interaction

We now consider why our SH winter QQO signal appears generally restricted to the mesosphere. It is well known that the Antarctic Peninsula is a hot spot for gravity wave activity at the edge of the southern polar cap (Hoffmann et al., 2013) and this region is consistently active during austral autumn, winter and spring. Many GWs are able to penetrate all the way up to the mesosphere before their amplitudes become so large that they break, and deposit their energy, thereby introducing perturbations in winds and temperatures. Correlation coefficients below the 0.1 hPa level (~65 km) in our Aura/MLS analysis are potentially low because few GWs break below this altitude. The strong eastward stratospheric winds of the polar night jet filter out many eastward propagating GWs creating a westward drag on winds in the mesosphere, which when combined with the Coriolis force generates a weak poleward flow. This flow is modulated by interannual variations in upward propagation of GWs and agrees with the view of (Solomon et al., 2018) who attribute the significant inter-annual variability of mesopause temperatures to the dominance of dynamical processes in their control. Further support for this view can be found in (Sato et al., 2012) who employed a high-resolution middle atmosphere general circulation model (GCM) to examine gravity wave propagation in the middle to high latitudes of the SH without the need for gravity wave parameterization. Gravity wave energy is generally weak in summer but in winter, gravity waves have large amplitudes and are distributed around the polar vortex in the upper stratosphere and mesosphere. The wave energy is not zonally uniformly distributed but is concentrated on the leeward side of

651 the Southern Andes and Antarctic Peninsula. Energy propagation extends several thousand
652 kilometres eastwards which explains the gravity wave distribution around the polar vortex
653 in winter.

654 Examining the Aura/MLS polar cap correlation plots in Fig. 2(b~~a~~) and 2(c~~b~~) in
655 detail, we see that maps of GW potential energy (PE) at 10 hPa calculated for the winter
656 months by Sato et al. (2012; their Fig. 2) is well reproduced at 0.01 hPa and higher altitudes,
657 and that the region of highest correlation becomes more concentrated as GWs are filtered
658 out with increasing altitude. It is also likely that GWs are strongly focussed into the polar
659 night wind jet (Wright et al., 2017). Wright et al. (2016) reported strong correlations
660 between GW potential energy and vertical wavelength with stratospheric winds, but not
661 local surface winds from a multi-instruments gravity-wave investigation over Tierra del
662 Fuego and the Drake Passage. The results of Sato et al. (2012), together with the
663 ~~focussing~~focusing of GWs into the polar night wind reported by Wright et al. (2016, 2017)
664 suggests GWs as a plausible explanation for the asymmetry in the polar projection plots of
665 the QQO correlation coefficient at 0.01 hPa and above.
666

667 4.8 Mechanisms for a 4 year cycle

668 The question remains as to why does this modulation have a quasi-four year cycle?
669 Zhang et al. (2017) detected both three- and four-year oscillations in zonal mean SABER
670 temperatures at 85 km altitude in the period 2002-2015 using Lomb-Scargle analysis, in
671 which the much stronger annual, semi-annual, quasi-biennial, and 11-year periods were
672 also present. The latitude range studied was limited to 50° S to 50° N because of the
673 satellite yaw cycle; the four-year oscillation was found to have a stronger peak in the SH.
674 Although the origin of the four-year oscillation is not discussed in Zhang et al. (2017), it is
675 suggested that the three-year oscillation is a sub-peak of the QBO, and is due to modulation

of the QBO possibly by the semiannual oscillation. Their analyzed SABER temperatures also show evidence of the four-year oscillation at 25 km altitude, but not at 45 km. We note that a QQO variability observed in Jupiter's equatorial winds has been inferred to result from forcing by gravity waves produced by deep convection (Cosentino et al., 2017).

Liu et al. (2017) examined variations in global gravity waves from 14 years of SABER temperatures between 2002 and 2015. Unfortunately, their study was limited to the latitude band 50° S to 50° N because of the TIMED 60-day yaw cycle. They applied multivariate linear regression to calculate trends of global GW potential energy and the responses of GW PE to solar activity, to the QBO and to ENSO. They found a positive trend in GW PE with a maximum of 12-15% per decade at 40° S - 50° S below 60 km altitude. This was interpreted as a possible indication of eddy diffusion increase in some locations, and at 50° S could be due to a strengthening of the polar stratospheric jets. ~~Increasing eddy diffusion was advanced as a possible explanation of increasing $CO_2$ trends with altitude (Emmert et al., 2012). However, Qian et al. (2019) have shown that sampling of SABER data in window lengths less than 60 days can lead to incorrect $CO_2$ values. As a result, increased eddy diffusion is no longer necessary to explain the anomalous $CO_2$ result.~~ The global gravity wave response to solar activity is negative in lower and mid-latitudes in the mesosphere lower-thermosphere (MLT) region. It is also negative to the QBO eastward wind phase in the tropics, and is more negative in the NH than in the SH MLT region. The response of global GWs to the ENSO index is positive in the tropical stratosphere (Geller et al., 2016).

Yasui et al. (2016) examined the seasonal and inter-annual variations of GWs (50 - 100 km) using an MF radar at Syowa Station (1999-2013). They found that the Antarctic summer inter-annual modulation could not be explained by the proposed mechanism of SSWs in the Arctic via inter-hemisphere coupling. Two other proposed mechanisms were

found to be the more likely origin of the modulation.~~:~~ these were: (a) modulation of the vertical filtering of GWs in association with breakdown of the polar vortex in the SH, and (b) tropical convection and propagation to the Antarctic region. Two of ~~T~~the periods noted in the Introduction in the study of the mesosphere over Central Europe reported by Offermann et al. (2015) (3.4 years and 5.5 years) fit well with the correlation results for Aura/MLS temperatures at different pressure levels in Fig. 2 of the present study. The amplitude of the oscillations they report (~1 K) are about half those observed in the QQO at Davis. Offermann et al. (2015) suggest harmonics of the 11-year solar cycle at 5.5 years, 3.6 years and 2.2 years as possible origins of these oscillations. In addition, Offermann et al. (2015) ~~they~~ state that ~~these type of~~ oscillations with similar periods are found in the GLOTI (Global Land Ocean Temperature Index) and NAO (North Atlantic Oscillation index) data. ~~,~~This is an interesting observation in the context of ~~s congruent with which supports~~ the correlation maps of the Davis QQO signal with Extended Range Sea Surface Temperature ~~r~~shown in Figure 5~~esults with the SSTs observed in this work~~. ~~Concerning possible origins of these oscillations, Offermann et al. (2015) suggest harmonics of the 11-year solar cycle at 5.5 years, 3.6 years and 2.2 years, in addition to synchronisation of adjacent atmospheric layers acting as independent non-linear oscillators.~~

## 5. Summary and Conclusions

The variability in winter temperatures derived from hydroxyl airglow observations at Davis Station are examined after seasonal, solar cycle and long-term linear trend terms are removed (in Part 1 of this work, French et al., 2020~~19~~). The following observations are made regarding this variability:

- A strong QQO feature (3-4 K peak-to-peak amplitude, 3.5 - 4.5 year period) has been observed in the mesopause region winter average temperatures measured at Davis research station which has been sustained over more than two solar cycles (24 years).
- Previous reports of QQO signals have tended to be associated with the ENSO phenomenon and sea surface temperatures, or the wind field over equatorial regions, but this is the first report of its presence at high latitude mesopause altitudes.
- Hydroxyl-layer equivalent winter average [AMJJAS] temperatures from both ~~Observations from both~~ Aura/MLS (from 2005) and TIMED/SABER (from 2002) in the vicinity of the station (within 500km) agree well with the Davis OH temperature QQO in amplitude, period and phase.~~of the station support the Davis QQO feature in amplitude, period and phase. The first point (L620-621) notes that the OH layer equivalent temperatures of both Aura/MLS and SABER in the vicinity of the station (within 500km) agree with the Davis OH temperature QQO in amplitude, period and phase.~~
- The Davis QQO pattern shows a significant positive correlation with the Aura/MLS 0.0046 hPa temperature field over ~~Correlation of the QQO pattern detected at Davis with the Aura/MLS 0.0046 hPaglobal temperature field over at 0.0046 hPa shows that the QQO has a significant positive correlation with~~ a large part of the Antarctic polar cap and southern Indian Ocean sectors and significant anti-correlation in the Southern Ocean below New Zealand. The polar cap winter average (AMJJAS; 65° S - 85° S) has a very similar QQO pattern to the Davis site revealing that the feature has a large spatial scale.~~-~~

- There is a general region of negative correlation at mid- to high latitudes, in the Northern Hemisphere (NH) summer, indicating that the QQO has opposite phases in the two hemispheres.
- Correlation of the SH polar cap average QQO signal shows that the pattern extends vertically at least from the mesopause region (~86 km) down to 0.1 hPa (~64 km) and then becomes anti-correlated in the upper stratosphere (1 – 10 hPa). Again, this pattern is opposite in the NH.
- Composite analysis with ERA5 geopotential anomaly indicate warm years of the QQO are associated with higher than average geopotential height anomalies over the polar cap, the East Antarctic sector of the Southern Ocean (sub-Africa) and the Amundsen Sea region and lower than average anomalies in the southern Pacific, Indian and Atlantic regions. Cold years are associated with the opposite and the effect is greater at higher altitudes (10 and 1 hPa levels). There is the indication of a connection with persistent near-surface circulation anomalies in the southern Indian Ocean and south-west Pacific Ocean, and variability in Antarctic sea ice.
- Composite analysis with ERA5 data also indicates the presence of distinctly different wave patterns in the ERA5 geopotential and meridional wind anomalies during the warm and cold years of the QQO, indicative of a potential role of planetary waves or atmospheric tides in the QQO.
- Correlation with the meridional wind anomaly at 86 km measured by the Davis medium frequency spaced antenna radar shows that about 51% of the mesopause temperature QQO can be explained by the adiabatic cooling (heating) resulting from meridional circulation. This result is supported by the anti-correlation

between temperature and Aura/MLS CO measurements on a global scale as reported by Lee et al. (2018).

- M~~The m~~odulation of the meridional circulation is possibly~~most likely~~ a result of the variation in~~of the~~ gravity wave filtering by the strong stratospheric winds during the polar night.

Formatted: Font color: Auto

Taken together, these points highlight the interconnectedness of the entire atmosphere-ocean system, and that the QQO may be a manifestation of some type of normal oscillatory atmospheric mode arising from atmosphere-ocean interactions. Our efforts to isolate a specific mechanism that would drive a QQO, such as combinations of ENSO, QBO, PVI, SAM (like those proposed by Li et al. (2016) in the SH summer) have not found anything definite in the winter data at this time, and further investigations are warranted.

As we have shown, the QQO signal is also present in the polar summer mesosphere, and consequently there are implications for multi-year variability in the summer polar phenomena of noctilucent clouds (or Polar Mesospheric Clouds (PMC)), and Polar Mesospheric Summer Echoes. It would be expected that the temperature perturbations of 3 – 4 K that accompany the QQO at the mesopause will tend to have the most significant influence where temperatures hover near the ice-aerosol formation threshold, perturbed by gravity waves, planetary waves and tides. Indeed, the QQO signal may explain part of the variability in the position of the low-latitude boundary and modelled occurrence of noctilucent clouds in the NH reported by Russell et al. (2014), and the albedo of PMC for the SH and NH reported by Liu et al. (2016). The implications of the QQO for long-term trends in these mesospheric phenomena deserves further study.

## Data Availability

All Davis hydroxyl rotational data described in this manuscript are available through the Australian Antarctic Data Centre website (under project AAS4157) via the following link - https://data.aad.gov.au/metadata/records/Davis_OH_airglow. The satellite data used in this paper were obtained from the Aura/MLS archive at the Goddard Earth Sciences (GES) Data and Information Services Center (DISC) Distributed Active Archive Center (DAAC) (see https://disc.gsfc.nasa.gov/ and https://mls.jpl.nasa.gov) and the SABER data archive (see http://saber.gats-inc.com/data.php) and are publicly available. The ERA5 reanalysis is publically available from the Copernicus Climate Data Store (https://climate.copernicus.eu/climate-data-store). ERSST and OI-SST data sets are publicly available from the NOAA Physical Science Division website (https://www.esrl.noaa.gov/psd/).

## Author Contribution

WJRF managed data collection, performed data analysis, and prepared the manuscript and figures with contributions from all co-authors.

ARK analysed Aura/MLS satellite data and provided interpretation and manuscript and figure editing.

FJM analysed SABER data, and provided interpretation and editing of the manuscript, figures, and references

## Competing Interests

The authors declare that they have no conflict of interest.

## Acknowledgements

The authors thank the dedicated work of the Davis optical physicists and engineers over many years in the collection of airglow data and calibration of instruments. We thank Dr. Damian Murphy for provision of the MFSA radar data from Davis. These projects are supported by the Australian Antarctic Science program (projects AAS 4157 and AAS 4025). Aura/MLS data used in this study were acquired as part of the NASA's Earth-Sun System Division and archived and distributed by the Goddard Earth Sciences (GES) Data and Information Services Center (DISC) Distributed Active Archive Center (DAAC). SABER were obtained from http://saber.gats-inc.com/data.php. ECMWF/ERA5 data were also obtained from the Copernicus Climate Data Store (https://climate.copernicus.eu/climate-data-store). ERA5, ERSST and OI-SST data sets were accessed via the KNMI Climate Explorer site (https://climexp.knmi.nl/); ERSST and OI-SST original data from the NOAA Physical Science Division (https://www.esrl.noaa.gov/psd/). CESM-WACCM data were obtained from the British Atmospheric Data Center (http://badc.nerc.ac.uk). We thank those teams and acknowledge the use of these data sets. This work contributes to the understanding of mesospheric change processes coordinated through the Network for Detection of Mesospheric Change (https://ndmc.dlr.de/).

# References


Baldwin, M. P., Birner, T., Brasseur, G., Burrows, J., Butchart, N., Garcia, R., Geller, M., Gray, L., Hamilton, K., Harnik, N., Hegglin, M. I., Langematz, U., Robock, A., Sato, K. and Scaife, A.: 100 Years of Progress in Understanding the Stratosphere and Mesosphere, Meteorol. Monogr., doi:10.1175/amsmonographs-d-19-0003.1, 2019.

~~Brasseur, G. P. and Solomon, S.: Aeronomy of the Middle Atmosphere, Springer Netherlands, Dordrecht., 2005.~~

Cosentino, R. G., Morales-Juberías, R., Greathouse, T., Orton, G., Johnson, P., Fletcher, L. N. and Simon, A.: New Observations and Modeling of Jupiter's Quasi-Quadrennial Oscillation, J. Geophys. Res. Planets, 122(12), 2719–2744, doi:10.1002/2017JE005342, 2017.

Dyrland, M. E., Mulligan, F. J., Hall, C. M., Sigernes, F., Tsutsumi, M. and Deehr, C. S.: Response of OH airglow temperatures to neutral air dynamics at 78°N, 16°E during the anomalous 2003–2004 winter, J. Geophys. Res., 115(D7), D07103, doi:10.1029/2009JD012726, 2010.

~~Emmert, J. T., Stevens, M. H., Bernath, P. F., Drob, D. P. and Boone, C. D.: Observations of increasing carbon dioxide concentration in Earth's thermosphere, Nat. Geosci., 5(12), 868–871, doi:10.1038/ngeo1626, 2012.~~

Espy, P. J., Hibbins, R. E., Jones, G. O. L., Riggin, D. M. and Fritts, D. C.: Rapid, large-scale temperature changes in the polar mesosphere and their relationship to meridional flows, Geophys. Res. Lett., 30(5), n/a-n/a, doi:10.1029/2002GL016452, 2003.

French, W.J.R.; Mulligan, F.J.; Klekociuk, A. R. .: Analysis of 24 years of mesopause

region OH rotational temperature observations at Davis, Antarctica. Part 1:Long-term trends., Atmos. Chem. Phys, 20202019 (submitted).

French, W. J. R. and Klekociuk, A. R.: Long-term trends in Antarctic winter hydroxyl temperatures, J. Geophys. Res., 116(D4), D00P09, doi:10.1029/2011JD015731, 2011.

French, W. J. R. and Mulligan, F. J.: Stability of temperatures from TIMED/SABER v1.07 (2002–2009) and Aura/MLS v2.2 (2004–2009) compared with OH(6-2) temperatures observed at Davis Station, Antarctica, Atmos. Chem. Phys., 10(23), 11439–11446, doi:10.5194/acp-10-11439-2010, 2010.

Garcia, R. R., and Solomon, S.: The effect of breaking gravity waves on the dynamics and chemical composition of the mesosphere and lower thermosphere, J. Geophys. Res., 90(D2), 3850-3868, doi:10.1029/JD090iD02p03850, 1985.

García-Comas, M., López-Puertas, M., Marshall, B. T., Wintersteiner, P. P., Funke, B., Bermejo-Pantaleón, D., Mertens, C. J., Remsberg, E. E., Gordley, L. L., Mlynczak, M. G. and Russell III, J. M.: Errors in Sounding of the Atmosphere using Broadband Emission Radiometry (SABER) kinetic temperature caused by non-local-thermodynamic-equilibrium model parameters, J. Geophys. Res., 113(D24), D24106, doi:10.1029/2008JD010105, 2008.

Geller, M. A., Zhou, T., Shindell, D., Ruedy, R., Aleinov, I., Nazarenko, L., Tausnev, N. L., Kelley, M., Sun, S., Cheng, Y., Field, R. D. and Faluvegi, G.: Modeling the QBO-Improvements resulting from higher-model vertical resolution, J. Adv. Model. Earth Syst., 8(3), 1092–1105, doi:10.1002/2016MS000699, 2016.

Formatted: Space After: 8 pt, Line spacing: Multiple 1.08 li, Widow/Orphan control

Formatted: Font: (Default) Calibri, 11 pt

Hoffmann, L., Xue, X. and Alexander, M. J.: A global view of stratospheric gravity wave hotspots located with Atmospheric Infrared Sounder observations, J. Geophys. Res. Atmos., 118(2), 416–434, doi:10.1029/2012JD018658, 2013.

Huang, B., Thorne, P. W., Banzon, V. F., Boyer, T., Chepurin, G., Lawrimore, J. H., Menne, M. J., Smith, T. M., Vose, R. S. and Zhang, H.-M.: Extended Reconstructed Sea Surface Temperature, Version 5 (ERSSTv5): Upgrades, Validations, and Intercomparisons, J. Clim., 30(20), 8179–8205, doi:10.1175/JCLI-D-16-0836.1, 2017.

Jiang, N., Neelin, J. D. and Ghil, M.: Quasi-quadrennial and quasi-biennial variability in the equatorial Pacific, Clim. Dyn., 12(2), 101–112, doi:10.1007/BF00223723, 1995.

Langhoff, S. R., Werner, H. J. and Rosmus, P.: Theoretical Transition Probabilities for the OH Meinel System, J. Mol. Spectrosc., 118, 507–529, 1986.

Lee, J. N., Wu, D. L., Ruzmaikin, A. and Fontenla, J.: Solar cycle variations in mesospheric carbon monoxide, J. Atmos. Solar-Terrestrial Phys., 170, 21–34, doi:10.1016/j.jastp.2018.02.001, 2018.

Li, T., Calvo, N., Yue, J., Russell, J. M., Smith, A. K., Mlynczak, M. G., Chandran, A., Dou, X., Liu, A. Z., Li, T., Calvo, N., Yue, J., III, J. M. R., Smith, A. K., Mlynczak, M. G., Chandran, A., Dou, X. and Liu, A. Z.: Southern Hemisphere Summer Mesopause Responses to El Niño–Southern Oscillation, J. Clim., 29(17), 6319–6328, doi:10.1175/JCLI-D-15-0816.1, 2016.

Liu, C. and Xue, F.: The relationship between the canonical ENSO and the phase transition of the Antarctic oscillation at the quasi-quadrennial timescale, Acta Oceanol. Sin., 29(6), 26–34, doi:10.1007/s13131-010-0073-4, 2010.

Liu, H.-L.: Variability and predictability of the space environment as related to lower atmosphere forcing, Sp. Weather, 14(9), 634–658, doi:10.1002/2016SW001450, 2016.

Liu, S. and Duan, A.: Impacts of the global sea surface temperature anomaly on the evolution of circulation and precipitation in East Asia on a quasi-quadrennial cycle, Clim. Dyn., 51(11–12), 4077–4094, doi:10.1007/s00382-017-3663-4, 2018.

Liu, X., Yue, J., Xu, J., Yuan, W., Russell, J. M., Hervig, M. E., and Nakamura, T.: Persistent longitudinal variations in 8 years of CIPS/AIM polar mesospheric clouds, J. Geophys. Res. Atmos., 121, 8390– 8409, doi:10.1002/2015JD024624, 2016.

Liu, X., Yue, J., Xu, J., Garcia, R. R., Russell, J. M., Mlynczak, M., Wu, D. L. and Nakamura, T.: Variations of global gravity waves derived from 14 years of SABER temperature observations, J. Geophys. Res. Atmos., 122(12), 6231–6249, doi:10.1002/2017JD026604, 2017.

Livesey, Nathaniel J., William G. Read, Paul A. Wagner, Lucien Froidevaux, A. L., Gloria L. Manney, Luis F. Millán Valle, Hugh C. Pumphrey, M. L. S., Michael J. Schwartz, Shuhui Wang, Ryan A. Fuller, Robert F. Jarnot, B. W. K. and Elmain Martinez, R. R. L.: Earth Observing System (EOS) Aura Microwave Limb Sounder (MLS) Version4.2x Level 2 data quality and description document Version 4.2x–3.1, , 1–163 [online] Available from: https://mls.jpl.nasa.gov/data/v4-2_data_quality_document.pdf, 2018.

Marsh, D. R., Mills, M. J., Kinnison, D. E., Lamarque, J.-F., Calvo, N. and Polvani, L. M.: Climate Change from 1850 to 2005 Simulated in CESM1(WACCM), J. Clim., 26(19), 7372–7391, doi:10.1175/JCLI-D-12-00558.1, 2013.

McDade, I. C.: The altitude dependence of the OH(X2Π) vibrational distribution in the nightglow: Some model expectations, Planet. Space Sci., 39(7), 1049–1057, doi:10.1016/0032-0633(91)90112-N, 1991.

Mertens, C. J., Mlynczak, M. G., Lopez-Puertas, M., Wintersteiner, P. P., Picard, R. H., Winick, J. R., Gordley, L. L. and Russell III, J. M.: Retrieval of kinetic temperature and carbon dioxide abundance from nonlocal thermodynamic equilibrium limb emission measurements made by the SABER experiment on the TIMED satellite, in Remote Sensing of Clouds and the Atmosphere VII, vol. 4882, p. 162, SPIE., 2003.

Morgenstern, O., Hegglin, M., Rozanov, E., O'Connor, F., Luke Abraham, N., Akiyoshi, H., Archibald, A., Bekki, S., Butchart, N., Chipperfield, M., Deushi, M., Dhomse, S., Garcia, R., Hardiman, S., Horowitz, L., Jöckel, P., Josse, B., Kinnison, D., Lin, M., Mancini, E., Manyin, M., Marchand, M., Marécal, V., Michou, M., Oman, L., Pitari, G., Plummer, D., Revell, L., Saint-Martin, D., Schofield, R., Stenke, A., Stone, K., Sudo, K., Tanaka, T., Tilmes, S., Yamashita, Y., Yoshida, K. and Zeng, G.: Review of the global models used within phase 1 of the Chemistry-Climate Model Initiative (CCMI), Geosci. Model Dev., 10(2), 639–671, doi:10.5194/gmd-10-639-2017, 2017.

Murphy, D. J., Alexander, S. P. and Vincent, R. A.: Interhemispheric dynamical coupling to the southern mesosphere and lower thermosphere, J. Geophys. Res. Atmos., 117(D8), n/a-n/a, doi:10.1029/2011JD016865, 2012.

Offermann, D., Goussev, O., Kalicinsky, C., Koppmann, R., Matthes, K., Schmidt, H., Steinbrecht, W. and Wintel, J.: A case study of multi-annual temperature oscillations in the atmosphere: Middle Europe, J. Atmos. Solar-Terrestrial Phys., 135, 1–11, doi:10.1016/j.jastp.2015.10.003, 2015.

949 Parkinson, C. L.: A 40-y record reveals gradual Antarctic sea ice increases followed by
950 decreases at rates far exceeding the rates seen in the Arctic, PNAS, 116, 14414-14423,
951 doi:10.1073/pnas.1906556116, 2019

952 Perminov, V. I., Semenov, A. I., Pertsev, N. N., Medvedeva, I. V., Dalin, P. A. and
953 Sukhodoev, V. A.: Multi-year behaviour of the midnight OH∗ temperature according to
954 observations at Zvenigorod over 2000–2016, Adv. Sp. Res., 61(7), 1901–1908,
955 doi:10.1016/J.ASR.2017.07.020, 2018.

956 Pisoft, P., Miksovsky, J., Kalvova, J., Raidl, A. and Zak, M.: Areal analysis of
957 oscillations in 500-hPa temperature field: a pseudo-2D wavelet transform approach, Int.
958 J. Climatol., 31(10), 1545–1553, doi:10.1002/joc.2167, 2011.

959 ~~Qian, L., Jacobi, C. and McInerney, J.: Trends and Solar Irradiance Effects in the~~
960 ~~Mesosphere, J. Geophys. Res. Sp. Phys., 124(2), 1343–1360,~~
961 ~~doi:10.1029/2018JA026367, 2019.~~

962 Raphael, M. N.: A zonal wave 3 index for the Southern Hemisphere, Geophys. Res. Lett.,
963 31, L23212, doi:10.1029/2004GL020365, 2004.

964 Reid, I. M., Spargo, A. J. and Woithe, J. M.: Seasonal variations of the nighttime O($^1$S)
965 and OH (8-3) airglow intensity at Adelaide, Australia, J. Geophys. Res. Atmos., 119(11),
966 6991–7013, doi:10.1002/2013JD020906, 2014.

967 Reynolds, R. W., Rayner, N. A., Smith, T. M., Stokes, D. C. and Wang, W.: An
968 Improved In Situ and Satellite SST Analysis for Climate, J. Clim., 15(13), 1609–1625,
969 doi:10.1175/1520-0442(2002)015<1609:AIISAS>2.0.CO;2, 2002.

970 Russell III, J. M., Mlynczak, M. G., Gordley, L. L., Tansock, J. and Esplin, R.: An

971 Overview of the SABER Experiment and Preliminary Calibration Results, SPIE Proc.,
972 3756, 277–288, doi:10.1117/12.366382, 1999.

973 Russell, J. M., Rong, P., Hervig, M. E., Siskind, D. E., Stevens, M. H., Bailey, S. M. and
974 Gumbel, J.: Analysis of northern midlatitude noctilucent cloud occurrences using satellite
975 data and modeling, J. Geophys. Res. Atmos., 119(6), 3238–3250,
976 doi:10.1002/2013JD021017, 2014.

977 Sato, K., Tateno, S., Watanabe, S., Kawatani, Y., Sato, K., Tateno, S., Watanabe, S. and
978 Kawatani, Y.: Gravity Wave Characteristics in the Southern Hemisphere Revealed by a
979 High-Resolution Middle-Atmosphere General Circulation Model, J. Atmos. Sci., 69(4),
980 1378–1396, doi:10.1175/JAS-D-11-0101.1, 2012.

981 von Savigny, C., McDade, I. C., Eichmann, K. U. and Burrows, J. P.: On the dependence
982 of the OH* Meinel emission altitude on vibrational level: SCIAMACHY observations
983 and model simulations, Atmospheric Chem. Phys., 12, 8813–8828, doi:10.5194/acp-12-
984 8813-2012, 2012.

985 Schmidt, H., Brasseur, G. P., Charron, M., Manzini, E., Giorgetta, M. A., Diehl, T.,
986 Fomichev, V. I., Kinnison, D., Marsh, D. and Walters, S.: The HAMMONIA chemistry
987 climate model: Sensitivity of the mesopause region to the 11-year solar cycle and CO2
988 doubling, J. Clim., 19(16), 3903–3931, doi:10.1175/JCLI3829.1, 2006.

989 Schwartz, M. J., Lambert, A., Manney, G. L., Read, W. G., Livesey, N. J., Froidevaux,
990 L., Ao, C. O., Bernath, P. F., Boone, C. D., Cofield, R. E., Daffer, W. H., Drouin, B. J.,
991 Fetzer, E. J., Fuller, R. A., Jarnot, R. F., Jiang, J. H., Jiang, Y. B., Knosp, B. W., Krüger,
992 K., Li, J.-L. F., Mlynczak, M. G., Pawson, S., Russell, J. M., Santee, M. L., Snyder, W.

993 V., Stek, P. C., Thurstans, R. P., Tompkins, A. M., Wagner, P. A., Walker, K. A., Waters,
994 J. W. and Wu, D. L.: Validation of the Aura Microwave Limb Sounder temperature and
995 geopotential height measurements, J. Geophys. Res., 113(D15),
996 doi:10.1029/2007jd008783, 2008.

997 Solomon, S. C., Liu, H., Marsh, D. R., McInerney, J. M., Qian, L. and Vitt, F. M.: Whole
998 Atmosphere Simulation of Anthropogenic Climate Change, Geophys. Res. Lett., 45(3),
999 1567–1576, doi:10.1002/2017GL076950, 2018.

1000 Torrence, C. and Compo, G. P.: A Practical Guide to Wavelet Analysis, Bull. Am.
1001 Meteorol. Soc., 79, 61–78, doi:10.1175/1520-
1002 0477(1998)079<0061:APGTWA>2.0.CO;2, 1998.

1003 Turner, J., Hosking, J.S., Marshall, G.J., Phillips, T., Bracegirdle, T.J.: Antarctic sea ice
1004 increase consistent with intrinsic variability of the Amundsen Sea Low, Clim. Dyn., 46,
1005 2391, doi:10.1007/s00382-015-2708-9, 2016.

1006 Turney, C. S. M., Fogwill, C. J., Klekociuk, A. R., van Ommen, T. D., Curran, M. A. J.,
1007 Moy, A. D., and Palmer, J. G.: Tropical and mid-latitude forcing of continental Antarctic
1008 temperatures, The Cryosphere, 9, 2405–2415, doi:10.5194/tc-9-2405-2015, 2015.

1009 Wright, C. J., Hindley, N. P., Moss, A. C. and Mitchell, N. J.: Multi-instrument gravity-
1010 wave measurements over Tierra del Fuego and the Drake Passage – Part 1: Potential
1011 energies and vertical wavelengths from AIRS, COSMIC, HIRDLS, MLS-Aura,
1012 SAAMER, SABER and radiosondes, Atmos. Meas. Tech., 9(3), 877–908,
1013 doi:10.5194/amt-9-877-2016, 2016.

1014 Wright, C. J., Hindley, N. P., Hoffmann, L., Alexander, M. J. and Mitchell, N. J.:

1015 Exploring gravity wave characteristics in 3-D using a novel S-transform technique:
1016 AIRS/Aqua measurements over the Southern Andes and Drake Passage, Atmos. Chem.
1017 Phys., 17(13), 8553–8575, doi:10.5194/acp-17-8553-2017, 2017.

1018 Yasui, R., Sato, K. and Tsutsumi, M.: Seasonal and Interannual Variation of Mesospheric
1019 Gravity Waves Based on MF Radar Observations over 15 Years at Syowa Station in the
1020 Antarctic, SOLA, 12(0), 46–50, doi:10.2151/sola.2016-010, 2016.

1021 Zhang, Y., Sheng, Z., Shi, H., Zhou, S., Shi, W., Du, H. and Fan, Z.: Properties of the
1022 Long-Term Oscillations in the Middle Atmosphere Based on Observations from
1023 TIMED/SABER Instrument and FPI over Kelan, Atmosphere (Basel)., 8(12), 7,
1024 doi:10.3390/atmos8010007, 2017.

1025

1026 Figures

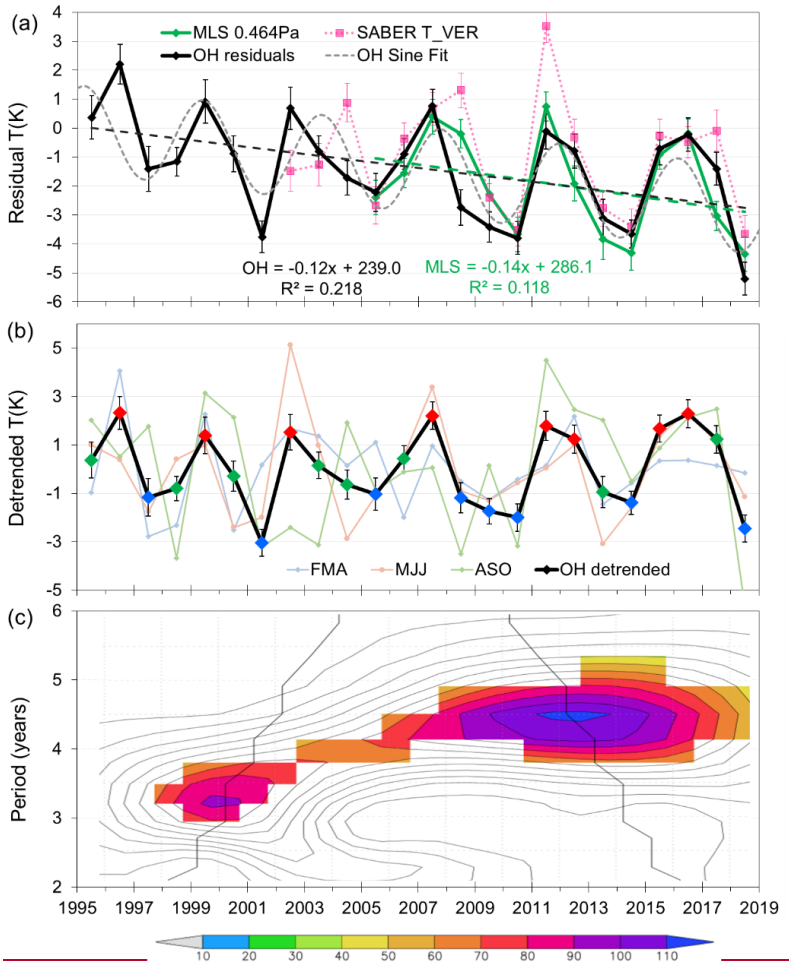


1027

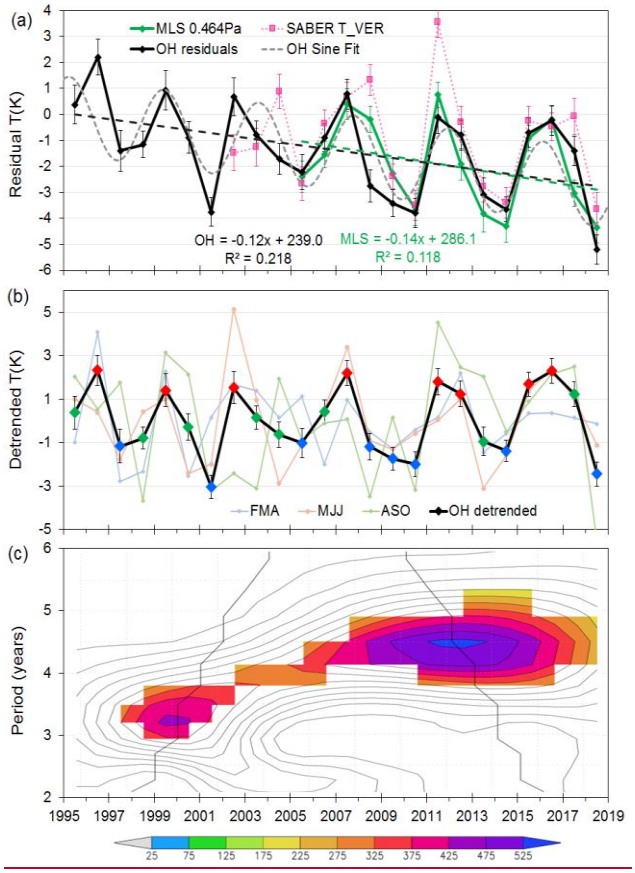


Figure 1. (a) Davis OH winter mean residual (solar response removed) temperatures (black line, standard error in mean error bars, dashed linear fit) compared with Aura/MLS [AMJJAS] mean residual temperatures for 0.0046 hPa (green line, standard error-in-mean error bars, dashed linear fit) and TIMED/SABER (pink dotted line, standard error-in-mean error bars). Gray dotted line is a sinusoid fit (peak-peak amplitude 3.0±0.1 K period 4.2±0.7 years) provided as a guide. (b) Detrended Davis OH winter mean temperatures [AMJJAS] (black line, long-term linear fit removed) compared to FMA, MJJ and ASO monthly averages (red, green and blue points mark warm, mid and cold years respectively for composite studies). (c) A Morlet wavelet transform (order 6) of the detrended Davis OH winter mean temperatures. Coloured sections are power significant above 90% significance level as per colour bar. The black line indicates the cone of influence; points outside have been influenced by the boundaries of the time series.

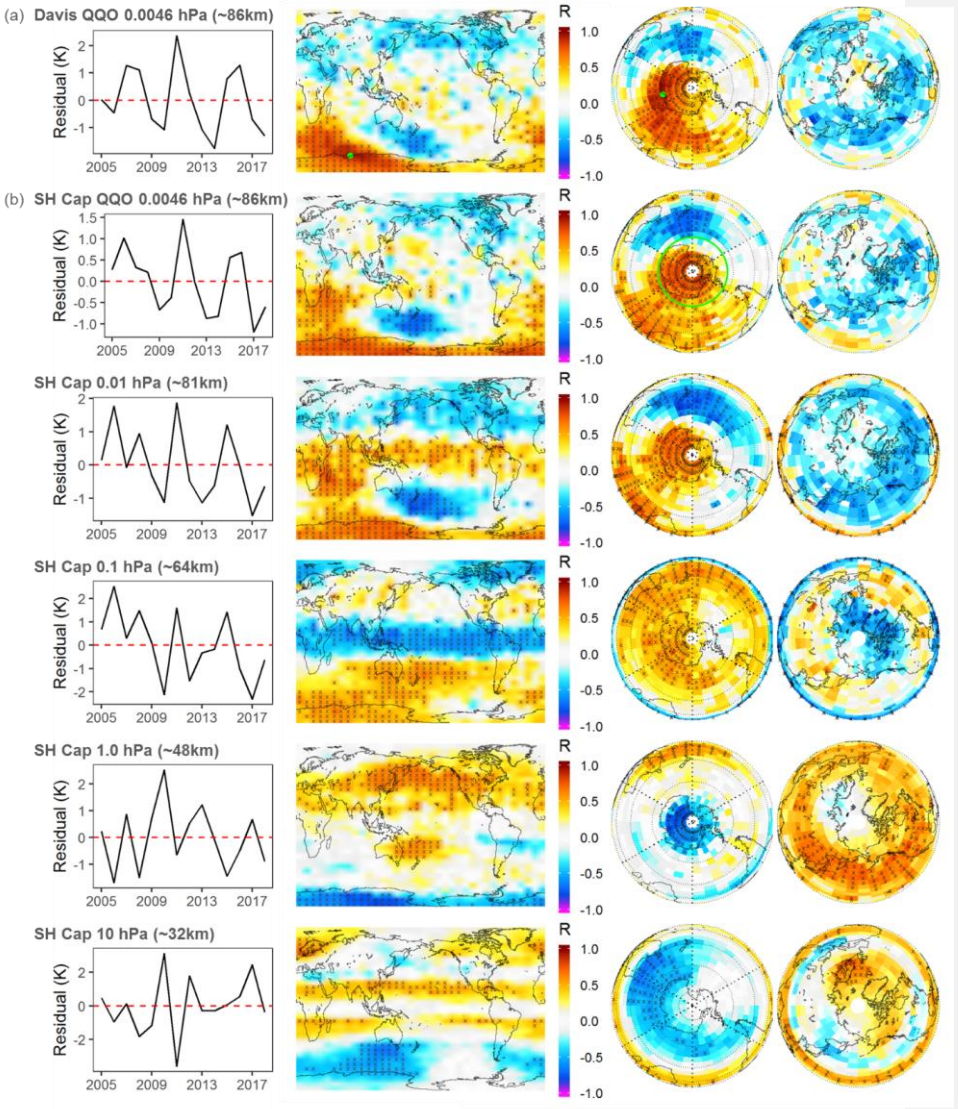
(a) Davis QQO 0.0046 hPa (~86km)
(b) SH Cap QQO 0.0046 hPa (~86km)
SH Cap 0.01 hPa (~81km)
SH Cap 0.1 hPa (~64km)
SH Cap 1.0 hPa (~48km)
SH Cap 10 hPa (~32km)
Residual (K)
2005
2009
2013
2017
R
1.0
0.5
0.0
-0.5
-1.0

1041

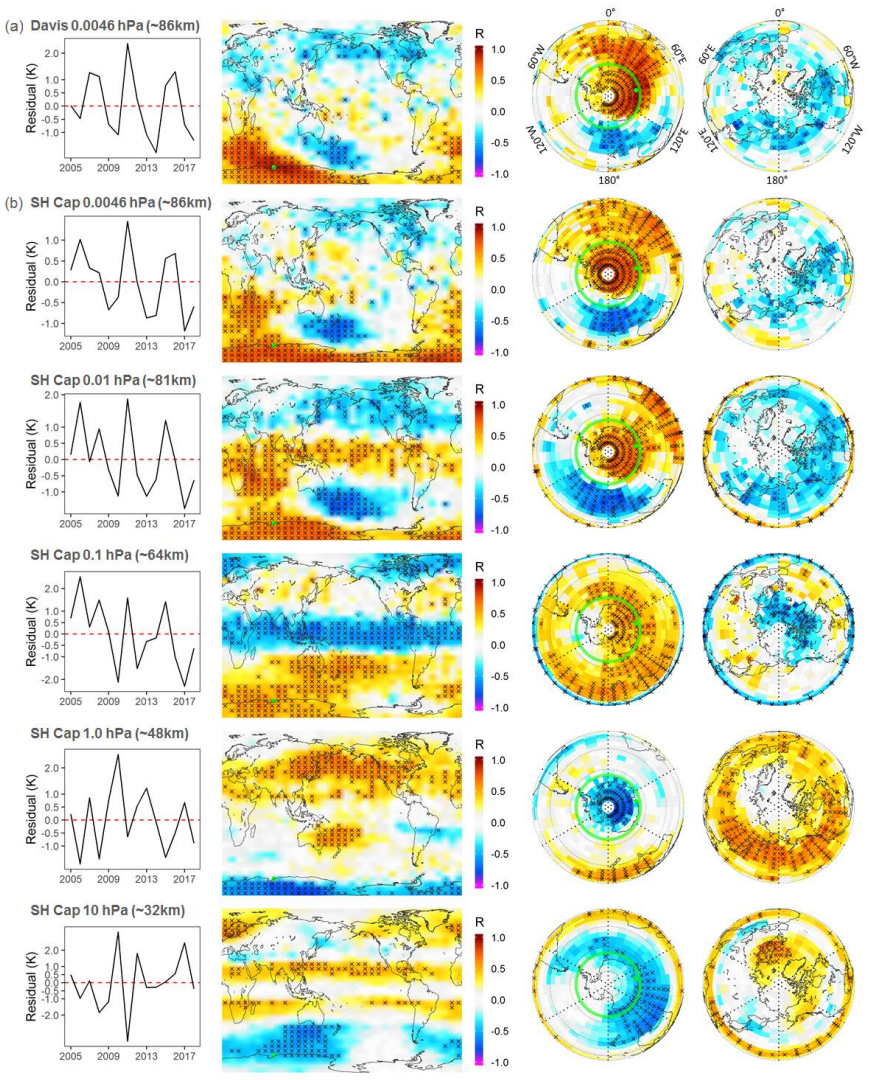


Figure 2. (a). Correlation of the Aura/MLS 0.0046 hPa grid box QQO residual temperature signal at Davis (left hand time series panel) with each grid box of the Aura/MLS 0.0046hPa global temperature field gridded in 5° x 10° bins. Equi-rectangular and polar projections of the correlation (R) are shown (crossed grid cells ~~hashed areas~~ are significant at the 90% level). Davis location indicated by green dot. (b) C~~As for (a), but c~~orrelation of the 0.0046 hPa SH polar cap winter average (65 °S - 85° S; AMJJAS; green circle) with each grid box of the Aura/MLS temperature fields at various pressure levels as indicated.

**Formatted:** Space After: 0 pt

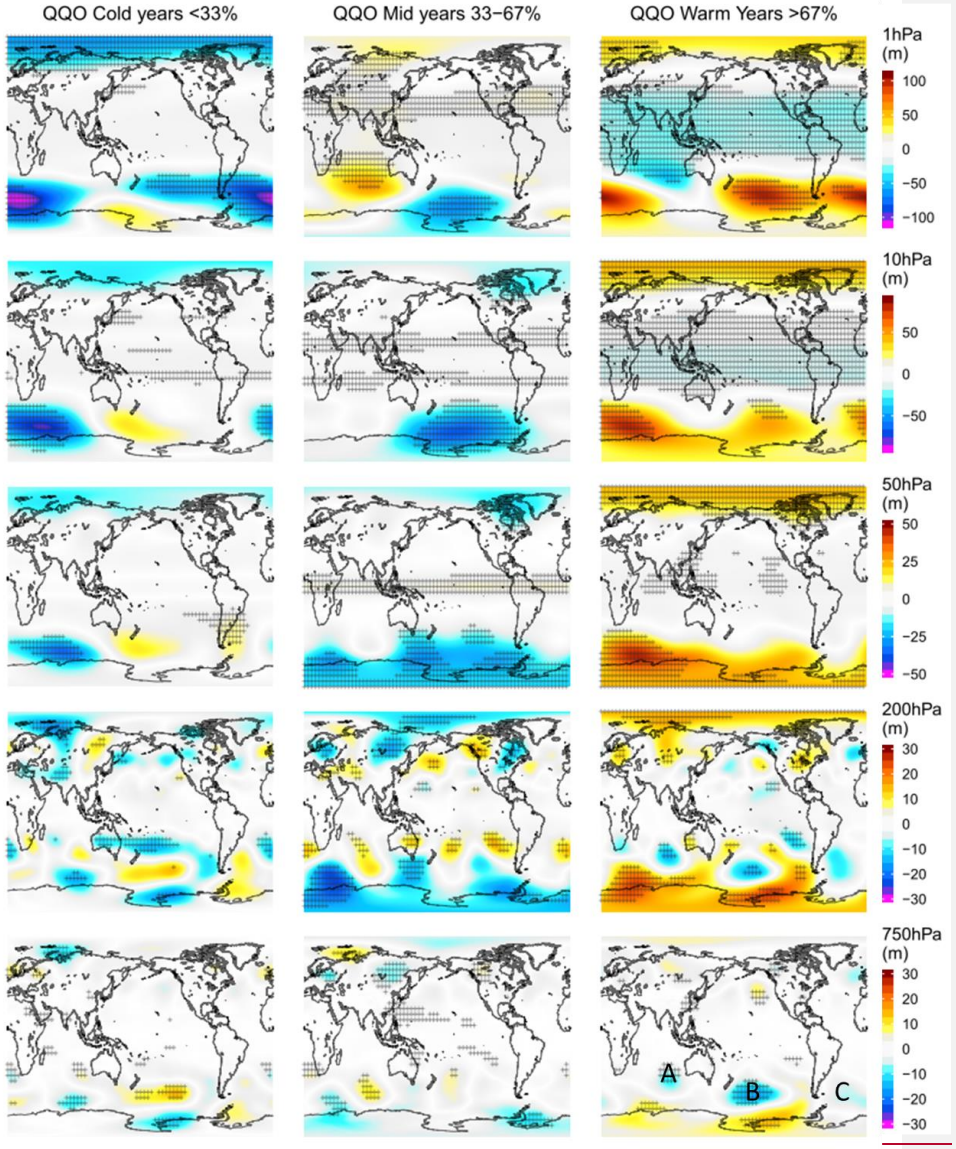
QQO Cold years <33%
QQO Mid years 33−67%
QQO Warm Years >67%
1hPa (m)
100
50
0
−50
−100
10hPa (m)
50
0
−50
50hPa (m)
50
25
0
−25
−50
200hPa (m)
30
20
10
0
−10
−20
−30
750hPa (m)
30
20
10
0
−10
−20
−30
A
B
C

1050

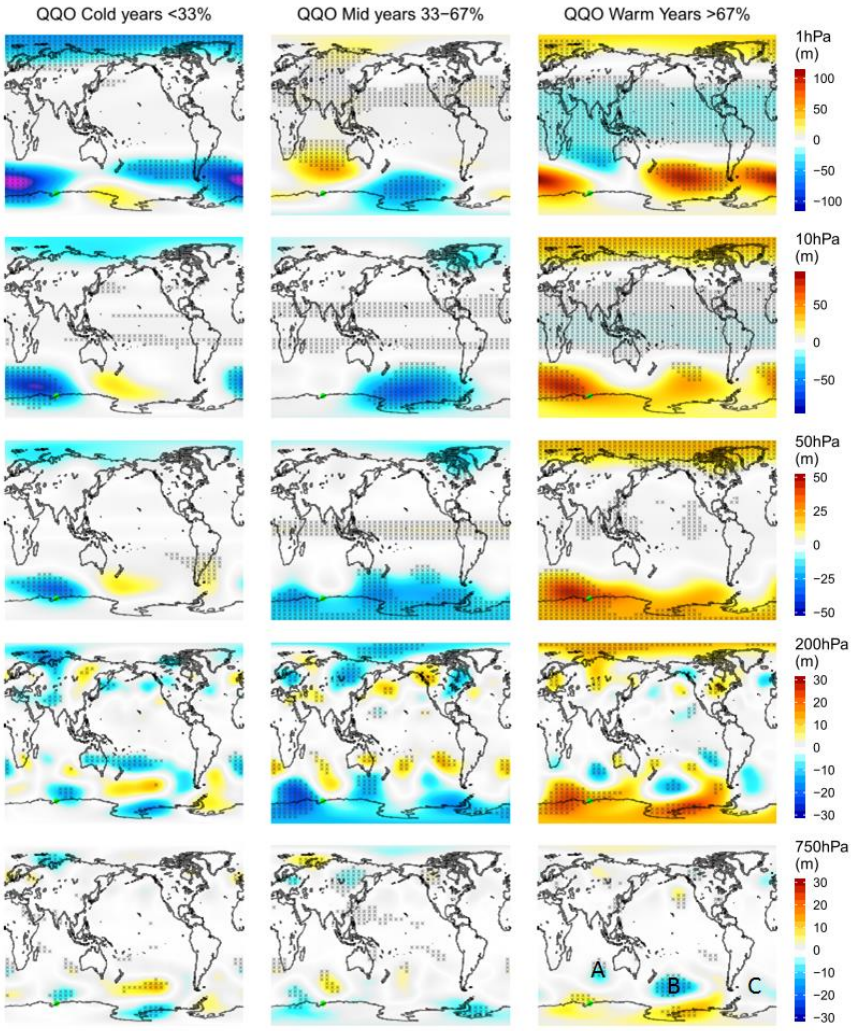


Figure 3. Composites of the ERA5 [AMJJAS] geopotential anomaly, for cold, mid and warm years of the Davis detrended winter average QQO signal. Pressure levels are indicated on the right hand colour bar. The colour scales are in m of geopotential height. Hashed areas on the plots are significant at the 90% level.

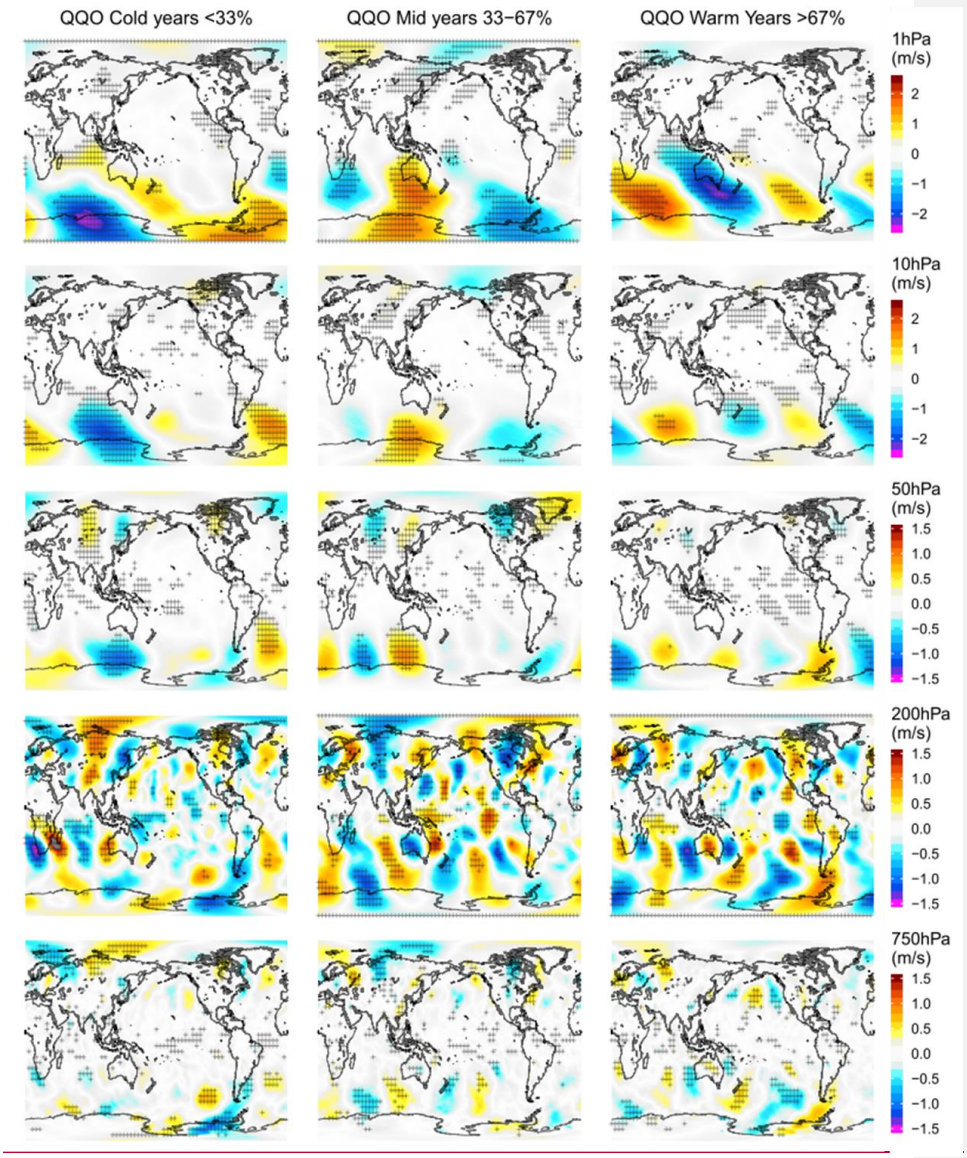
QQO Cold years <33%
QQO Mid years 33−67%
QQO Warm Years >67%
1hPa (m/s)
2
1
0
−1
−2
10hPa (m/s)
2
1
0
−1
−2
50hPa (m/s)
1.5
1.0
0.5
0.0
−0.5
−1.0
−1.5
200hPa (m/s)
1.5
1.0
0.5
0.0
−0.5
−1.0
−1.5
750hPa (m/s)
1.5
1.0
0.5
0.0
−0.5
−1.0
−1.5

1056

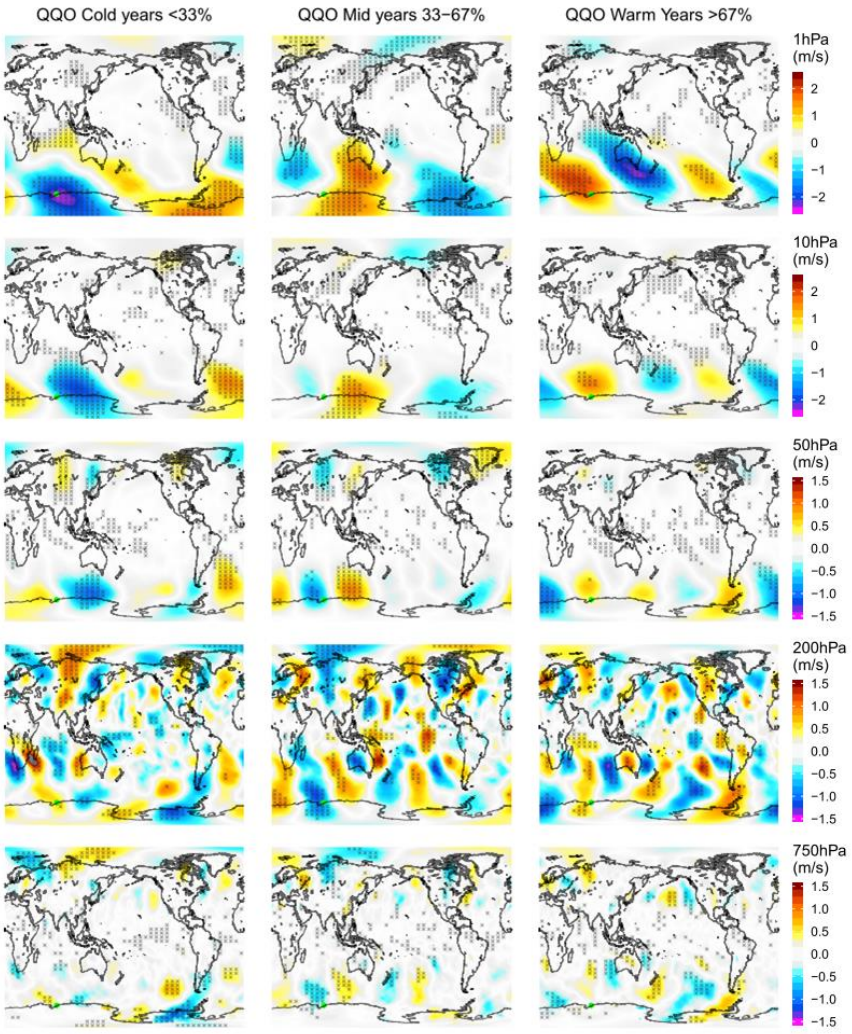


Figure 4. Composites of the ERA5 [AMJJAS] meridional wind anomaly, for cold, mid and warm years of the Davis detrended winter average QQO signal. Pressure levels are indicated on the right hand colour bar. The colour scales are in m/s. Hashed areas on the plots are significant at the 90% level. Zonal wind anomaly equivalent in Fig S3 (supplementary).

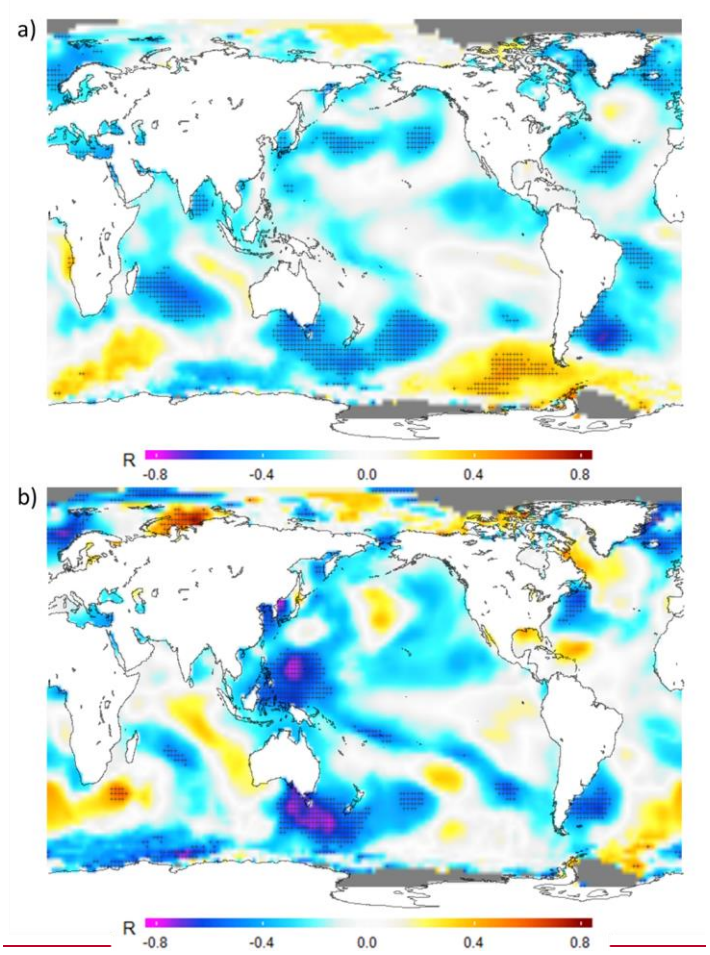


1065

1066

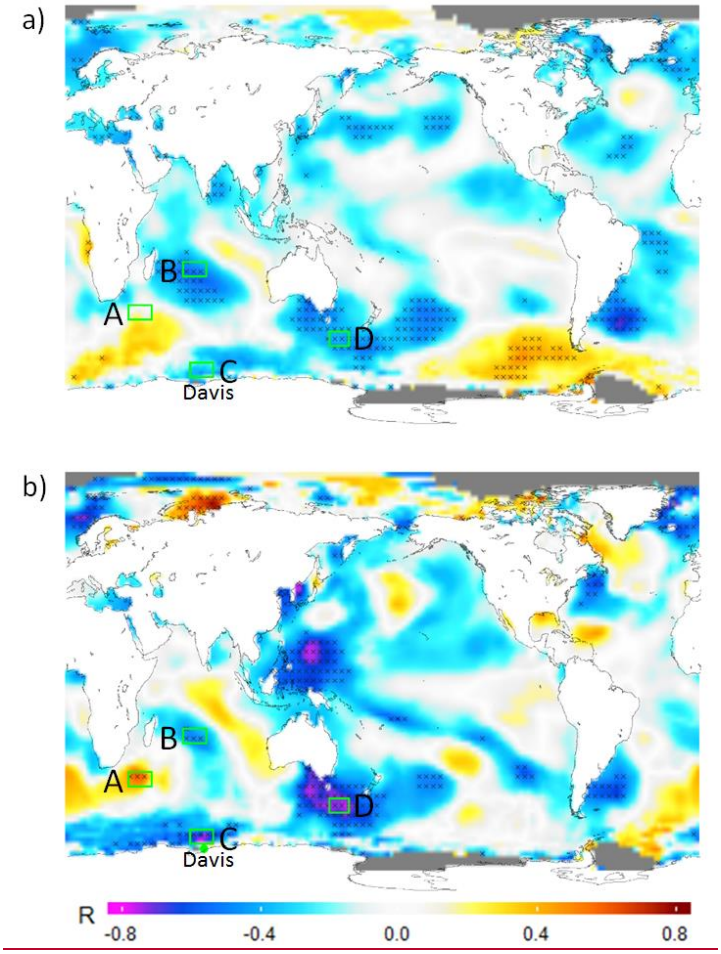


Figure 5. Correlation maps of the Davis OH residual (24 year) QQO signal (a) and MLS 0.0046hPa [AMJJAS] polar cap average residual (14 year) QQO signal (b) with the Extended Range Sea Surface Temperature [AMJJAS] average anomalies. Cross h~~H~~atched points ~~colours~~ are significant at the 90% level (every second grid point marked). Grey areas are permanent sea ice.

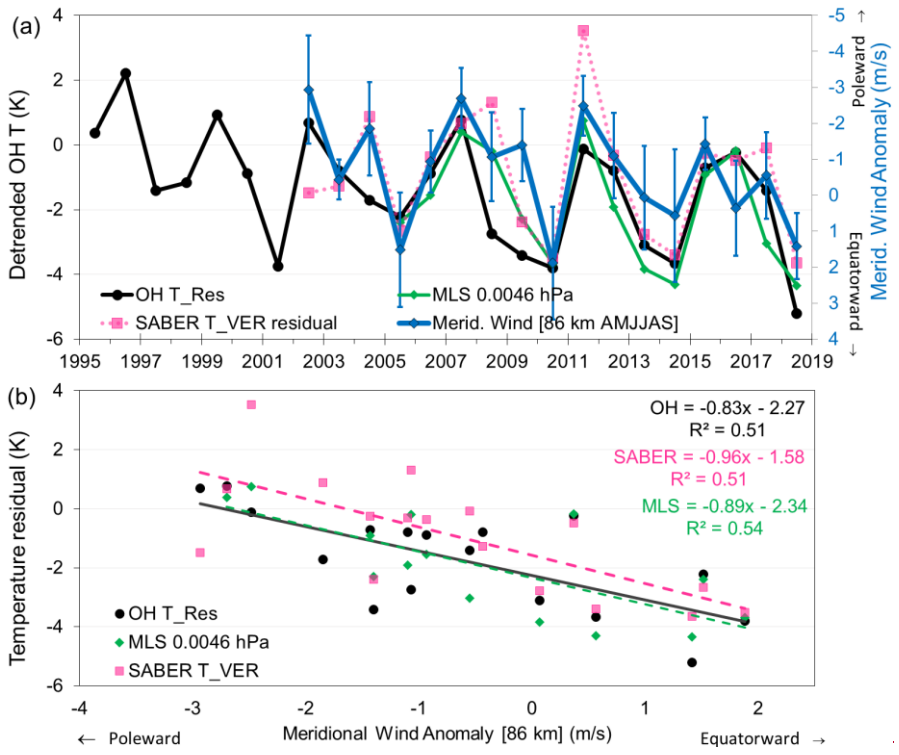
(a)
Detrended OH T (K)
Meridional Wind Anomaly (m/s)
Poleward
Equatorward
OH T_Res
SABER T_VER residual
MLS 0.0046 hPa
Merid. Wind [86 km AMJJAS]
(b)
Temperature residual (K)
OH = -0.83x - 2.27
R² = 0.51
SABER = -0.96x - 1.58
R² = 0.51
MLS = -0.89x - 2.34
R² = 0.54
OH T_Res
MLS 0.0046 hPa
SABER T_VER
← Poleward
Meridional Wind Anomaly [86 km] (m/s)
Equatorward →

1074

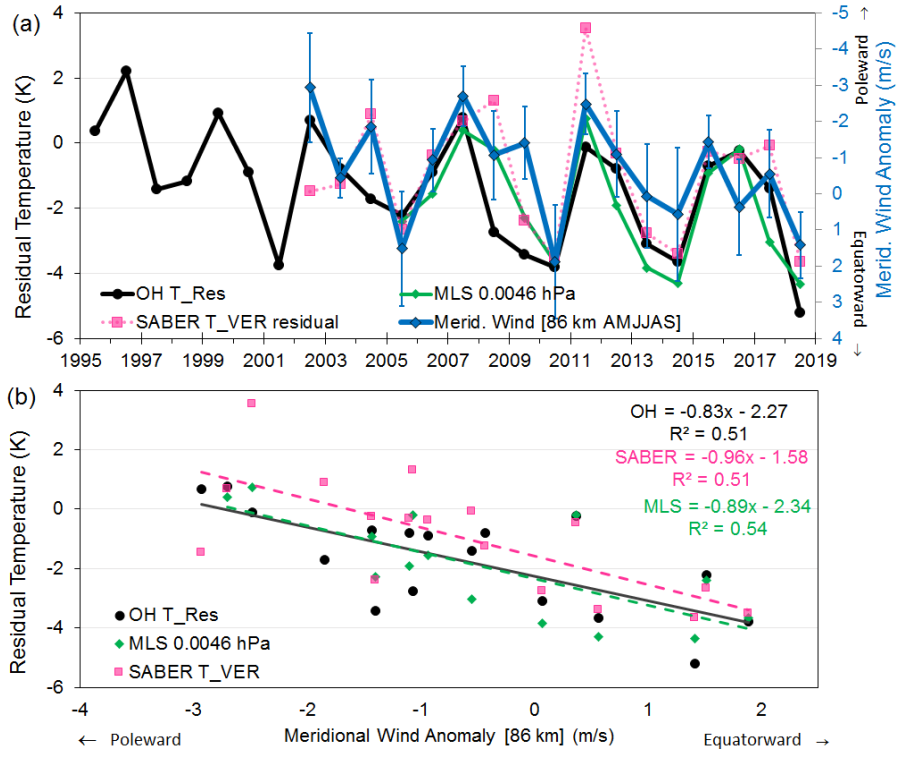


Figure 6~~6~~. (a) Davis OH, Aura/MLS (0.464 Pa level) and SABER (T_VER) residual temperatures compared to the AMJJAS mean meridional wind at 86km measured by MFSA radar at Davis. (b) The relationship between Davis OH, Aura/MLS and SABER residual temperatures and meridional winds at 86 km above Davis. OH and SABER are fit over a common era (2002-2018) for comparison. MLS is fit over 2005-2018.

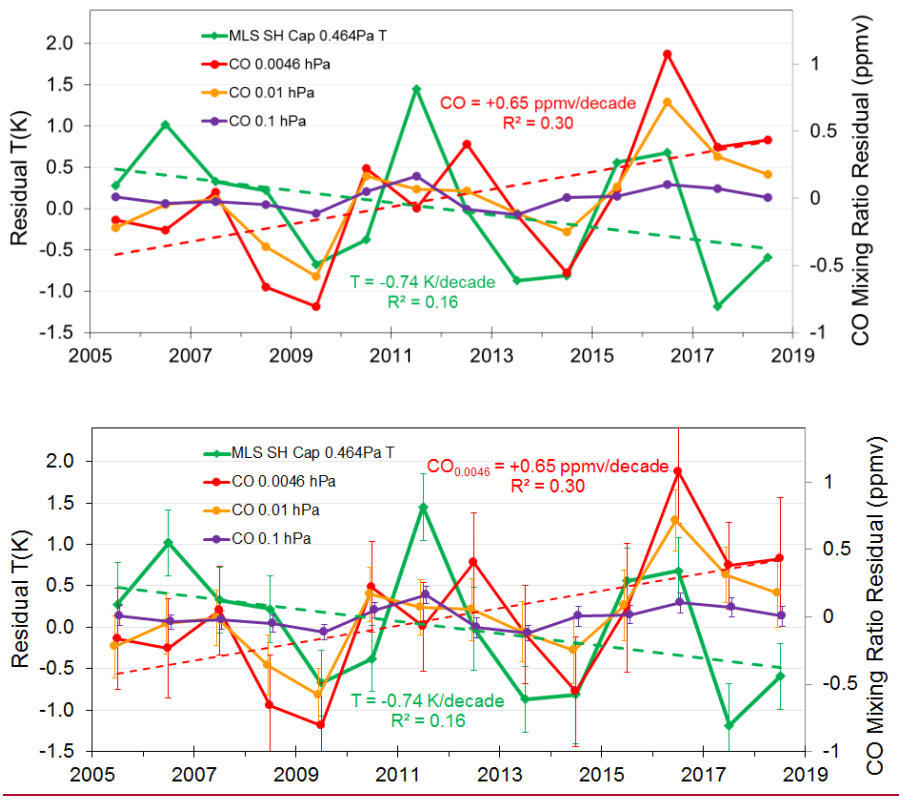


Figure 7~~8~~. Comparison of Aura/MLS SH polar cap (65° S - 85° S) winter time series of temperature at 0.0046 hPa (green line and dashed linear fit -0.74 K/decade) with CO mixing ratio at 0.0046 hPa, 0.01 hPa and 0.1 hPa (red line with dashed fit +0.65 ppmv/decade, orange line and purple line respectively). The data have been averaged over months AMJJAS, and had seasonal and solar cycle variations subtracted.

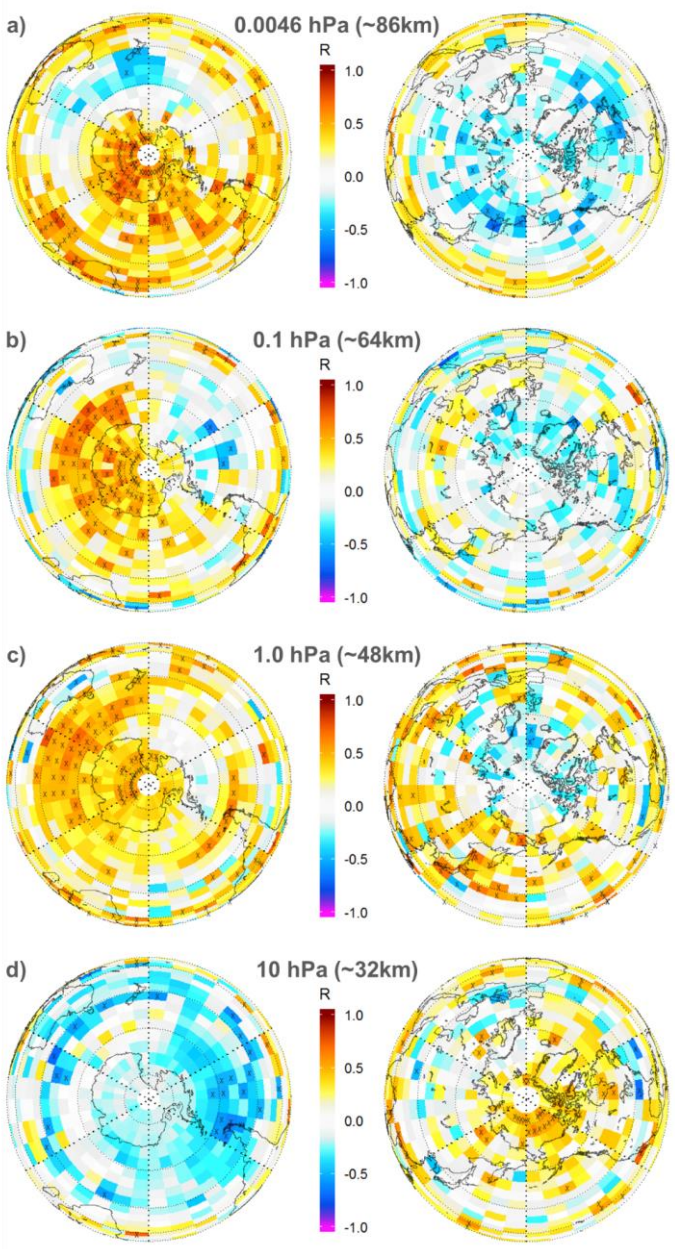
a)
0.0046 hPa (~86km)
R
1.0
0.5
0.0
-0.5
-1.0
b)
0.1 hPa (~64km)
R
1.0
0.5
0.0
-0.5
-1.0
c)
1.0 hPa (~48km)
R
1.0
0.5
0.0
-0.5
-1.0
d)
10 hPa (~32km)
R
1.0
0.5
0.0
-0.5
-1.0

1095

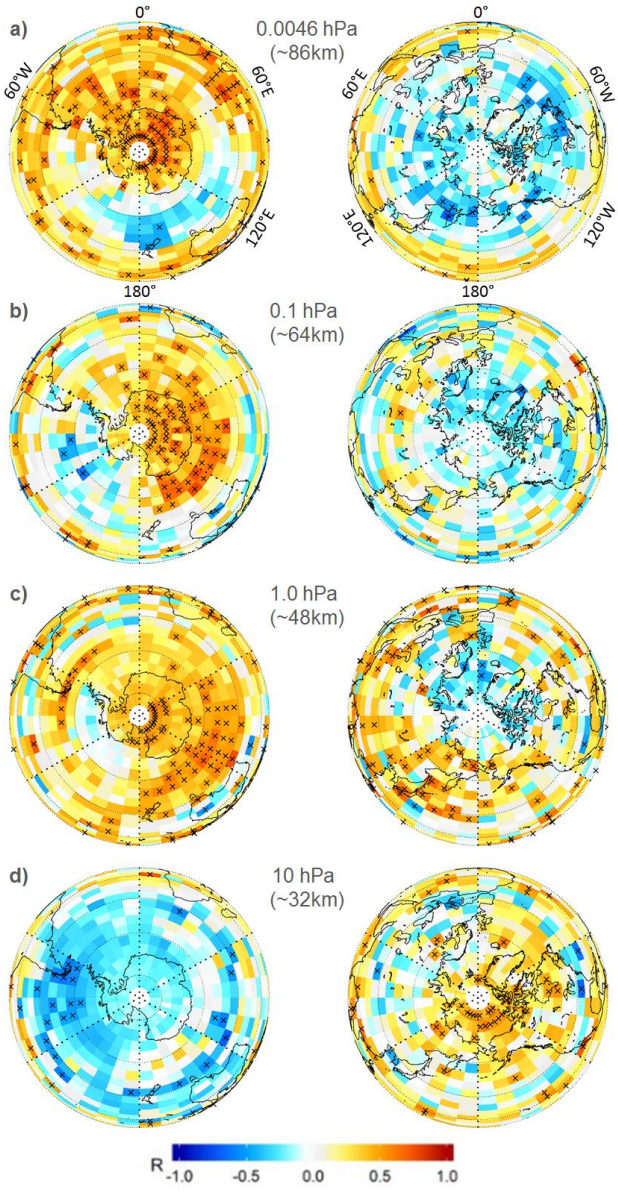


Figure 89. SH and NH projection maps of correlation between the detrended Aura/MLS 0.0046 hPa, SH polar cap (65° S - 85° S), AMJJAS average temperature time series with residual Aura/MLS CO mixing ratio in each grid box at the pressure levels indicated. Crosses indicate the correlation is significant at the 90% level.

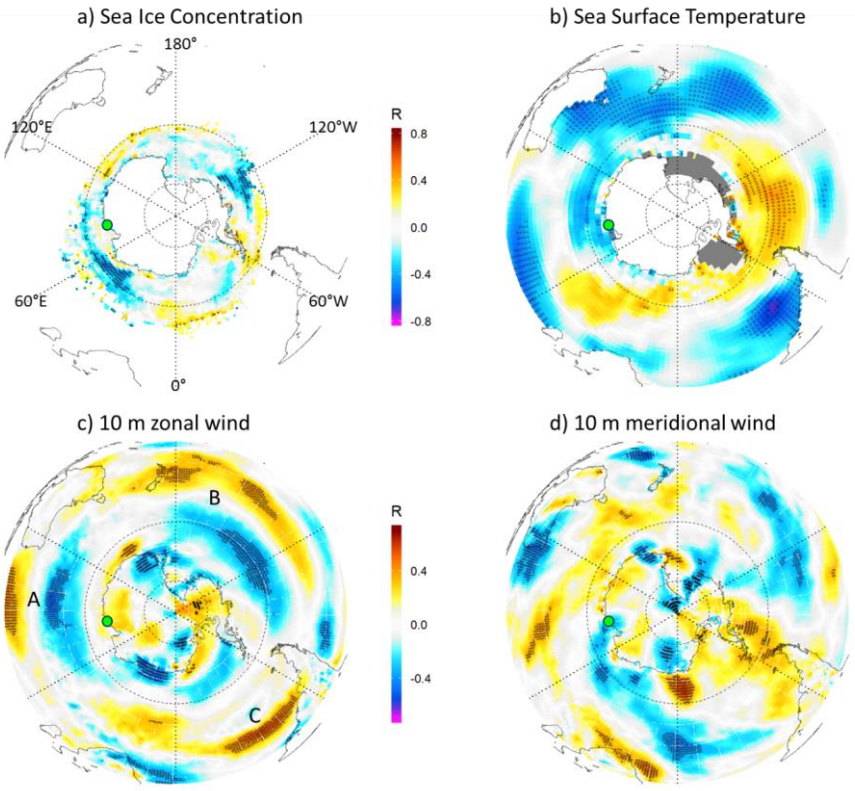
a) Sea Ice Concentration
b) Sea Surface Temperature
c) 10 m zonal wind
d) 10 m meridional wind
180°
120°E
120°W
60°E
60°W
0°
R
0.8
0.4
0.0
-0.4
-0.8
A
B
C

1101

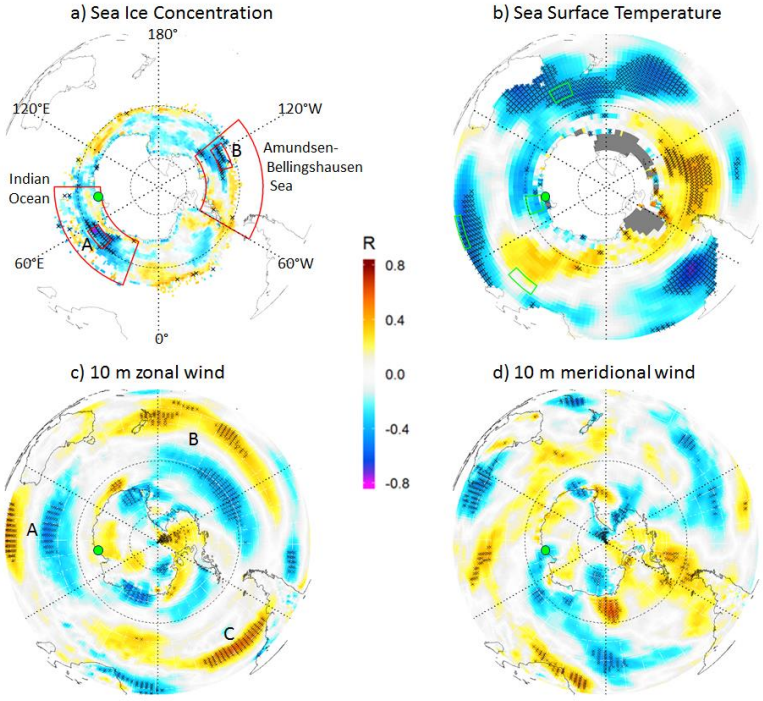
a) Sea Ice Concentration
b) Sea Surface Temperature
c) 10 m zonal wind
d) 10 m meridional wind
180°
120°E
120°W
60°E
60°W
0°
Indian
Ocean
Amundsen-
Bellingshausen
Sea
A
B
C
R
0.8
0.4
0.0
-0.4
-0.8

1102

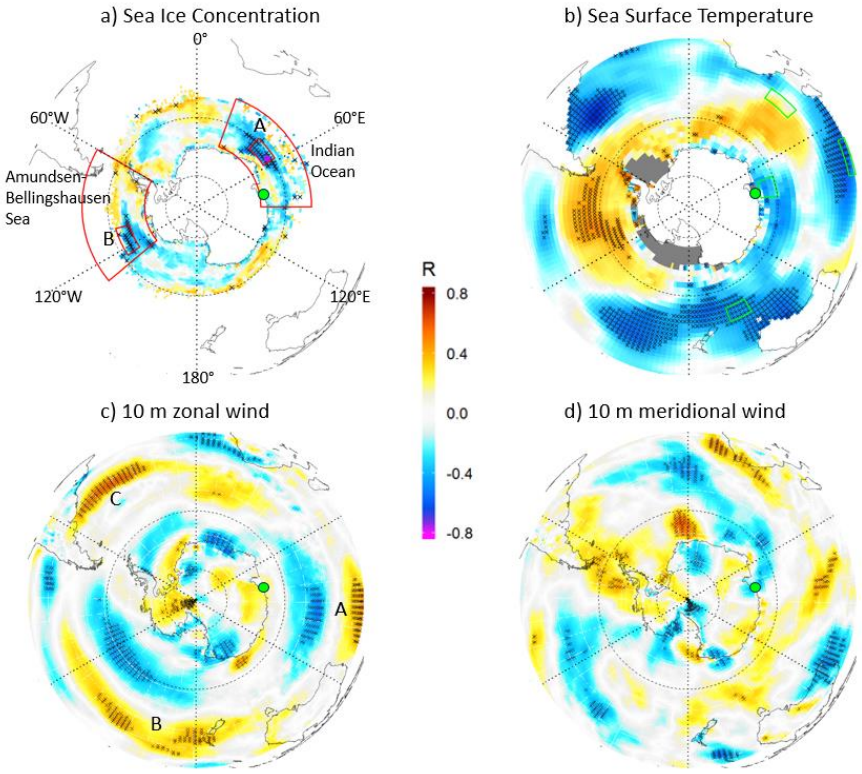


Figure 9~~7~~. Correlation maps of Davis OH 24 year QQO signal (green dot) with a) Sea Ice Concentration (OI-SST; Reynolds et al., 2002) b) Sea surface temperature (ERSSTv5) c) Surface (10m) Zonal wind anomaly (ERA5) and d) Surface (10m) Meridional wind anomaly (ERA5). Hashed areas are significant at the 90% level

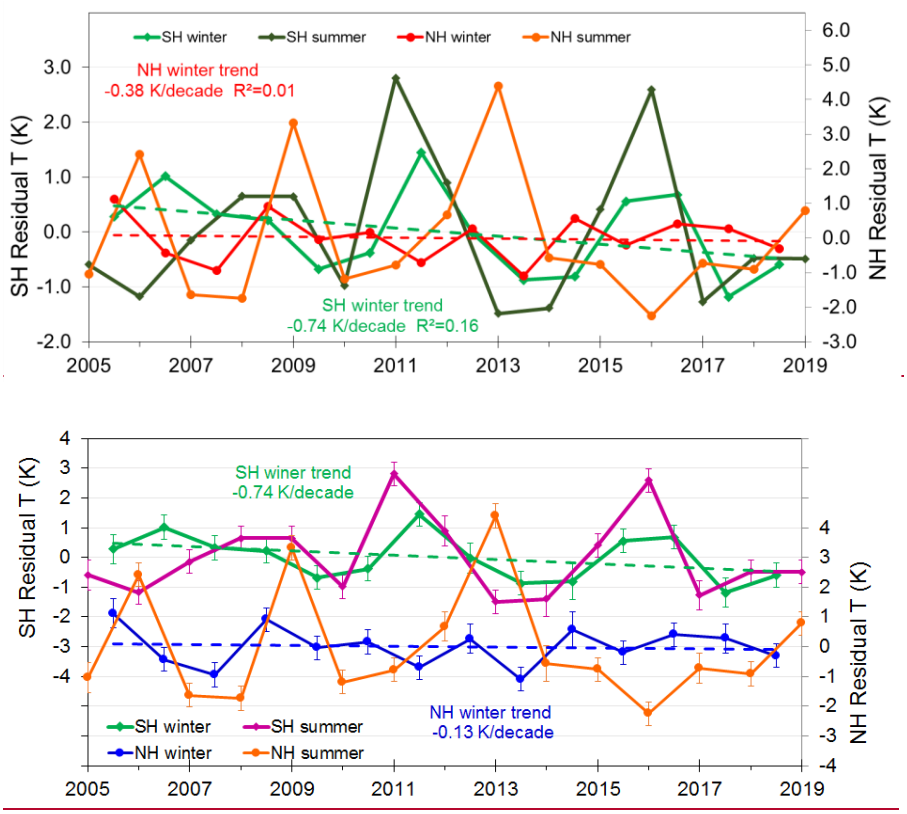


Figure. 10. Time series of Aura/MLS temperature residuals at the 0.0046hPa pressure level averaged over the SH polar cap (65° S - 85° S) for winter months (AMJJAS; light green line) and summer months (ONDJF~~A~~M; purple~~dark green~~ line), and the NH polar cap (65° N - 85° N) for summer months (AMJJAS; orange line) and winter months (ONDJF~~A~~M; blue~~red~~ line). Scales offset 3K for clarity.

# Supplementary Figures

French, Klekociuk and Mulligan - Analysis of 24 years of mesopause region OH rotational temperature observations at Davis, Antarctica. Part 2: Evidence of a quasi-quadrennial oscillation (QQO) in the polar mesosphere.

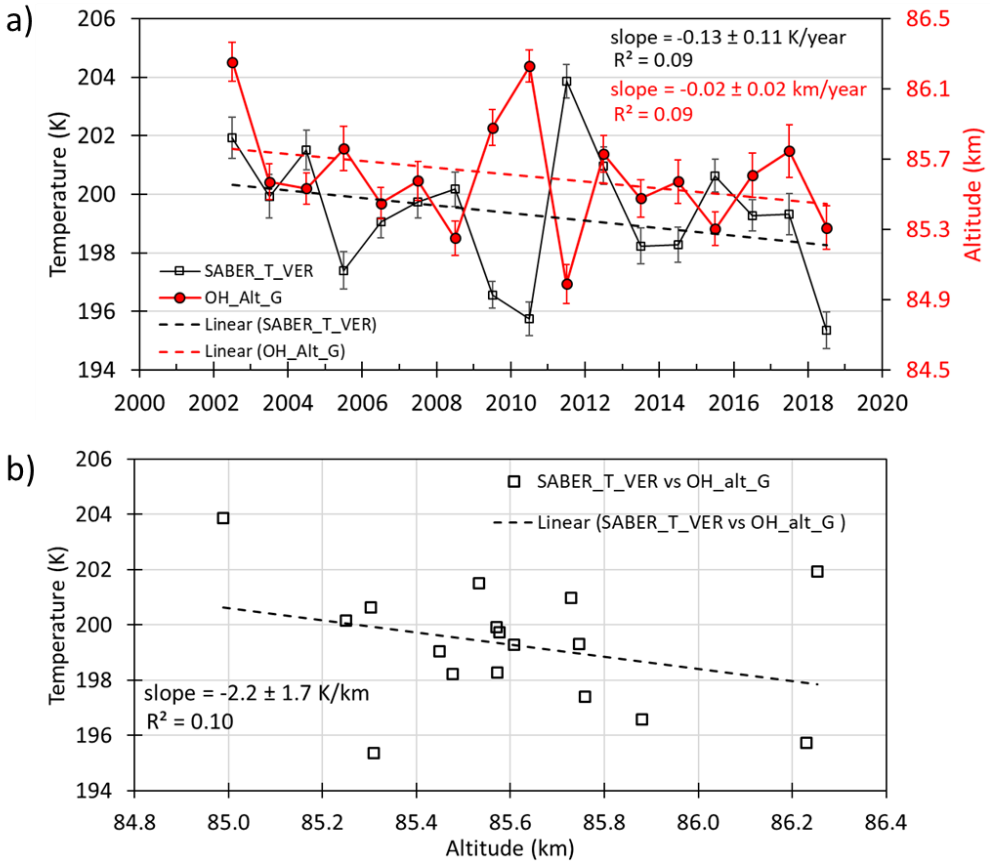


Figure S1. (a) OH layer equivalent temperatures (black) calculated from SABER VER weighted temperature profiles and the centroid altitude of a Gaussian fit to the SABER VER profiles (red) for the years 2002 to 2018 (day 106-259 of each year). The values are the average of all profiles measured by SABER within a 500 km radius of Davis station. (b) A scatter plot of the OH layer equivalent temperatures and the corresponding altitude of the OH layer shown in panel (a).

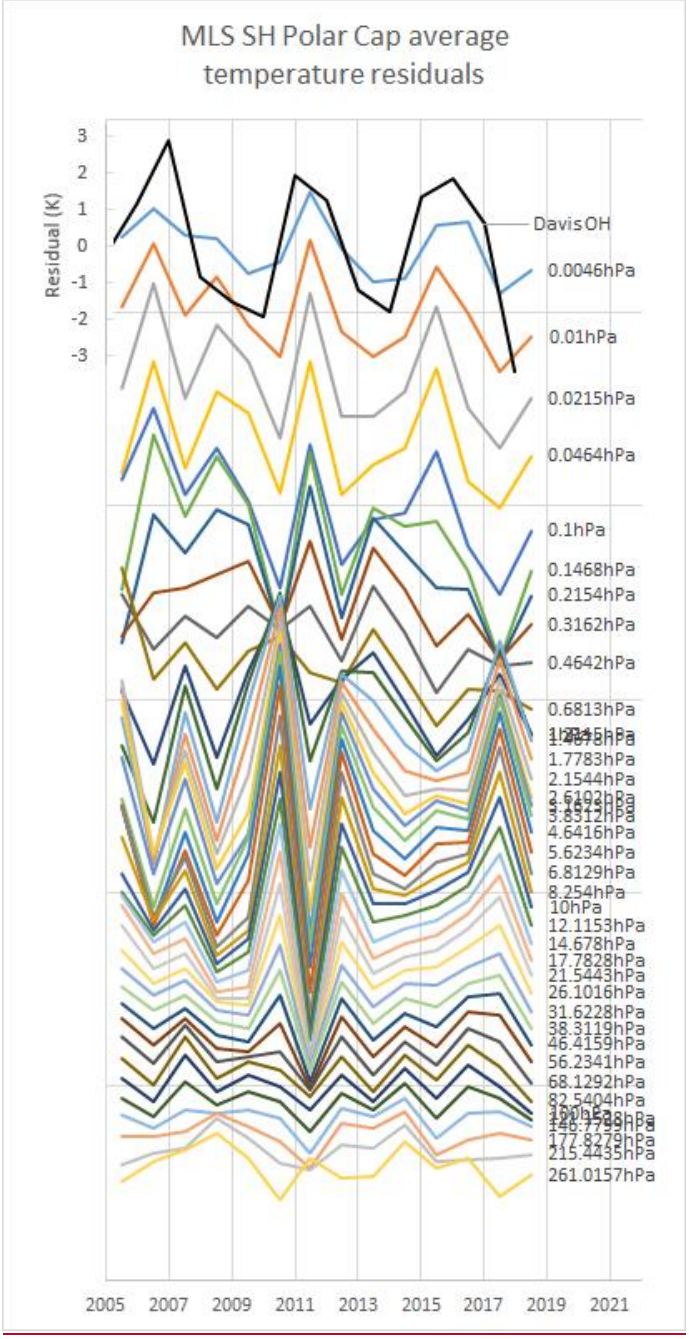


Figure S2. Additional pressure levels to compliment Figure 2b showing time series of Aura/MLS [AMJJAS] polar cap (65-85°S) averages at the native pressure levels indicated.

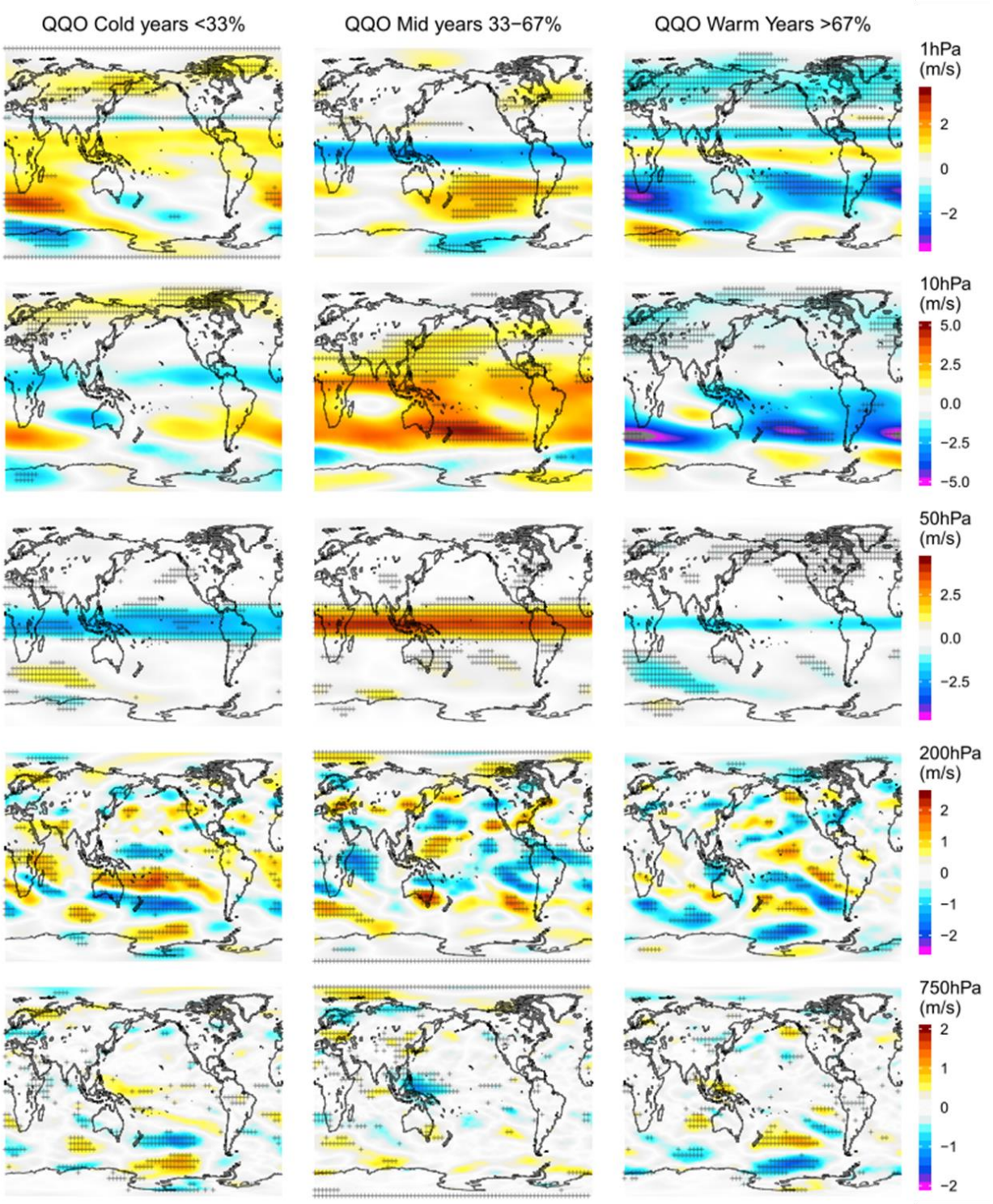
QQO Cold years <33%
QQO Mid years 33−67%
QQO Warm Years >67%
1hPa
(m/s)
2
0
−2
10hPa
(m/s)
5.0
2.5
0.0
−2.5
−5.0
50hPa
(m/s)
2.5
0.0
−2.5
200hPa
(m/s)
2
1
0
−1
−2
750hPa
(m/s)
2
1
0
−1
−2

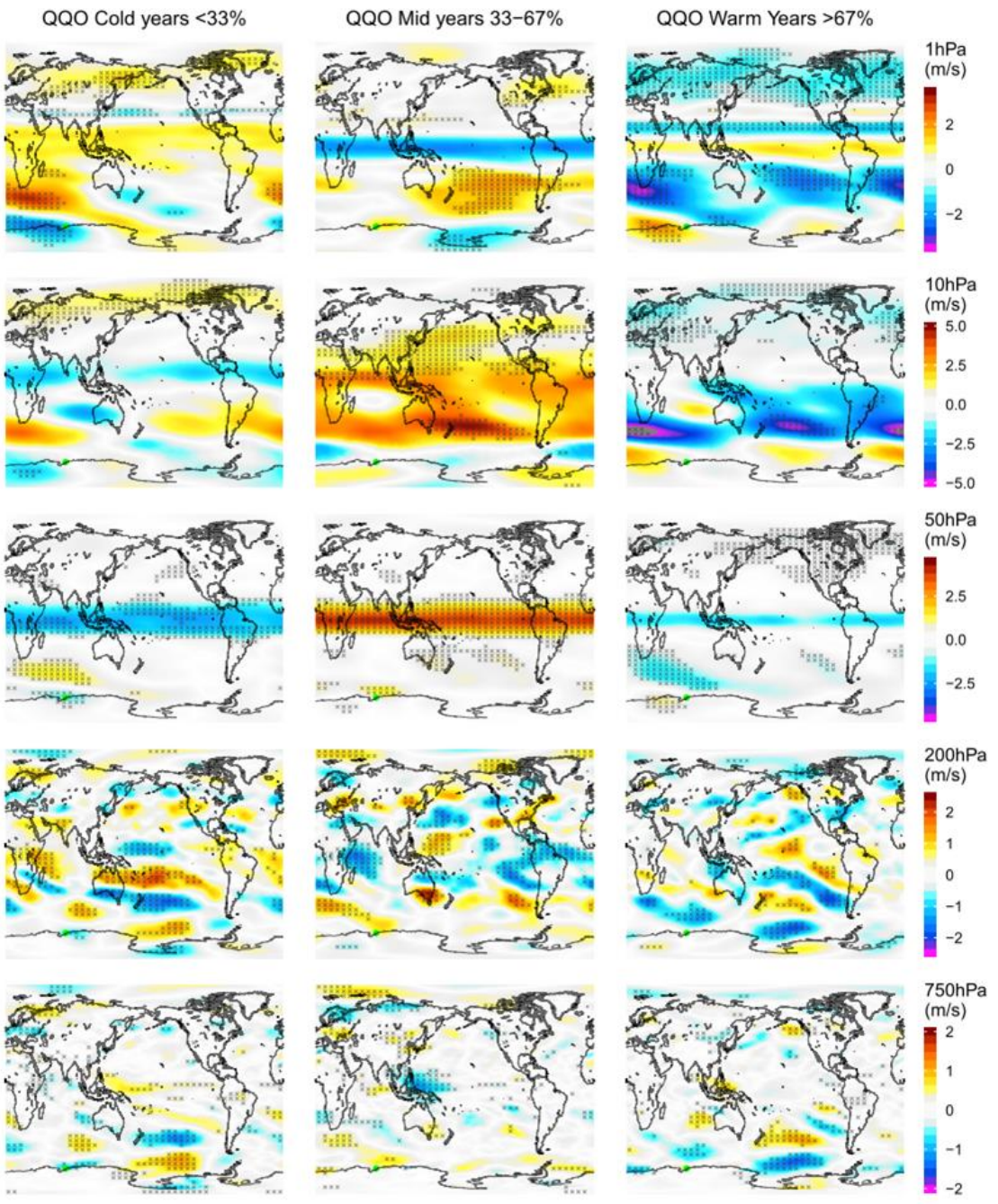


Figure S3~~2~~. Composites of the ERA5 [AMJJAS] zonal wind anomaly, for cold, mid and warm years of the Davis detrended winter average QQO signal. Pressure levels are indicated on the right hand colour bar. The colour scales are in m/s. Hashed areas on the plots are significant at the 90% level.

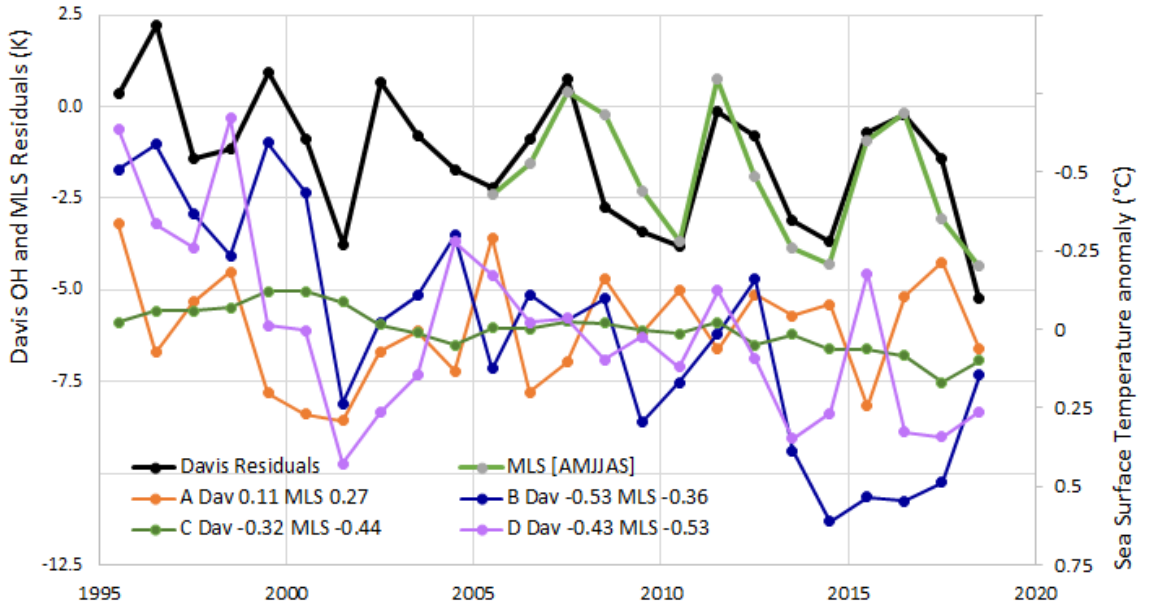


Figure S4. Time series of Sea Surface Temperature (SST) anomalies for the regions marked A, B, C and D on Fig. 5 compared to the Davis OH and Aura/MLS residual temperatures. Correlation coefficients for each series are provided in the legend caption.

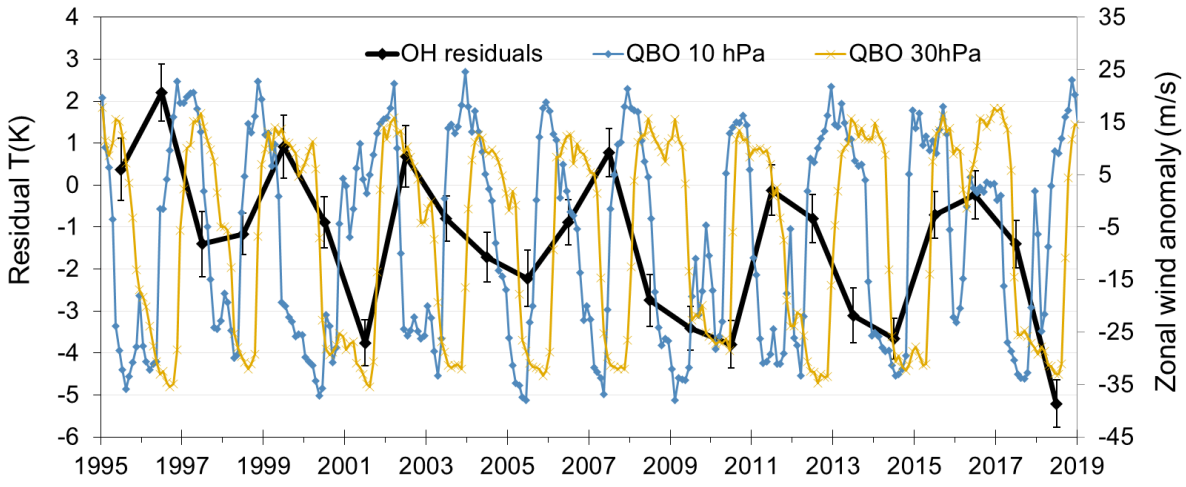


Figure S5~~4~~. Davis OH winter mean residual temperatures (K) (black line; 1995-2018), and the corresponding 10 hPa (blue) and 30 hPa (yellow) standardized monthly averaged zonally averaged zonal wind (m/s) at the equator (known as the Quasi-Biennial Oscillation (QBO). QBO data were obtained from the 30 hPa and 10 hPa Singapore QBO data (https://www.geo.fu-berlin.de/en/met/ag/strat/produkte/qbo/).

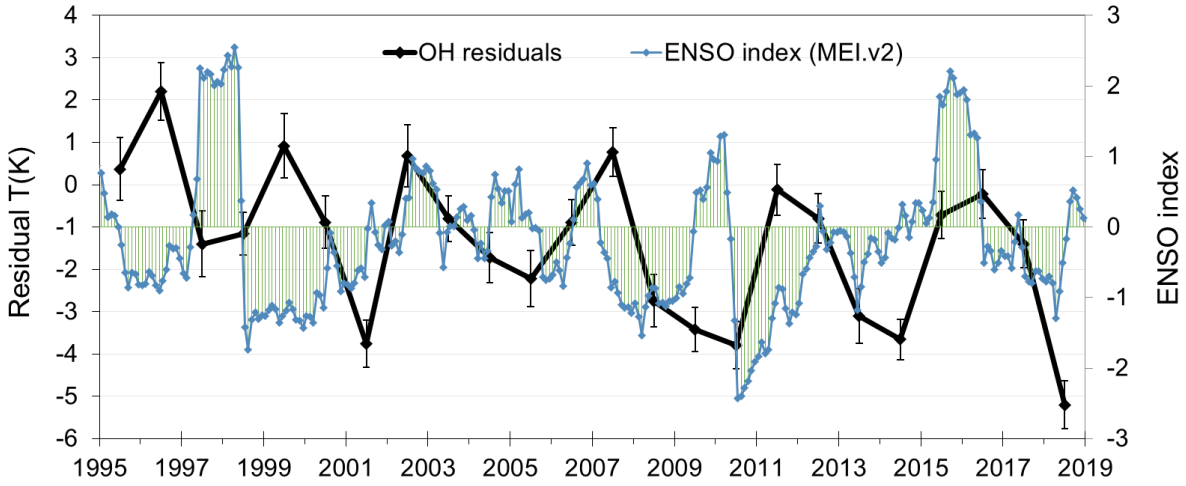


Figure S~~65~~. Davis OH winter mean residual temperatures (K) (black line; 1995-2018), and the corresponding values of the Multivariate El Nino Southern Oscillation Index (MEIv2). The time series is bimonthly so the Jan value represents the Dec-Jan value and is centered between the months. Details and current values were obtained from NOAA ESRL (Earth System Research Laboratory) Physical Sciences Division (PSD) MEI webpage (https://www.esrl.noaa.gov/psd/data/correlation/meiv2.data).

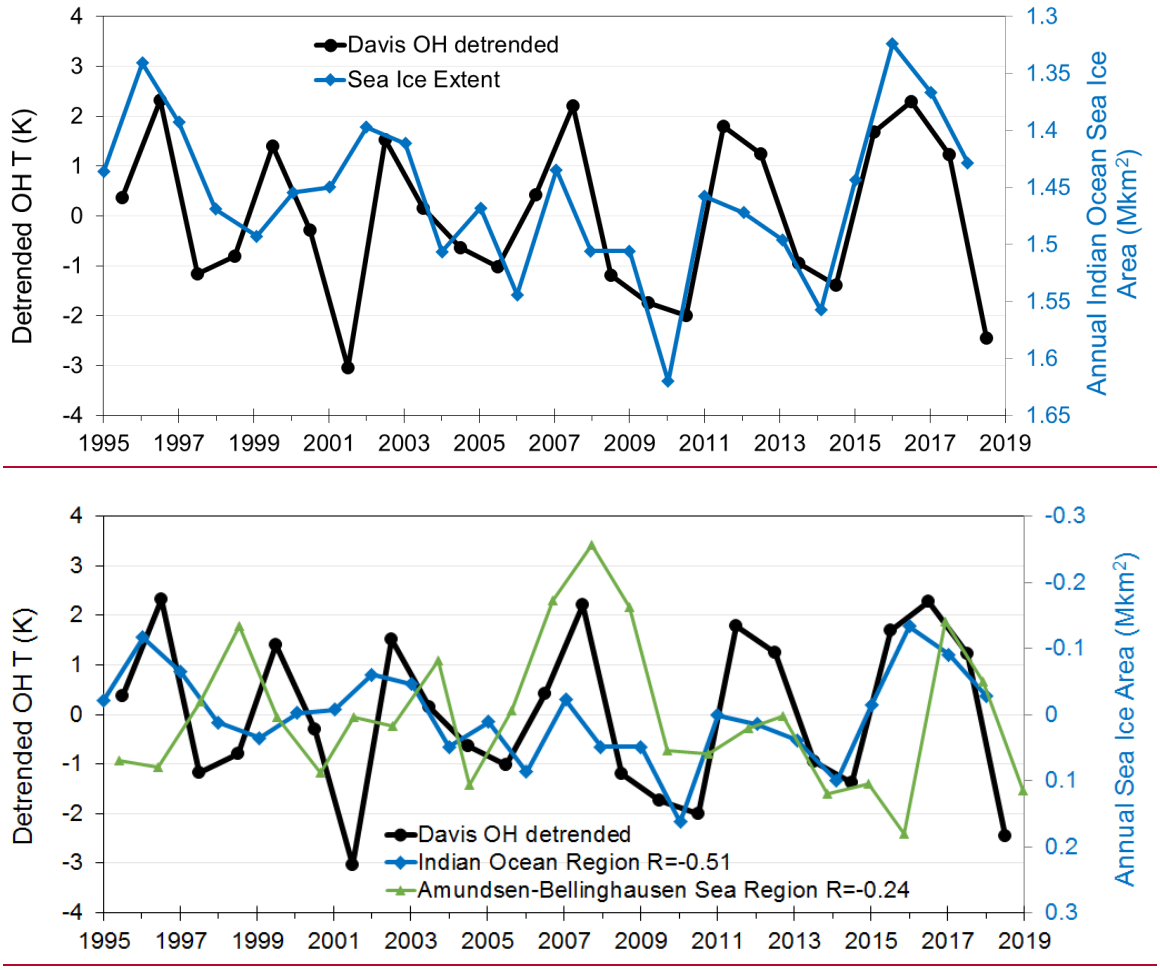


Figure S7. Detrended Davis OH winter mean temperatures compared to the Annual Indian Ocean (blue line; R=-0.51) and Amundsen-Bellinghausen Sea Region (green line; R=-0.24) Sea Ice Area (Mkm$^2$ from Parkinson, 2019). Note inverted scale for sea ice area.

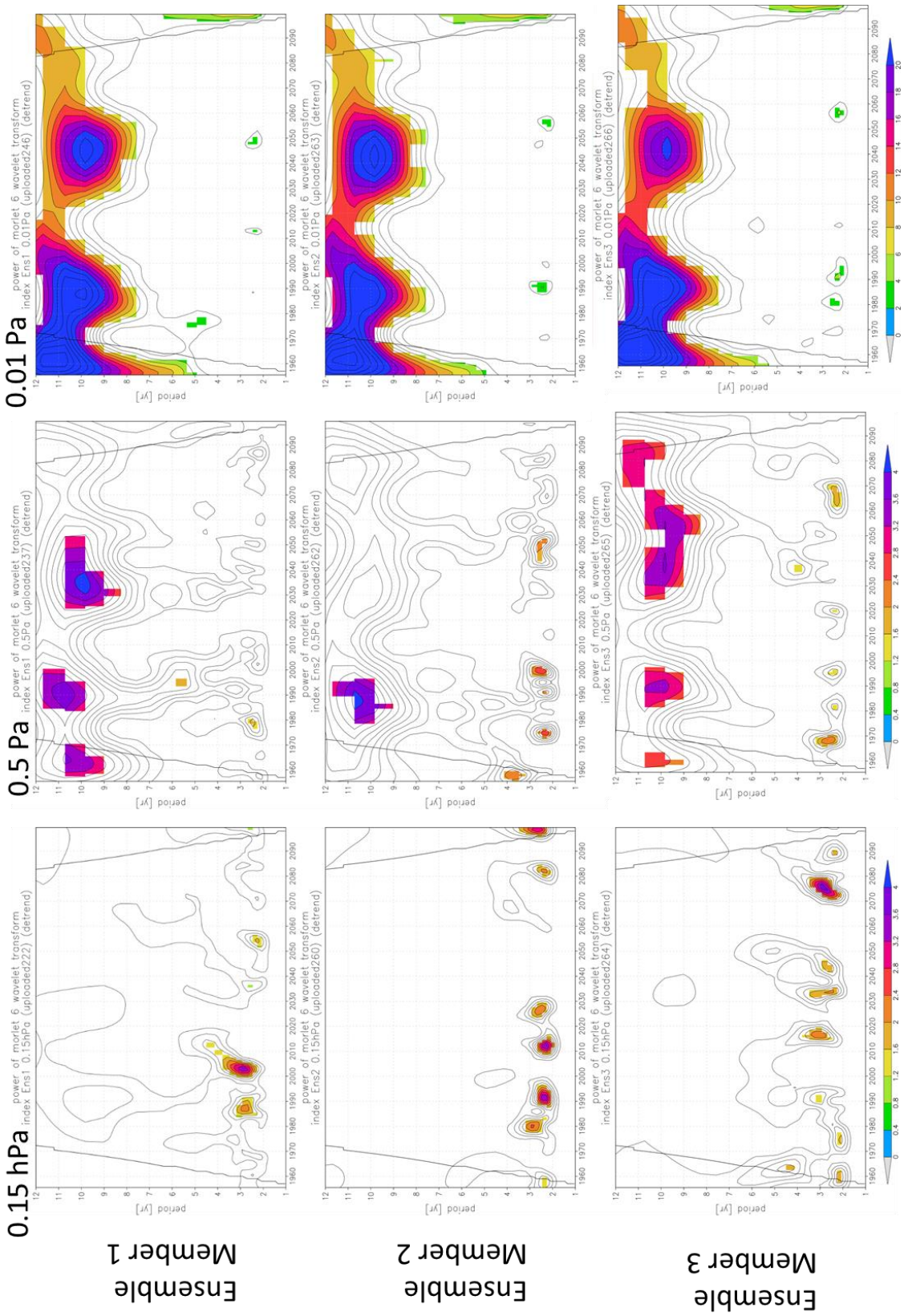


Figure S8. Wavelet spectra of CESM-WACCM Ref-C2 runs for CCMI-1 of polar cap average (65°S - 85 °S) temperature for AMJJAS. Shown are spectra for each of 3 ensemble members (columns) at three pressures (rows; 0.15 hPa, 0.5 Pa (0.005 hPa) and 0.01 Pa (0.0001 hPa)).